NAVAL POSTGRADUATE SCHOOL

MONTEREY, CALIFORNIA

THESIS

ULTRA LOW-VOLTAGE ENERGY HARVESTING

by

Alan P. Cabiling

September 2013

Thesis Advisor: Alexander L. Julian
Second Reader: Roberto Cristi

Approved for public release; distribution is unlimited

Report Documentation Page

Form Approved
OMB No. 0704-0188

1. REPORT DATE	2. REPORT TYPE	3. DATES COVERED
SEP 2013	**N/A**	**-**

4. TITLE AND SUBTITLE
Ultra Low-Voltage Energy Harvesting

5a. CONTRACT NUMBER
5b. GRANT NUMBER
5c. PROGRAM ELEMENT NUMBER

6. AUTHOR(S)

5d. PROJECT NUMBER
5e. TASK NUMBER
5f. WORK UNIT NUMBER

7. PERFORMING ORGANIZATION NAME(S) AND ADDRESS(ES)
Naval Postgraduate School Monterey, CA 93943-5000

8. PERFORMING ORGANIZATION REPORT NUMBER

9. SPONSORING/MONITORING AGENCY NAME(S) AND ADDRESS(ES)

10. SPONSOR/MONITOR'S ACRONYM(S)
11. SPONSOR/MONITOR'S REPORT NUMBER(S)

12. DISTRIBUTION/AVAILABILITY STATEMENT
Approved for public release, distribution unlimited

13. SUPPLEMENTARY NOTES

14. ABSTRACT

The U.S. Navy has many opportunities to take advantage of energy sources that are usually wasted because these low power sources yield such low-voltages that a normal voltage converter is not efficient enough to harvest the energy. Low-voltage energy is available in many forms including solar, thermal, vibration, and electro-magnetic. The power that can be obtained from these sources on a small scale can be taken advantage of by using an ultra-low power boost converter that is specifically designed for energy harvesting applications. These energy sources with a very small footprint can be used in military and defense applications such as wireless sensor networks, industrial monitoring, and varieties of portable and wearable devices. The theory of power conversion, synchronous rectification, and maximum power point tracking is discussed. A discussion of the benefits of using an energy converter made specifically for energy harvesting is also covered. A commercially available energy harvester converter is simulated using a simulation program with integrated circuit emphasis, and a solar application is tested with hardware. The hardware experiments explore the startup sequence of the circuit, the switching profile of the converter, and a test of the circuits efficiency.

15. SUBJECT TERMS

16. SECURITY CLASSIFICATION OF:			17. LIMITATION OF ABSTRACT	18. NUMBER OF PAGES	19a. NAME OF RESPONSIBLE PERSON
a. REPORT	b. ABSTRACT	c. THIS PAGE			
unclassified	**unclassified**	**unclassified**	**SAR**	**97**	

THIS PAGE INTENTIONALLY LEFT BLANK

REPORT DOCUMENTATION PAGE			*Form Approved OMB No. 0704-0188*
Public reporting burden for this collection of information is estimated to average 1 hour per response, including the time for reviewing instruction, searching existing data sources, gathering and maintaining the data needed, and completing and reviewing the collection of information. Send comments regarding this burden estimate or any other aspect of this collection of information, including suggestions for reducing this burden, to Washington headquarters Services, Directorate for Information Operations and Reports, 1215 Jefferson Davis Highway, Suite 1204, Arlington, VA 22202-4302, and to the Office of Management and Budget, Paperwork Reduction Project (0704-0188) Washington DC 20503.			
1. AGENCY USE ONLY ***(Leave blank)***	**2. REPORT DATE** September 2013	**3. REPORT TYPE AND DATES COVERED** Master's Thesis	
4. TITLE AND SUBTITLE ULTRA LOW-VOLTAGE ENERGY HARVESTING		**5. FUNDING NUMBERS**	
6. AUTHOR(S) Alan P. Cabiling			
7. PERFORMING ORGANIZATION NAME(S) AND ADDRESS(ES) Naval Postgraduate School Monterey, CA 93943-5000		**8. PERFORMING ORGANIZATION REPORT NUMBER**	
9. SPONSORING /MONITORING AGENCY NAME(S) AND ADDRESS(ES) N/A		**10. SPONSORING/MONITORING AGENCY REPORT NUMBER**	
11. SUPPLEMENTARY NOTES The views expressed in this thesis are those of the author and do not reflect the official policy or position of the Department of Defense or the U.S. government. IRB protocol number ____N/A____.			
12a. DISTRIBUTION / AVAILABILITY STATEMENT Approved for public release; distribution is unlimited		**12b. DISTRIBUTION CODE** A	

13. ABSTRACT (maximum 200 words)

The U.S. Navy has many opportunities to take advantage of energy sources that are usually wasted because these low power sources yield such low-voltages that a normal voltage converter is not efficient enough to harvest the energy. Low-voltage energy is available in many forms including solar, thermal, vibration, and electro-magnetic.

The power that can be obtained from these sources on a small scale can be taken advantage of by using an ultra-low power boost converter that is specifically designed for energy harvesting applications. These energy sources with a very small footprint can be used in military and defense applications such as wireless sensor networks, industrial monitoring, and varieties of portable and wearable devices.

The theory of power conversion, synchronous rectification, and maximum power point tracking is discussed. A discussion of the benefits of using an energy converter made specifically for energy harvesting is also covered. A commercially available energy harvester converter is simulated using a simulation program with integrated circuit emphasis, and a solar application is tested with hardware. The hardware experiments explore the startup sequence of the circuit, the switching profile of the converter, and a test of the circuit's efficiency.

14. SUBJECT TERMS Energy harvesting, power conversion, boost converter, maximum power point tracking, synchronous converter, renewable energy			**15. NUMBER OF PAGES** 97
			16. PRICE CODE
17. SECURITY CLASSIFICATION OF REPORT Unclassified	**18. SECURITY CLASSIFICATION OF THIS PAGE** Unclassified	**19. SECURITY CLASSIFICATION OF ABSTRACT** Unclassified	**20. LIMITATION OF ABSTRACT** UU

NSN 7540-01-280-5500

Standard Form 298 (Rev. 2-89)
Prescribed by ANSI Std. 239-18

THIS PAGE INTENTIONALLY LEFT BLANK

Approved for public release; distribution is unlimited

ULTRA LOW-VOLTAGE ENERGY HARVESTING

Alan P. Cabiling
Lieutenant, United States Navy
B.S., University of Washington, 2006

Submitted in partial fulfillment of the
requirements for the degree of

MASTER OF SCIENCE IN ELECTRICAL ENGINEERING

from the

NAVAL POSTGRADUATE SCHOOL
September 2013

Author: Alan P. Cabiling

Approved by: Alexander L. Julian
Thesis Advisor

Roberto Cristi
Second Reader

R. Clark Robertson
Chair, Department of Electrical and Computer Engineering

THIS PAGE INTENTIONALLY LEFT BLANK

ABSTRACT

The U.S. Navy has many opportunities to take advantage of energy sources that are usually wasted because these low power sources yield such low-voltages that a normal voltage converter is not efficient enough to harvest the energy. Low-voltage energy is available in many forms including solar, thermal, vibration, and electro-magnetic.

The power that can be obtained from these sources on a small scale can be taken advantage of by using an ultra-low power boost converter that is specifically designed for energy harvesting applications. These energy sources with a very small footprint can be used in military and defense applications such as wireless sensor networks, industrial monitoring, and varieties of portable and wearable devices.

The theory of power conversion, synchronous rectification, and maximum power point tracking is discussed. A discussion of the benefits of using an energy converter made specifically for energy harvesting is also covered. A commercially available energy harvester converter is simulated using a simulation program with integrated circuit emphasis, and a solar application is tested with hardware. The hardware experiments explore the startup sequence of the circuit, the switching profile of the converter, and a test of the circuit's efficiency.

THIS PAGE INTENTIONALLY LEFT BLANK

TABLE OF CONTENTS

THIS PAGE INTENTIONALLY LEFT BLANK

LIST OF FIGURES

LIST OF TABLES

THIS PAGE INTENTIONALLY LEFT BLANK

LIST OF ACRONYMS AND ABBREVIATIONS

AC	Alternating Current
BAT	Battery
C	Capacitor
CCM	Continuous Conduction Mode
C_{STOR}	Storage Capacitor
D	Duty Cycle
DC	Direct Current
DCM	Discontinuous Conduction Mode
EVM	Evaluation Module
GND	Ground
GPS	Global Positioning System
I	Current
I-V	Current-Voltage
IC	Integrated Circuit
I_{MP}	Maximum Power Current
I_{SC}	Short Circuit Current
L	Inductor
L_{BST}	Boost Inductor
MOSFET	Metal-Oxide Semiconductor Field Effect Transistor
MPPT	Maximum Power Point Tracking
OV	Over-Voltage
P	Power
PFM	Pulse Frequency Modulation
P_{MAX}	Maximum Power
PV	Photovoltaic
R	Resistance
RF	Radio Frequencies
S	Switch
SPICE	Simulation Program with Integrated Circuit Emphasis
T	Switching Cycle

t_{active}	Active Time
t_{cycle}	Cycle Time
UV	Under-Voltage
V	Voltage
V_{BAT}	Battery Voltage
V_{IN}	Input Voltage
V_{MP}	Maximum Power Voltage
V_{OC}	Open Circuit Voltage
V_{SOURCE}	Source Voltage
V_{STOR}	Storage Voltage
WSN	Wireless Sensor Network
η	Efficiency

EXECUTIVE SUMMARY

Energy harvesting has emerged as a method of extracting power from sources that only produce micro-watts of power. These power sources are usually constrained by size due to the environment that they are designed for. With these small sources of power, it is imperative that the conversion techniques used to harvest the energy is as efficient as possible. The technologies that make energy harvesting an efficient and viable form of power generation are covered in this thesis.

In military and defense applications, energy harvesting can be used to provide power for wireless sensor networks, industrial monitoring, environmental monitoring, or any other sensor network that requires small amounts of energy. Devices that are able to be powered with energy harvesters can be particularly desirable in areas that are inaccessible or where regular battery replacement is very difficult. This technology allows for a greater range of sensors to be placed where conventional renewable energy devices may not produce enough power due to the environment such as prolonged cloud cover in solar applications.

Many different technologies are incorporated to ensure that the small sources of energy are used to the maximum potential. When dealing with such small power harvesters, steps to make the circuit more efficient are essential. Since electrical power conversion is at the basis of harvesting these small sources of power, boost converter theory is first discussed to explain the conversion of the small voltages harvested in millivolts to the volts required by most electronic circuits.

In order to expand on conventional boost conversion techniques, the concept of synchronous conversion is discussed. Synchronous conversion is the technology that allows for transistors with a much lower voltage drop than conventional diodes to be used in the boost converter. Synchronous conversion is essentially an actively controlled converter where the switches are electronically controlled to provide the required amount of boosted voltage.

Another important issue addressed in this research is maximum power point tracking, a technology that allows the maximum extraction of power from different harvesting sources. In a solar cell, the most efficient way of extracting power is not by maximizing the voltage but by operating based on the solar cell's particular current-voltage characteristics. Typically, a solar cell produces the most power at about 80 percent of its maximum voltage. Maximum power point tracking will adjust the voltage pulled from the source to ensure that it remains at its most efficient operating point. This operating point can adjust due to different operating conditions that affect power generation. For example, if the solar cell is producing less voltage due to cloud cover, the maximum power point tracking will adjust and maintain the voltage at 80 percent. This can also be altered for different sources such as thermo-electric harvesters which are most efficient at about 50 percent. Finally, there are many energy storage options when considering energy harvesters such as rechargeable batteries and supercapacitors.

A Texas Instruments BQ25504 Ultra Low Power Boost Converter was simulated and tested in hardware. The simulation demonstrated such features of the converter as cold-starting, which allows the converter to bypass the internals when battery voltage is low and operate as an unregulated boost converter. The under-voltage and over-voltage features were also tested, demonstrating the energy storage protection features. The voltage and current waveforms were also shown for the different operating conditions. The same circuit was also tested in hardware, testing all the features that were demonstrated in the simulation and also showing the maximum power point tracking technology.

The theory of converters was covered as well as the technologies that aid in energy harvesting. A commercially available converter was analyzed in simulation and hardware experiments, demonstrating the technologies that make energy harvesting viable in using ultra low voltage sources. These technologies are all combined to make energy harvesting possible for use in many different applications in the defense community as well as commercially.

ACKNOWLEDGMENTS

I would like to thank my thesis advisor, Professor Alexander Julian, for inspiring the topic of research. I appreciate his trust in letting me pursue a topic that allowed for both of us to learn something new.

I would also like to thank my wife, Johanna, for constantly pushing me to keep the progress going. Without her, this thesis might not have been completed on time. To the rest of my family, I thank them for believing in me and always telling me that I was capable of great things.

THIS PAGE INTENTIONALLY LEFT BLANK

I. INTRODUCTION

A. BACKGROUND

This thesis was inspired while taking a course in advanced electrical machinery systems. In this course, which covered electrical generator theory, we discussed a previous thesis where a student designed a linear electromagnetic generator that was small enough to be handheld. This small generator could then be carried by a person to power any of the multitudes of electronic devices that have become part of our everyday lives. Although the energy harvested would be small, it would make use of physical energy that would otherwise be wasted. Another problem that needed a solution was the possibility of harvesting energy from something like the vibration of a delivery truck. The vibration of the delivery truck could then be used to possibly power a small Global Positioning System (GPS) unit to give the instantaneous position of a package. With technologies such as the handheld generator and other small sources of power, a conversion process is needed to harvest the small voltages produced and convert it into a more useful voltage.

1. Energy Needs in the Department of Defense

The Navy is also looking for new technologies to harness renewable power. The Secretary of the Navy has expressed his concern about making energy usage a topic that must be taken seriously. According to the Secretary of the Navy,

> Reforming energy use and policy within the Department of the Navy will assure the long-term energy security of the United States, encourage development of efficiencies, and promote environmental stewardship. In doing so, we will improve the combat and operational effectiveness of our Forces and maintain our position as the finest Navy and Marine Corps in the world. [1]

The Navy and other military entities could have broad applications for an energy harvester. Typically, any electrical requirement that is small and would benefit from less interaction such as changing batteries or being located in a remote location could be a potential candidate for this technology.

2. Applications

Texas Instruments claims that the BQ25504, which will be studied in this thesis, is one of the most efficient of its kind on the market. It has proposed many uses for this energy harvesting circuit, especially when used in a wireless sensor network (WSN) application. Texas Instruments provides the list below as some of the advertised uses for this technology [2]:

- Agriculture (gravity feed systems, water tank levels, pump levels)
- Air pollution
- Area monitoring
- Forest fire detection
- Greenhouse monitoring
- Home and building automation
- Industrial monitoring
- Landslide detection
- Machine health monitoring (machinery condition-based systems)
- Structural monitoring (monitor movement within buildings and infrastructure, monitor assets, retrieve daily data)
- Waste/water monitoring

B. OBJECTIVE

The various technologies integrated into a typical energy harvesting circuit are discussed in this thesis. The BQ25504 is a commercially available energy harvesting circuit that is available from Texas Instruments and is the circuit that is studied in this thesis. A review of the technologies that make energy harvesters is given to introduce topics in power conversion. Applications of this circuit are discussed with respect to the areas of industry that will make the most use of this technology. The device is modeled in a simulation program with integrated circuit emphasis (SPICE) program, and a startup sequence is observed. The circuit hardware is then implemented to observe the startup sequence and the general properties of the circuit. The simulation and the hardware implementation are compared. Overall, the viability of energy harvesters that could prove useful to the military and other industrial applications is discussed in this thesis.

C. PREVIOUS WORK

A previous Naval Postgraduate School student completed a thesis topic that considered the possibility of a miniature electromechanical generator that utilized human motion [3]. In this thesis, a miniature generator was designed and modeled to test the viability of this approach. The student's design in [3] was able to achieve a maximum output voltage of 1.7 V and a peak power output of 130 mW. Energy harvesting designs such as these are able to take energy that is produced as a byproduct of the main action. For example, walking has the objective of getting from one point to another, but having the sole of a shoe absorb the energy impact of the foot hitting the ground is basically wasting some of the energy expended. Utilizing an energy harvester at the sole of a shoe could potentially absorb the footstep energy while simultaneously generating electrical energy.

CAP-XX, an Australian capacitor manufacturer, specializes in thin profile supercapacitors. These thin profile capacitors are perfect for situations that require circuit topologies that are very small. CAP-XX has conducted two experiments: harvesting energy from a solar cell without a converter and using the same energy harvester boost converter that is discussed in this thesis [4].

Using the Texas Instruments BQ25504 energy harvesting intelligent converter, the people at CAP-XX were able to show the advantages and disadvantages of using a boost converter on small variable sources of input power. As a control experiment, a supercapacitor was connected to a photovoltaic (PV) source with a diode in between. The advantages of this circuit were a simple design and a fast charge. The disadvantages were that the capacitor could not be charged when the source voltage was less than the capacitor voltage. The capacitor was able to be charged in approximately 3.5 hours.

The second circuit that was tested utilized the BQ25504. The advantages gained by using the boost converter are that the capacitor can be charged despite the source voltage falling below the capacitor voltage. The disadvantages are that the charging time is very slow, about 67 hours. The last circuit tested also utilized the BQ25504 but added a bypass diode. This allowed for the capability of low source voltage charging with the

speed of the direct connection topology. The last circuit was able to charge the supercapacitor in two hours.

The Massachusetts Institute of Technology has done research in the field of low voltage energy harvesting by investigating the use of multiple sources to power a single power unit [5]. Often, a single small source may be sufficient for small loads, but if the power is able to be drawn from multiple sources, the range of devices that can be powered by low voltage harvesters increases. As stated in [5], "Circuits to harvest thermal differences typically produce only 0.02 to 0.15 V, while low-power photovoltaic cells can generate 0.2 to 0.7 V and vibration-harvesting systems can produce up to 5 V. Coordinating these disparate sources of energy in real time to produce a constant output is a tricky process." Being able to harvest energy not just from one source, such as solar, but to harvest it from multiple sources at the same time provides a great increase in the capability of the energy harvesters. Their research also discussed the problem of finding a very efficient circuit to be able to utilize the nano-voltages that the harvesters could generate. Along with using circuit optimization techniques, the researchers were also able to use a single inductor for three different power sources to increase the efficiency. Overall, this technology enables the ability to harvest energy from different sources, either providing power when one source is unavailable or being able to provide more power to a larger load.

The Imperial College of London conducted research on harvesting energy from electro-magnetic waves at radio frequencies (RF), another form of nano-power that falls into the energy harvesting spectrum [6]. In this research they measured the power available from multiple RF sources, the results of which are shown in Table 1.

Table 1. London RF survey measurements. (From [6])

Band name	Frequency (MHz)	Average P ($\mu W/cm^2$)	Maximum P ($\mu W/cm^2$)
DTV	470 - 610	$0.89x10^{-3}$	0.046
GSM 900	925 - 960	0.036	1.93
GSM 1800	1805 - 1876	0.084	6.39
WiFi	2400 - 2473	$0.18x10^{-3}$	$6.47x10^{-3}$
3G	2110 - 2170	0.012	0.24

The London researchers also used the Texas Instruments BQ25504 energy harvester that is used in this thesis's research. According to the London researcher's findings, "Efficiencies of up to 40% were achieved with a single banded rectenna operating at GSM 900, and efficiencies higher than 20% were achieved for TV and 3G" [6]. This research demonstrated another viable means to harvest energy that otherwise goes wasted.

D. THESIS ORGANIZATION

The reasons and motivation in choosing this research were introduced in this chapter. The basics of electrical power conversion and the theory that is behind an energy harvesting circuit is covered in Chapter II. The main circuit that will be modeled in simulation and tested in hardware is covered in Chapter III. The results of the circuit simulation as well as the results from the hardware tests are covered in Chapter IV. Concluding thoughts on the thesis as well as recommendations for further study are examined in Chapter V.

THIS PAGE INTENTIONALLY LEFT BLANK

II. OPERATION OF LOW VOLTAGE ENERGY HARVESTERS

Low-voltage energy harvesters are capable of capturing very small sources of energy from heat, light, etc. and converting that power to a higher voltage that is normally used by electronic circuitry. The simplest circuit to design that would capture energy is shown in Figure 1. This circuit topology results in quick charging and, due to the direct connection of the power harvester to the energy storage device, is very efficient. Other than a power source and the energy storage device, all that is needed is a diode to prevent the storage device from discharging. Without the diode, the storage device would discharge when the power source voltage dropped to less than the voltage of the storage device.

As an example of an application of this circuit, if in a solar battery charger the level of illumination were to drop due to cloud cover, the diode would prevent discharging of the battery when the source voltage becomes lower than battery voltage. The drawback of a simple circuit like this is that once the source voltage is lower than the battery voltage, the power source will not be able to charge the energy storage device due to the diode being reverse biased.

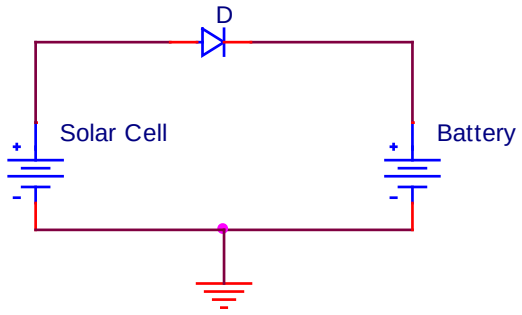

Figure 1. Simple energy harvesting circuit.

A more efficient solution is to use a device that is specifically suited to the demands of ultra-low energy harvesting. Although this adds complexity to the design of the system, the overall efficiency is increased. This device also allows the energy storage

device to be charged even if the power supply output decreases due to adverse conditions. A simple implementation of the converter is shown in Figure 2.

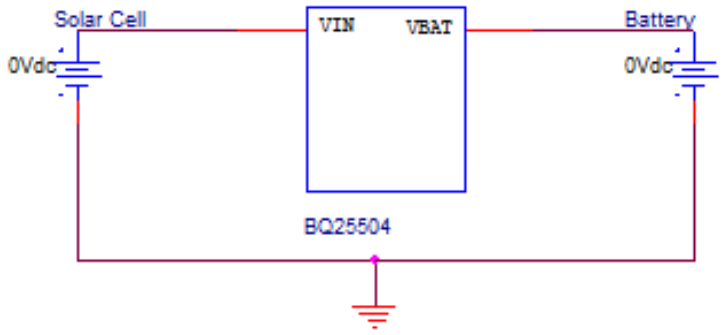

Figure 2. Harvesting circuit with boost converter.

A. THEORY OF OPERATION

Converting low voltages to higher voltages is usually accomplished in alternating current (AC) sources using a transformer, but with direct current (DC) sources a boost converter is required. The boost convert in an energy harvester is unique in that it must be able to operate on ultra-low power. This low power conversion ability is achieved using metal-oxide semiconductor field effect transistors (MOSFETs) operated in synchronous rectification. Another technology that is helpful when attempting to harvest small amounts of energy is maximum power point tracking (MPPT), which allows the optimal extraction of power from the source. Finally, issues related to different energy storage options for energy harvesting circuits are addressed.

1. Boost Converters

The main technology that energy harvesters rely upon is the ability to convert ultra-low voltages to a voltage that is typically used by normal circuitry. Energy harvester converters can take an input voltage on the order of 100 mV and increase it to a typical battery voltage of one to three V. This conversion is a DC-to-DC process and is achieved by using a boost converter. A simple boost converter is shown in Figure 3.

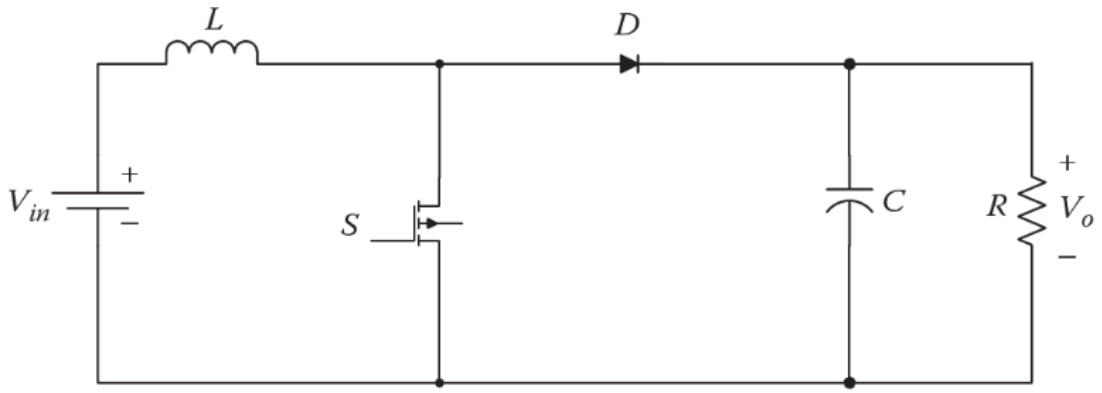

Figure 3. Conventional boost converter. (From [7])

In the circuit shown in Figure 3, the input voltage (V_{IN}) is from an energy harvester such as a PV source, and the inductor (L) is used to temporarily store energy. When the switch (S) is closed as shown in Figure 4, the voltage source is not connected to the load and only charges the inductor. The charge stored previously on the capacitor (C) provides voltage to the load while the switch is closed.

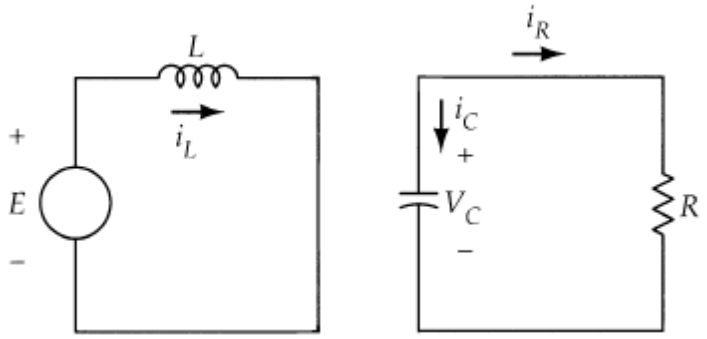

Figure 4. Conventional boost converter with switch closed. (From [8])

When the switch is open as shown in Figure 5, the stored energy in the inductor adds to the energy provided by the source and “boosts” the output voltage across the load to a value higher than that of the V_{IN} alone.

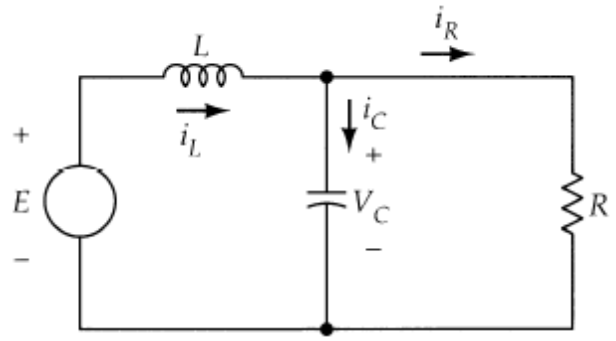

Figure 5. Conventional boost converter with switch open. (From [8])

The basic operation of a boost converter in continuous conduction mode (CCM) can be derived by observing the circuit in two different states, with the switch open and the switch closed as seen in [8]. With the switch closed as in Figure 4, the excitation voltage is

$$E = v_L \tag{1}$$

where v_L is the voltage across the inductor. Relating inductor current to inductor voltage, we obtain

$$E = L\frac{di_L}{dt} \tag{2}$$

where L is the value of inductance and i_L is inductor current. Equation (2) is then solved for the change in current to get

$$\Delta I = \frac{E}{L}\Delta t \tag{3}$$

and

$$\mathrm{I}_{MAX} - \mathrm{I}_{MIN} = \frac{E}{L}DT \tag{4}$$

where the duty cycle (D) is the ratio of the time that the switch is on to the total period of the switching cycle (T).

With the switch open as in Figure 5, E is now

$$E = v_L + V_C \tag{5}$$

where capacitor voltage V_C is added to v_L. Again, relating the inductor current to inductor voltage, we get

$$E = L\frac{di_L}{dt} + V_C . \tag{6}$$

Equation (6) can be solved for the change in current to get

$$\Delta I = \frac{E - V_C}{L}\Delta t \tag{7}$$

and

$$\mathrm{I}_{MAX} - \mathrm{I}_{MIN} = \frac{E - V_C}{L}(1 - D)T . \tag{8}$$

Setting equation (4) and equation (8) equal to each other relates the two circuit states and gives

$$-\frac{E}{V}DT = \frac{(E - V_C)}{L}(1 - D)T . \tag{9}$$

Simplifying equation (9), we get the capacitor voltage

$$V_C = \frac{E}{1 - D} \tag{10}$$

where V_C is also the output voltage. When D is less than one, the output V_C is higher than the input E. Thus, the fundamentals of a boost converter show that the input voltage can be boosted, and the boost amount is determined by D.

The size of the inductor used in a boost converter determines whether the converter operates in CCM or discontinuous conduction mode (DCM). A boost converter that is operating in CCM is shown in Figure 6. In CCM, the inductor current never reaches zero and is always providing power.

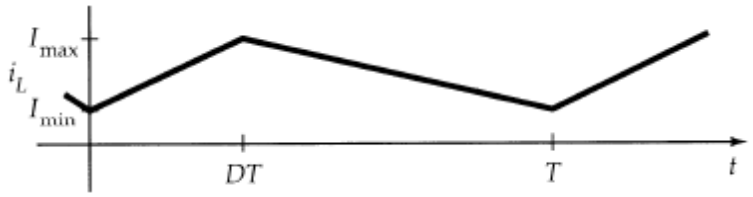

Figure 6. Boost converter inductor current in CCM. (From [8])

A boost converter that is operating in DCM is shown in Figure 7. In DCM the inductor is not large enough and causes inductor current to fall to zero for a period of time.

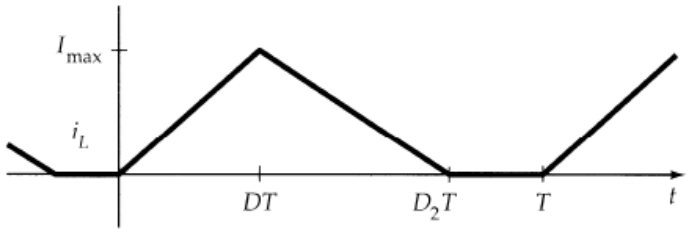

Figure 7. Boost converter inductor current in DCM. (From [8])

A higher converter gain is achieved in CCM as shown in Figure 8. Thus, converter operation in CCM is preferred, and the size of the inductor must be chosen accordingly.

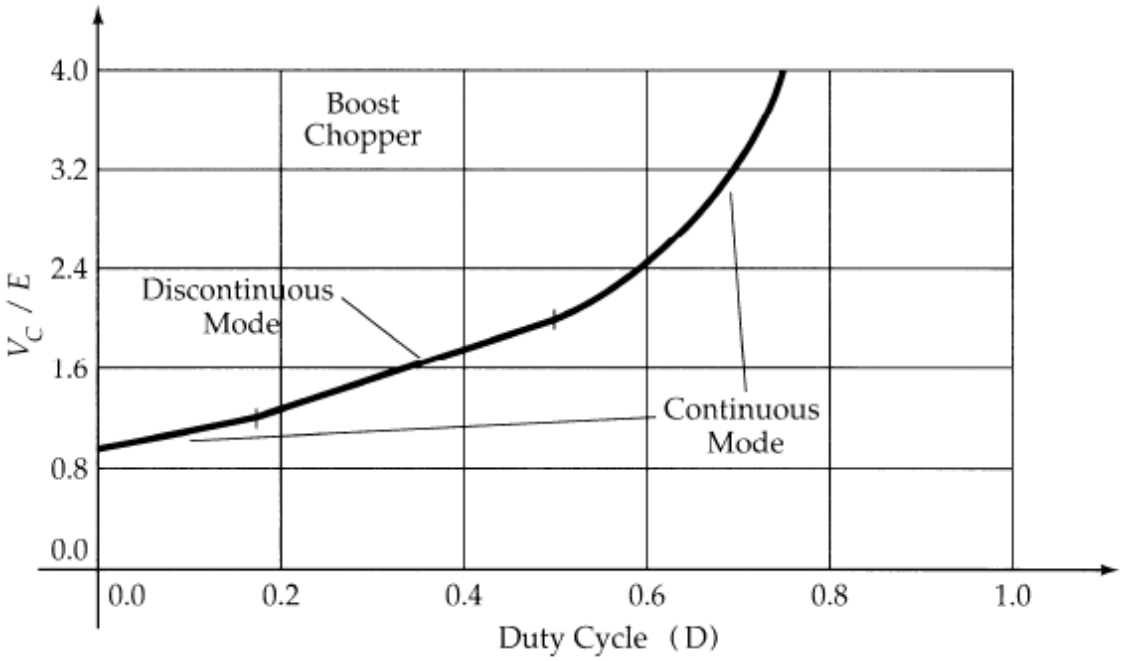

Figure 8. Boost converter gain in DCM and CCM. (From [8])

2. Synchronous Rectification

As can be seen in the boost converter in Figure 1, the circuit uses a diode. Diodes typically have a voltage drop at the semiconductor junction of 0.7 V in a silicon based device. This voltage drop is relatively small in normal power electronics that involve power levels on the order of Watts. The energy harvester on the other hand, having an input in the microwatts, cannot afford such a voltage drop.

Synchronous rectification is also known as active rectification. This is because synchronous rectification replaces the diodes in a normal power conversion circuit with electronic switches that are switched on and off through control circuitry. The diodes that are usually the cause of much of the switching losses in a converter are now replaced by electronically controlled switches. A synchronous boost converter illustrating the replacement of the diode with an actively controlled transistor is shown in Figure 9.

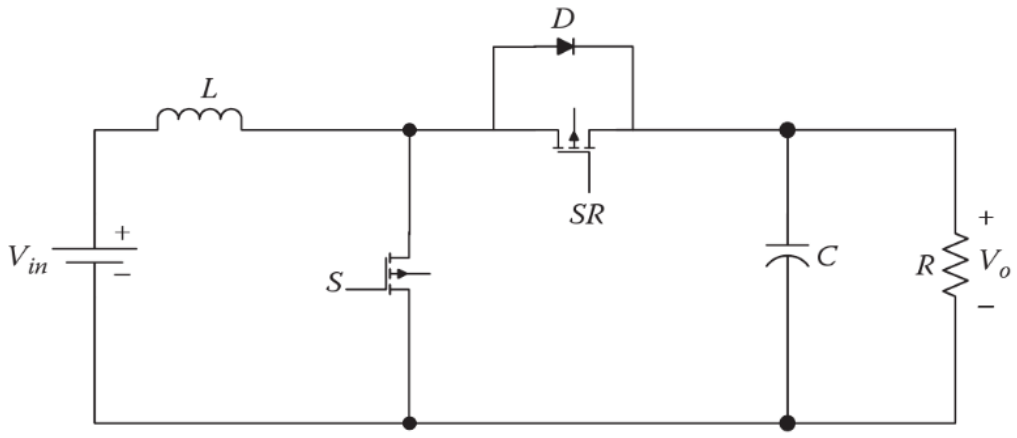

Figure 9. Synchronous boost converter. (From [7])

The relative gains in efficiency when using a synchronous converter over the conventional topology is shown in Figure 10. A synchronous converter is more efficient than a diode based converter throughout the range of output voltages.

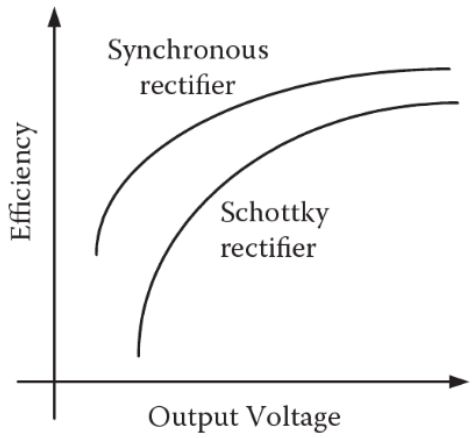

Figure 10. Conventional rectifier versus synchronous rectifier efficiency. (From [7])

3. Maximum Power Point Tracking

Energy harvesting technology often incorporates PV cells as the source of input power. The current-voltage (I-V) curve of a PV cell determines the output power characteristics. A typical PV I-V curve is shown in Figure 11. The open circuit voltage V_{OC} is the voltage produced by the PV cell with no load connected, while the short circuit current I_{SC} is the current produced by the PV cell when shorted. The maximum power P_{MAX} produced by the cell is

$$P_{MAX} = V_{MP} I_{MP} \tag{11}$$

which is the product of the maximum power current I_{MP} and the maximum power voltage V_{MP}. The maximum power P_{MAX} occurs when the area of the dotted rectangle is greatest as shown in Figure 11. When the voltage produced by the PV cell increases or decreases from V_{MP}, the cell does not operate at its maximum efficiency. The graph of output power is shown below the I-V curve, showing how P_{MAX} changes with voltage and current.

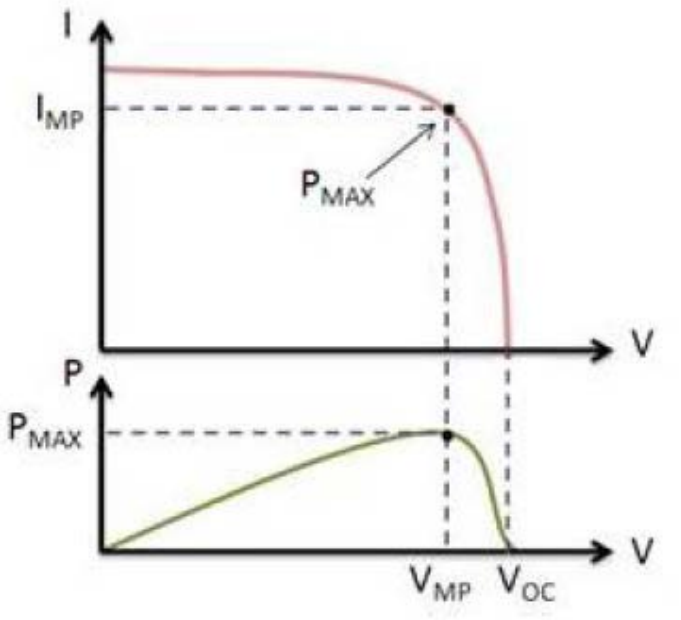

Figure 11. Typical solar cell I-V curve. (From [9])

The MPPT increases the efficiency in harvesting energy from a PV cell by regulating the input voltage to ensure it remains as close as possible to V_{MP}. In a PV cell the MPPT typically regulates voltage to 80 percent of V_{OC}.

Different harvesting sources will have different maximum power points where they operate most efficiently. As an example, in thermoelectric harvester, a 50 percent MPPT is used.

4. Energy Storage

When harvesting energy in the microwatt levels, there are many energy storage options available. Conventional rechargeable batteries, thin-film batteries, conventional capacitor, and supercapacitors can all be used with the energy harvester studied in this thesis. One benefit of using an intelligent boost converter is the ability of the converter to protect the energy storage device. Deep discharge of a battery could lead to irreversible damage. Overcharging a capacitor can also lead to damage of the storage device. Finally, the temperature of the storage device could lead to damage if allowed to reach high enough temperatures.

B. DEVICE SELECTION

The circuit that was analyzed in this thesis is the Texas Instruments BQ25504 Ultra Low Power Boost Converter with battery management for energy harvester applications. Other chips can provide the same boosting function as the BQ25504, but this particular chip was chosen for the intelligence incorporated into the integrated circuit (IC). The chip contains the technologies to improve efficiencies discussed earlier. The basic block diagram and interconnections of the chip are shown in Figure 13. Self-contained within the chip is the boost converter, the boost charge controller used for the synchronous rectification and the MPPT controller. In addition to these efficiency enhancing features, it has a small package size and a low cost. The package itself measures just three square millimeters and is shown in Figure 12. For the types of applications that can benefit from an energy harvesting circuit, size and relatively low cost are determining factors in the future of the particular chip.

Figure 12. BQ25504 chip size reference.

The synchronous converter, which is the heart of the system, is shown in Figure 13. The boost inductor (LBST) is the input of the converter, and the storage voltage (VSTOR) is the output of the converter. The boost charge controller is what controls the switching transistors to make this a synchronous converter. The cold-start unit enables the circuit to run as an unregulated boost converter when VSTOR is less than a certain voltage to quickly send power to the load without powering the main device. The device

MPPT controller samples V_{OC} to determine the MPPT setting, which is also adjustable depending on the applications. The chip also has adjustable settings for battery "overvoltage (OV)" and "undervoltage (UV)" which protect the energy storage device.

The BQ25504 also comes with technology to protect the energy storage device. To prevent deep discharging batteries, which can cause damage, the power load is designed to switch from the battery to the VSTOR pin whenever the battery voltage is below the UV setting. To prevent overcharging of the storage element, the battery is no longer charged when the battery voltage is above the OV setting.

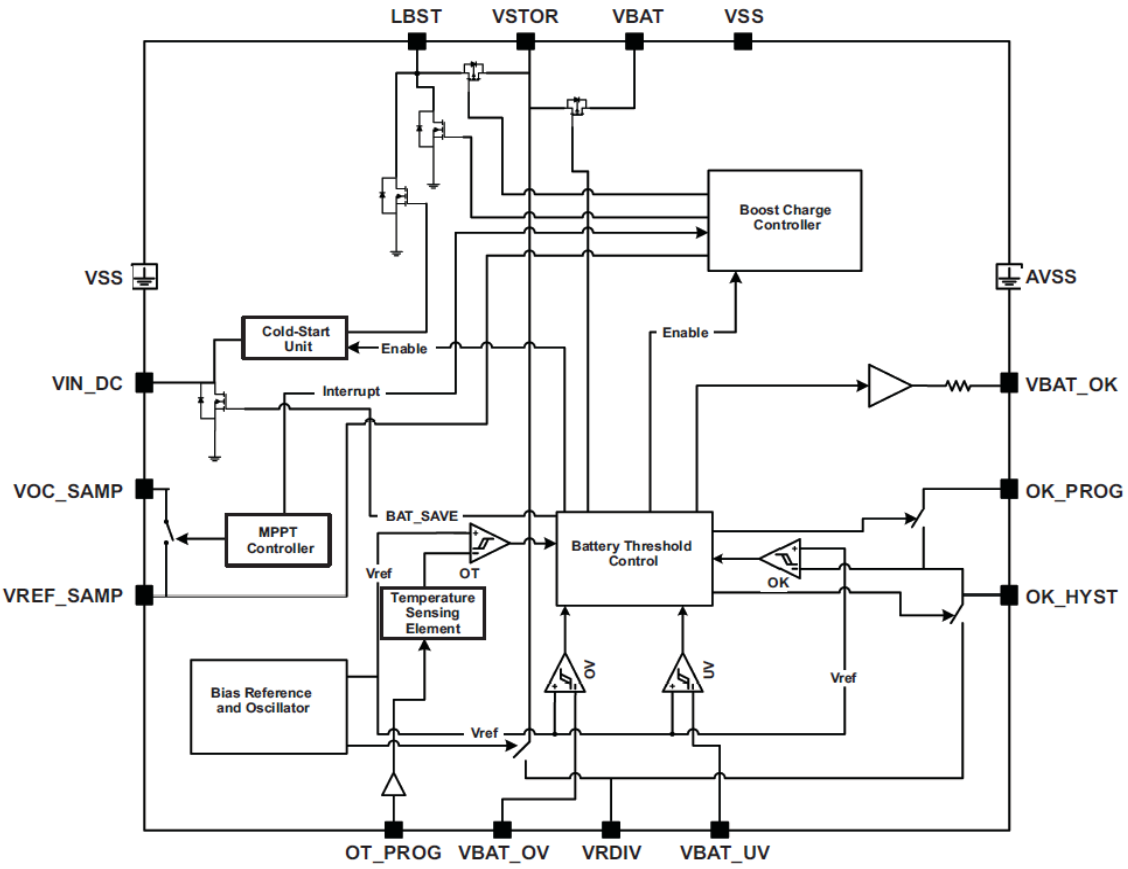

Figure 13. Block diagram of BQ25504 circuit. (From [10])

THIS PAGE INTENTIONALLY LEFT BLANK

III. SIMULATION AND HARDWARE MODEL

A. SPICE SIMULATION

Texas Instruments provides a SPICE program called TINA-TI. This program was used to model the circuit and observe its behavior. The schematics of the actual BQ25504 chip are proprietary, and we were not able study them in detail. The model is shown in Figure 14, and the basic functions of the chip can be seen in Figure 13. The BQ25504 does have other intelligent capabilities but only the functions that were of interest to this thesis were modeled in the simulation. A solar cell model with an output voltage of 500 mV and 400 µA was used with a 470 nF capacitor as the output energy storage device.

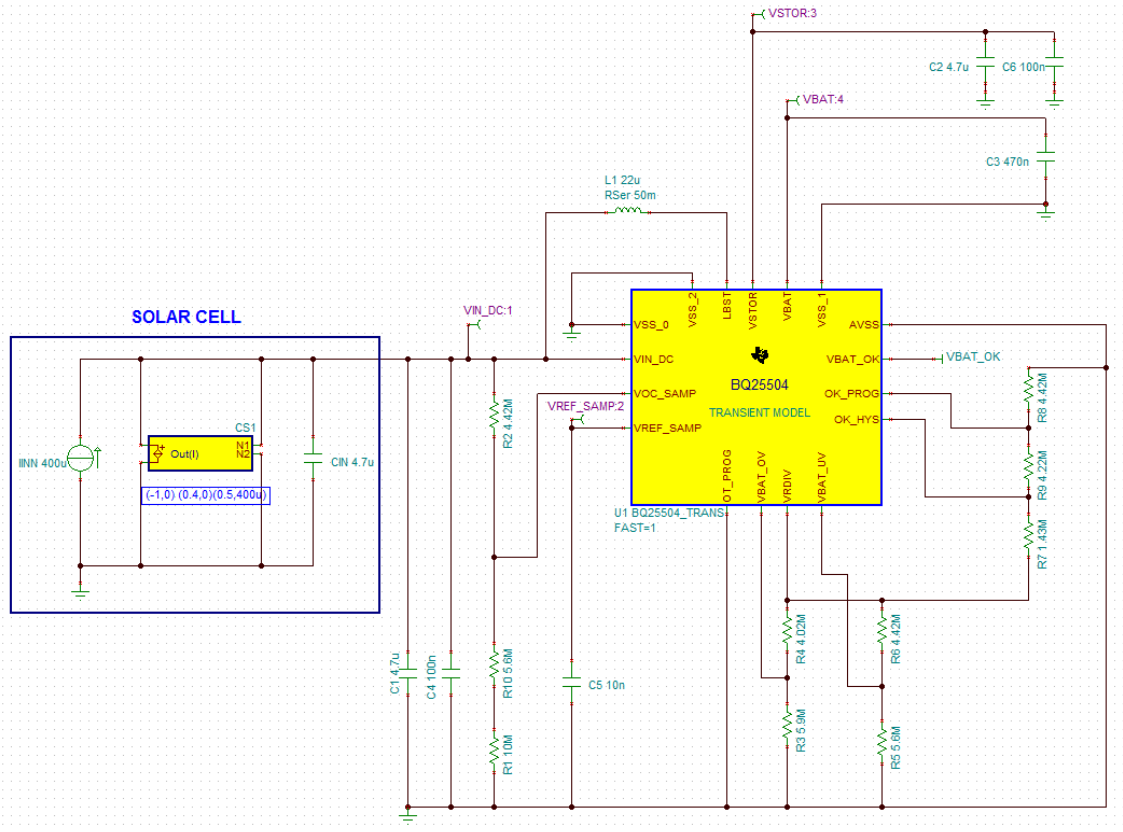

Figure 14. TINA-TI SPICE model of BQ25504 harvesting circuit.

Since a solar cell was being simulated and tested in hardware, a MPPT setting of 80 percent was used. The reference voltage was set as

$$V_{REF} = V_{OC}\left(\frac{R_1 + R_{10}}{R_1 + R_{10} + R_2}\right) \tag{12}$$

where R_1 =10 MΩ, R_{10} = 5.6 MΩ, and R_2 = 4.42 MΩ, making a voltage divider. This voltage divider can be adjusted to alter the MPPT set point. Using these resistance values and setting V_{OC} = 500mV, we get V_{REF} =389.6 mV which gives an MPPT set point of 77.9 percent.

B. HARDWARE MODEL

An evaluation module (EVM) was used to test the BQ25504 Ultra Low Power Boost Converter. The EVM can be seen in Figure 15. The EVM circuit correlated almost exactly to the SPICE model shown in Figure 14 with the exceptions that the capacitor between the battery (BAT) and ground (GND) was reduced from 100 μF to 0.47 nF and the storage device was not included to reduce simulation run times. For the test input, a power supply was used to verify circuit operation. A solar cell was also used to verify real-world applications of the circuit.

The circuit shown in Figure 16 was used instead of a battery. Although a rechargeable battery was used to verify the practicality of this circuit, the simulated battery allows quick changes in battery voltage V_{BAT} instead of waiting for a real battery to discharge. The diode (D_1) was connected between a resistor and a separate power supply. The power supply provided the input for V_{BAT}, while the diode only allowed power to flow in one direction to emulate a battery. The resistor acts as the load. In this way, the battery power supply can be manipulated to simulate a battery charging and discharging.

The list of equipment used for the hardware experiments is shown in Table 2. The power supply was used to supply the input voltage, and a second power supply was used to emulate the battery. The graphs in the results section of the thesis were taken with a four channel oscilloscope. Voltage and current measurements were taken with a multi-meter.

Table 2. Laboratory equipment used.

Power Supply	Agilent E3631A DC Power Supply
Oscilloscope	Tektronix TDS3014B
Multimeter	Fluke 45 Dual Display
Solar Cell	0.5 W Solar Panel/4.5V RS2770045
Battery	2300 mAH Ni-NH Rechargeable

The measured component values that were used are listed in Table 3. The components D_1 and R_1 were used for the simulated battery.

Table 3. Component values used in hardware tests.

D_1	IN4001
R_1	10.0 Ω
R_{IN}	20.8 Ω
R_{LOAD} (startup evaluation)	10.02 kΩ
R_{LOAD} (solar charging evaluation)	108.7 kΩ

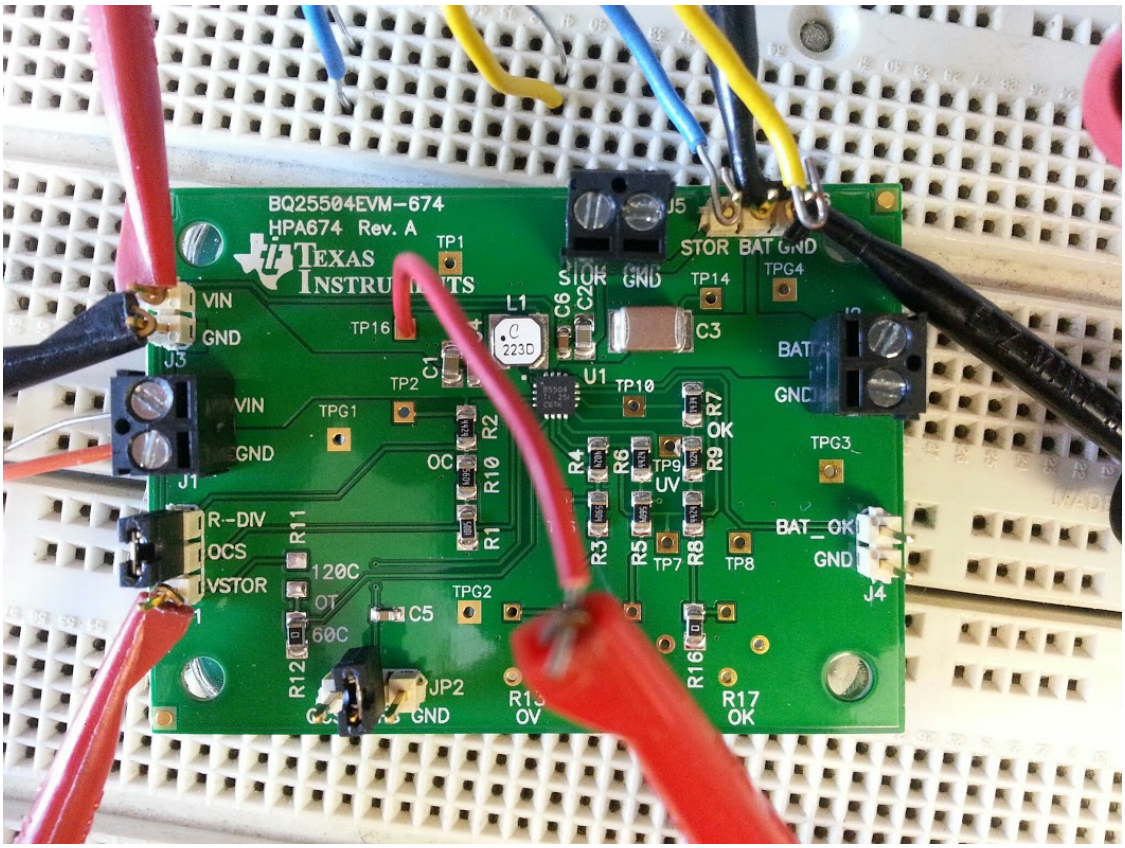

Figure 15. Hardware model test setup using BQ25504 EVM.

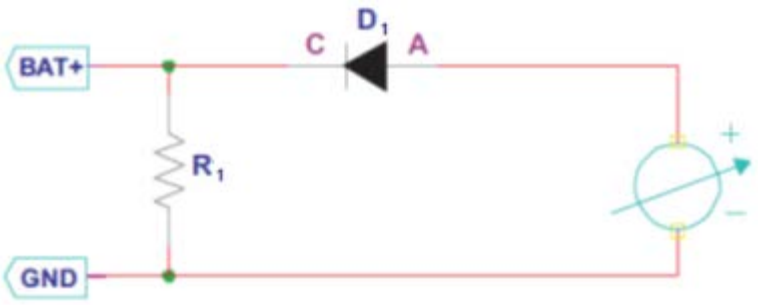

Figure 16. Hardware simulated battery. (From [11])

IV. RESULTS

A. CONVERTER SIMULATION OPERATION

The circuit simulation was conducted in TINA-TI, and the various aspects of the circuits operation were observed. The simulation demonstrated the major technologies that enable this energy harvesting circuit to be more efficient than a directly connected source or a typical boost converter.

The simulation was run for 1.4 s to allow the transients to settle and to allow the device to start up and show a couple of charging cycles. The overall input voltage, which was provided by a PV source, is shown in Figure 17, and the inductor current is shown in Figure 18. At time zero, the simulation is started and the solar cell begins to provide power to the circuit. When the circuit is initially energized, V_{STOR} is less than 1.8 V as shown in Figure 24, and V_{IN} is greater than the minimum cold-start voltage of 330 mV. In this condition, the boost converter is unregulated with no input from the MPPT circuitry. This condition is not as efficient as when the boost regulation circuitry is operating. The cold-start condition exists until the storage capacitor (C_{STOR}) is charged to 1.8 V at which point the main boost regulator starts. This mode occurs from time zero to 252 ms and is the initial thick green band shown in Figure 17.

The next spike in V_{IN} is due to the regulator shutting off for 24 ms. The regulator is shut off before the main boost regulator starts so that the V_{OC} of the input can be measured and a reference voltage (V_{REF}) can be obtained for the MPPT circuitry. The regulator is turned off at 252 ms and turned on at 276 ms. After V_{REF} has been established, the main boost regulator can start.

The main boost regulator is on between 276 ms and 457 ms at which time the V_{BAT} OV is reached, causing the regulator to switch off. The next two downward spikes at 457 ms and 868 ms are due to the regulator switching on briefly to maintain the charge on the capacitor.

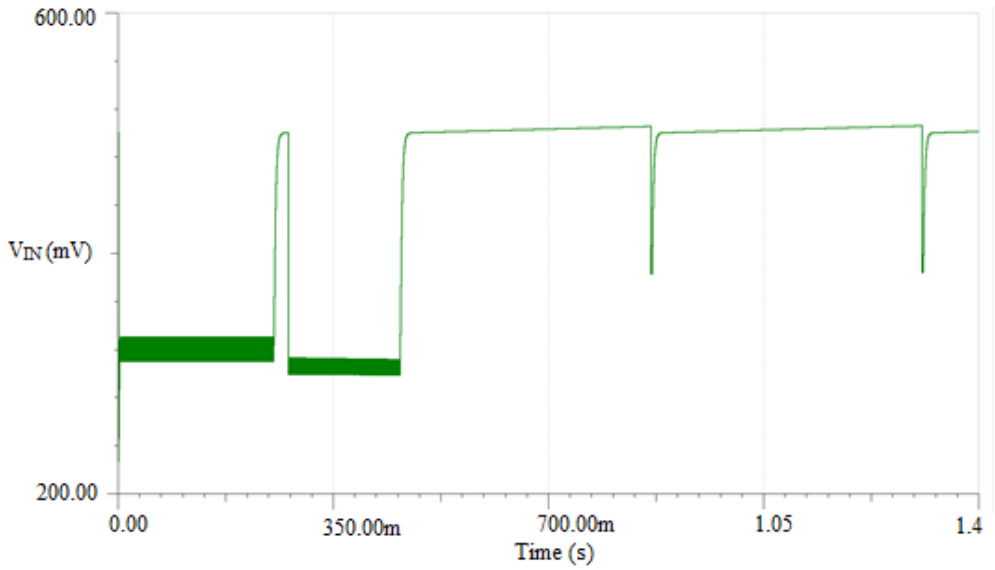

Figure 17. Simulated input voltage during startup.

The current through L_{BST} is shown in Figure 18. The current spike timing matches with the drops in V_{IN}. Also, with the unregulated boost converter at the start of the simulation, it can be seen that the current is much less than the current when the main boost regulator is started. The peak inductor current is 6 mA with the unregulated boost converter and 50 mA with the regulated boost converter.

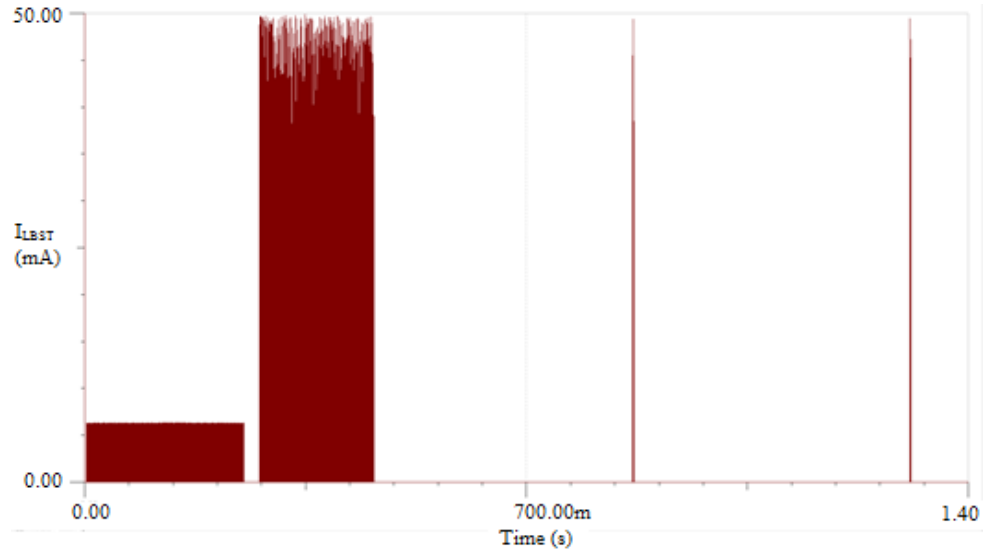

Figure 18. Simulated boost inductor current during startup.

The time that the boost converter is active is shown in Figure 19, which is a more detailed view of V_{IN} during the initial unregulated boost. A more detailed view of the initial current into the inductor only during unregulated boost is shown in Figure 20. The average voltage is calculated as

$$V_{AVE} = \frac{V_{MAX} - V_{MIN}}{2}. \tag{13}$$

While the boost converter is unregulated, V_{AVE} is 320 mV. The time that the boost converter is active t_{active} is shown in Figure 19. The total time of the boost cycle t_{cycle} is shown in Figure 20. The converter is active for 89 µs with a total cycle period of 567 µs. The duty cycle percentage can be calculated as

$$D = \frac{t_{active}}{t_{cycle}} 100\%, \tag{14}$$

yielding an unregulated duty cycle of 15.7 percent.

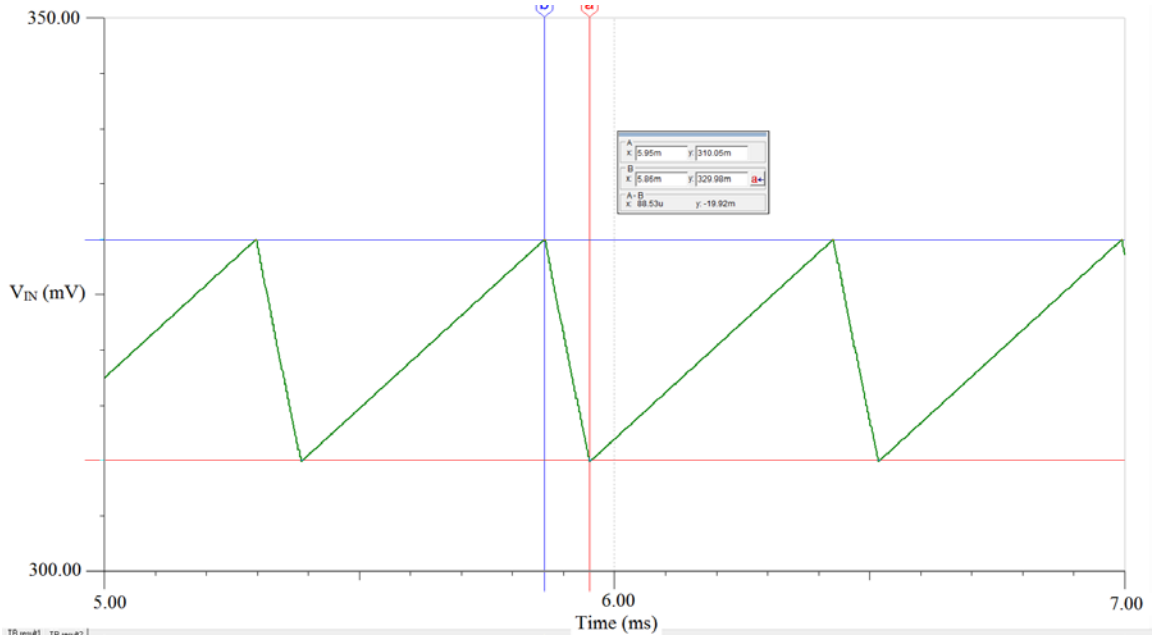

Figure 19. Input voltage during unregulated boost showing t_{active}.

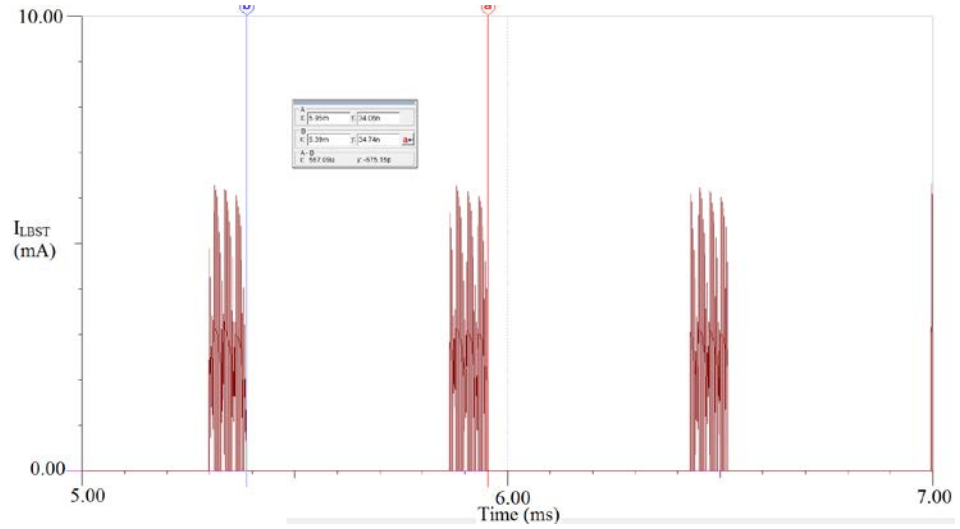

Figure 20. Inductor current during unregulated boost showing t_{cycle}.

The time that the boost converter is active is shown in Figure 21, which is a more detailed view of V_{IN} during the regulated boost operating area. A more detailed view of the initial current into the inductor during regulated boost operation is shown in Figure 22. The average voltage is calculated using equation (13) as 305.9 mV. The converter t_{active} is measured in Figure 21, and t_{cycle} is measured in Figure 22. The converter is active for 6.8 µs with a total cycle period of 325 µs. Duty cycle percentage can be calculated using equation (14) and is 2.1 percent.

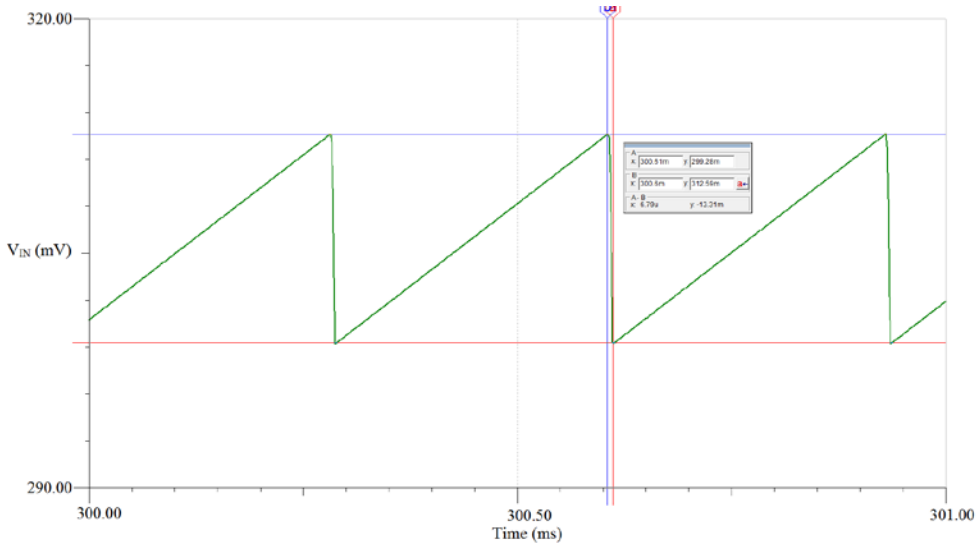

Figure 21. Input voltage during regulated boost.

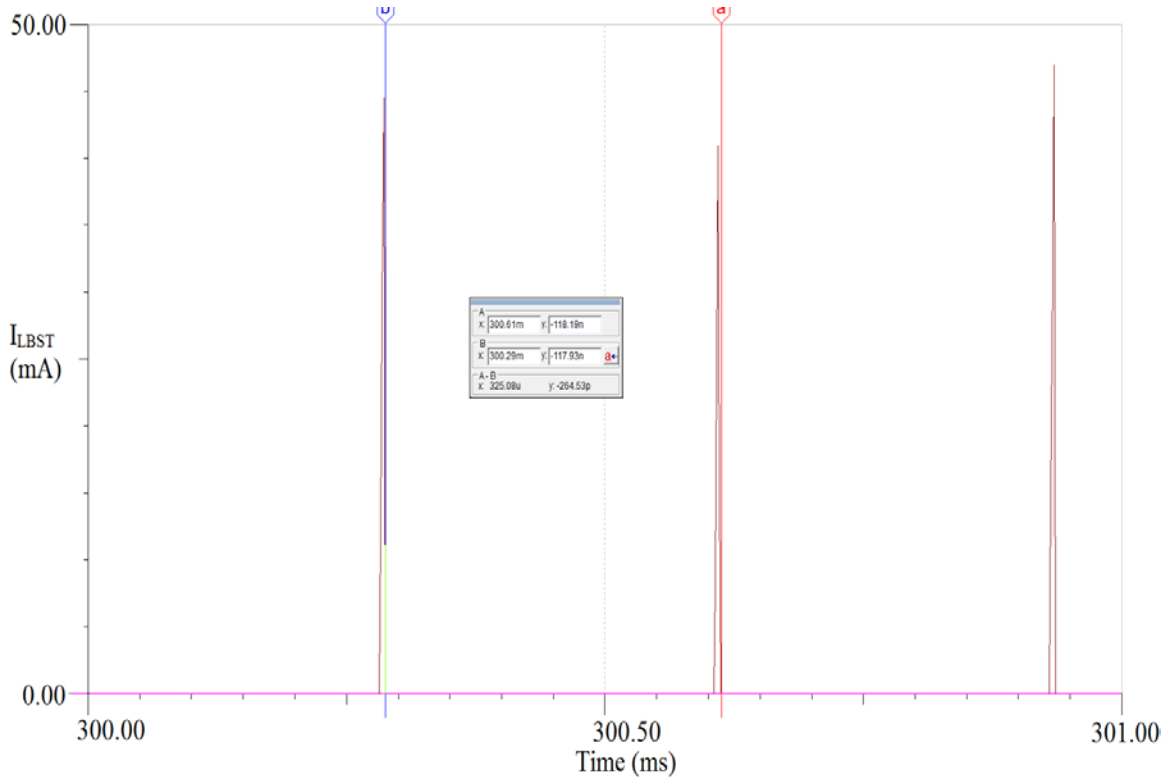

Figure 22. Inductor current during regulated boost.

The circuit reference voltage V_{REF} is shown in Figure 23. The circuit reference voltage V_{REF} is used by the circuit to calculate the MPPT set point from equation (12). The first sampling of V_{REF} occurs after the cold-start operation terminates to give the MPPT circuitry an initial reference point. The initial sample can be seen at 252 ms. Since the initial sample only lasts for 24 ms, V_{REF} was not able to charge up to the full V_{OC}. The next V_{REF} sample occurs at 534 ms, at which point V_{REF} has sufficient time to charge to V_{OC}. The voltage V_{REF} only charges up to about 393 mV due to the MPPT setting. The expected voltage was about 390 mV from the calculations showing that the simulated V_{REF} is accurate.

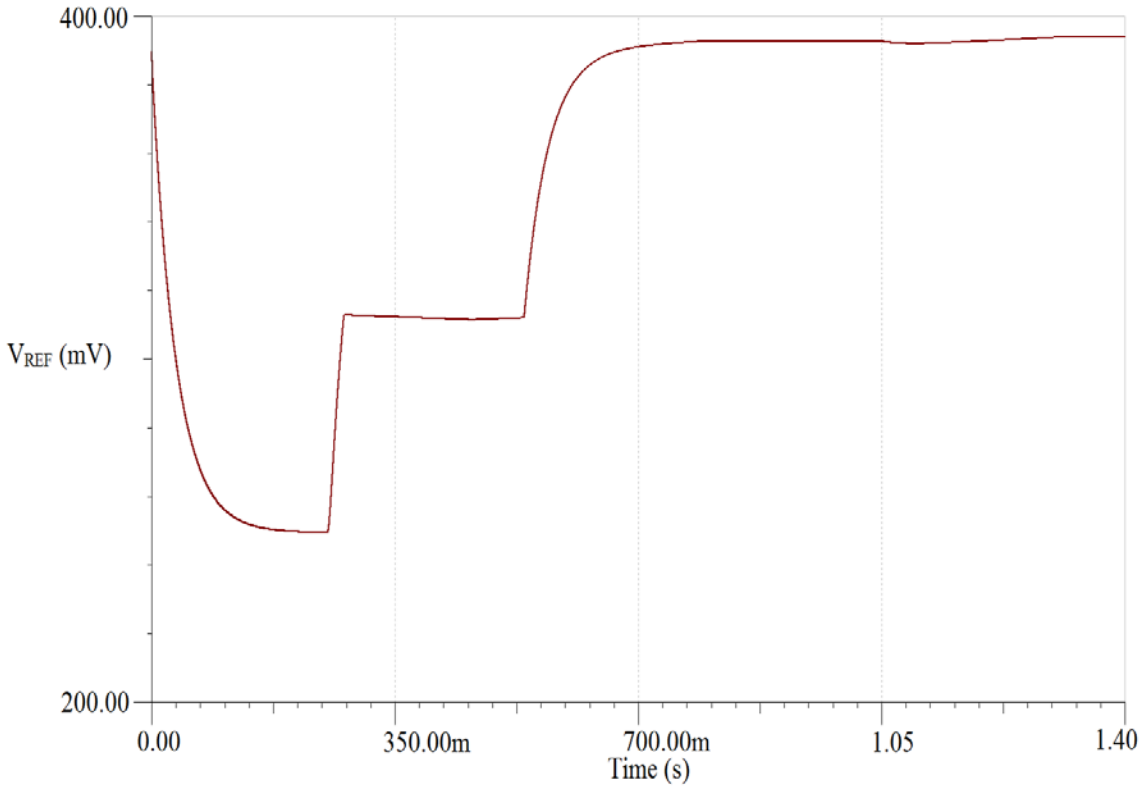

Figure 23. Simulated reference voltage during startup.

The voltage V_{STOR} is shown in Figure 24, where V_{STOR} charges initially due to the converter providing power via the unregulated boost converter until 252 ms, where V_{STOR}=1.8 V, which is the set point that switches the converter from unregulated to regulated boost modes. The boost converter turning off can be seen by the voltage no longer increasing on V_{STOR} for the 24 ms that V_{REF} is being sampled. Once V_{REF} has been sampled and the regulated boost mode resumes, it can be seen that the rate of V_{STOR} rising has increased in the time period 276 ms to 457 ms. When V_{STOR} charges to 3.1 V the V_{SOTR} OV setting is reached and the converter turns off. As V_{STOR} drops below the 3.1 V set point, it can be seen that the converter periodically turns on to keep V_{STOR} charged to the set point.

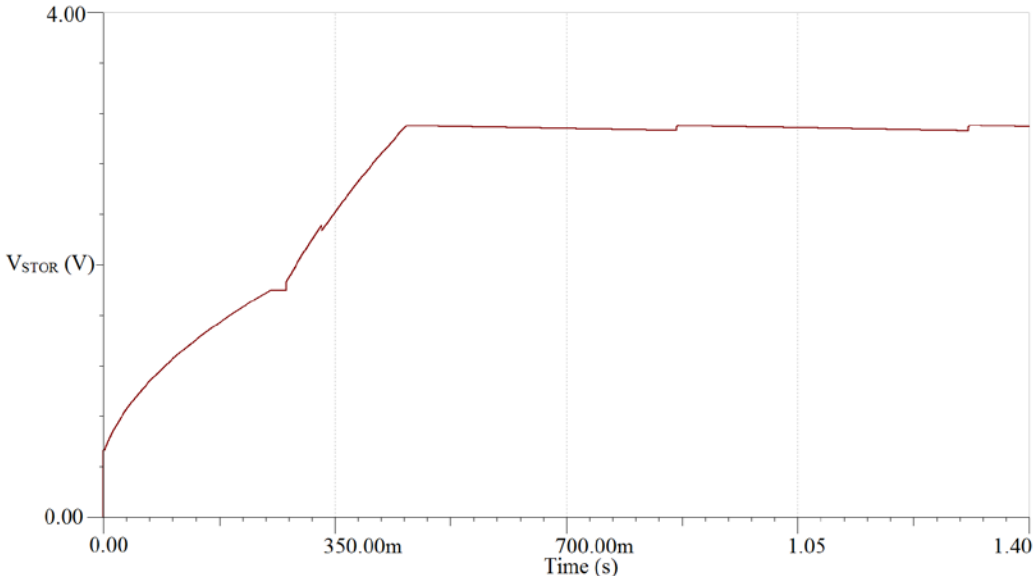

Figure 24. Simulated storage voltage during startup.

The battery voltage V_{BAT} is shown in Figure 25 and is almost identical to the behavior of V_{STOR} with the exception that at 331 ms, V_{STOR}=2.2 V, which is the V_{BAT} UV setting at which V_{BAT} begins charging. This explains the large spike in V_{BAT} at 331 ms.

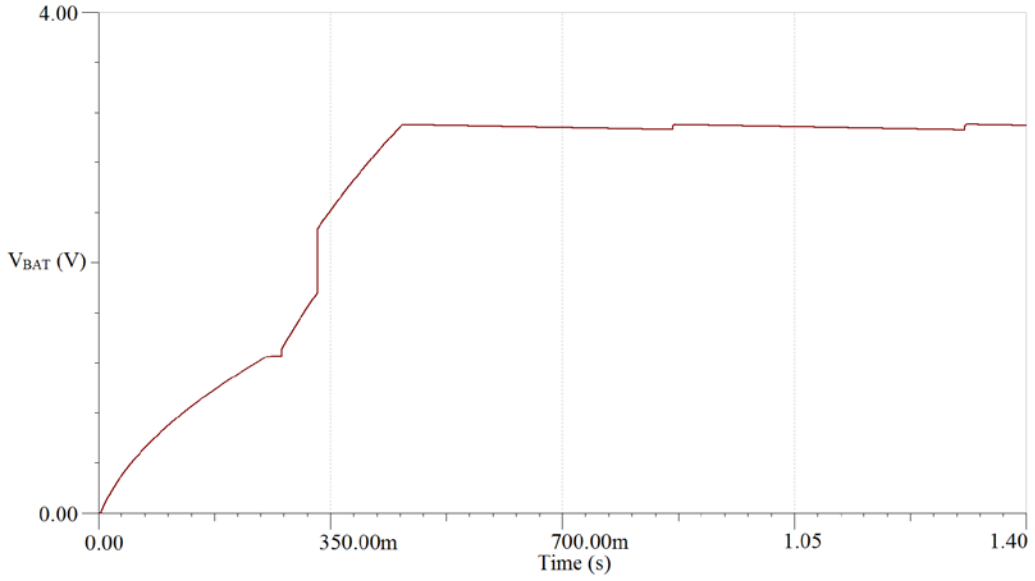

Figure 25. Simulated battery voltage during startup.

B. CONVERTER HARDWARE OPERATION

The hardware experiments were conducted to verify the different technologies at the basis of the energy harvesting converter.

1. Startup with no Battery and 10 kΩ Load

The initial hardware experiment demonstrates the cold-start ability of the circuit. The expected hardware results from the manufacturer are shown in Figure 26. The boost converter switching cycle can be seen on channel one (V_{phase}), measured on the output of L_{BST}. The storage voltage V_{STOR} is shown on channel two, and the input source voltage ($V_{p/s\#1}$) is shown on channel three. When initially energized, the boost converter is immediately turned on as shown by the converter switching pattern and the rise in V_{STOR}. Since V_{STOR} was initially less than 1.8 V the converter begins in cold-start mode. Due to this being an initial startup, V_{STOR} only charges to about 2.4 V due to the soft-start characteristic. While the converter is off, the 10 kΩ resistor connected to the load causes V_{STOR} to discharge. When the converter turns on again, V_{STOR} charges to the full OV setting. The voltage V_{STOR} continues to be charged until it reaches the OV setting and then discharges to the hysteresis point. The boost converter periodically energizes to maintain V_{STOR}.

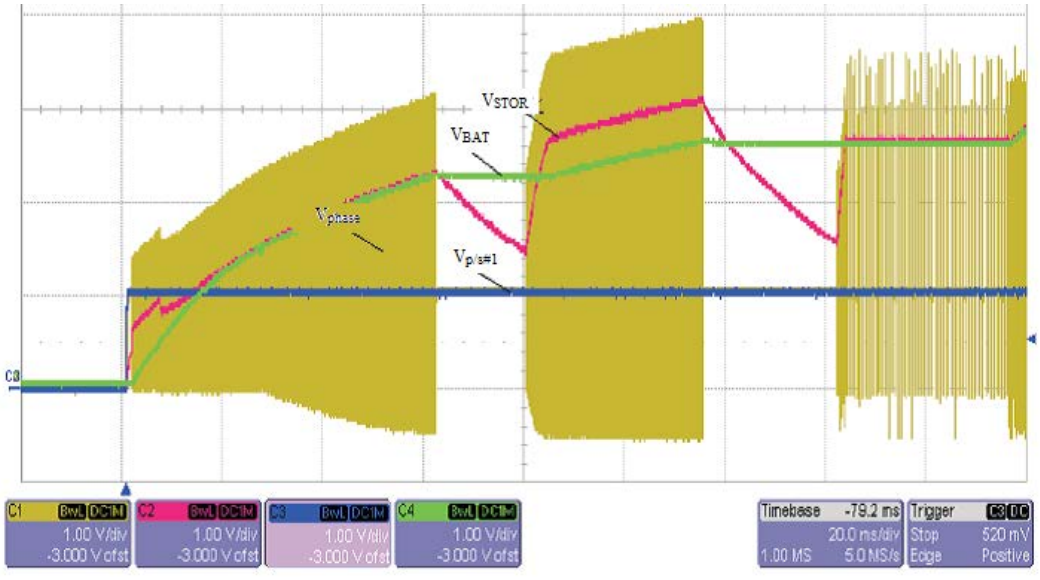

Figure 26. Expected startup with no battery and 10 kΩ load. (From [8])

The measured hardware results showing the cold-start features are shown in Figure 27. A power supply was used to provide the input voltage of one V. The converter switching pattern can be seen on channel one, V_{STOR} is shown on channel two, and V_{IN} is shown on channel three. The lab results are almost identical to the expected waveforms. The operation of the startup of the circuit is actually easier to see from the lab results. The initial converter startup can be seen, and V_{STOR} initially charges to the lower OV setting of 2.8 V. The voltage V_{STOR} then discharges after reaching the OV setting due to the load resistance. After the converter starts again, the full OV setting of 3.1 V is reached by V_{STOR}. Once the OV setting is reached the periodic converter pulses show that the converter maintains the V_{STOR} value of 3.1 V.

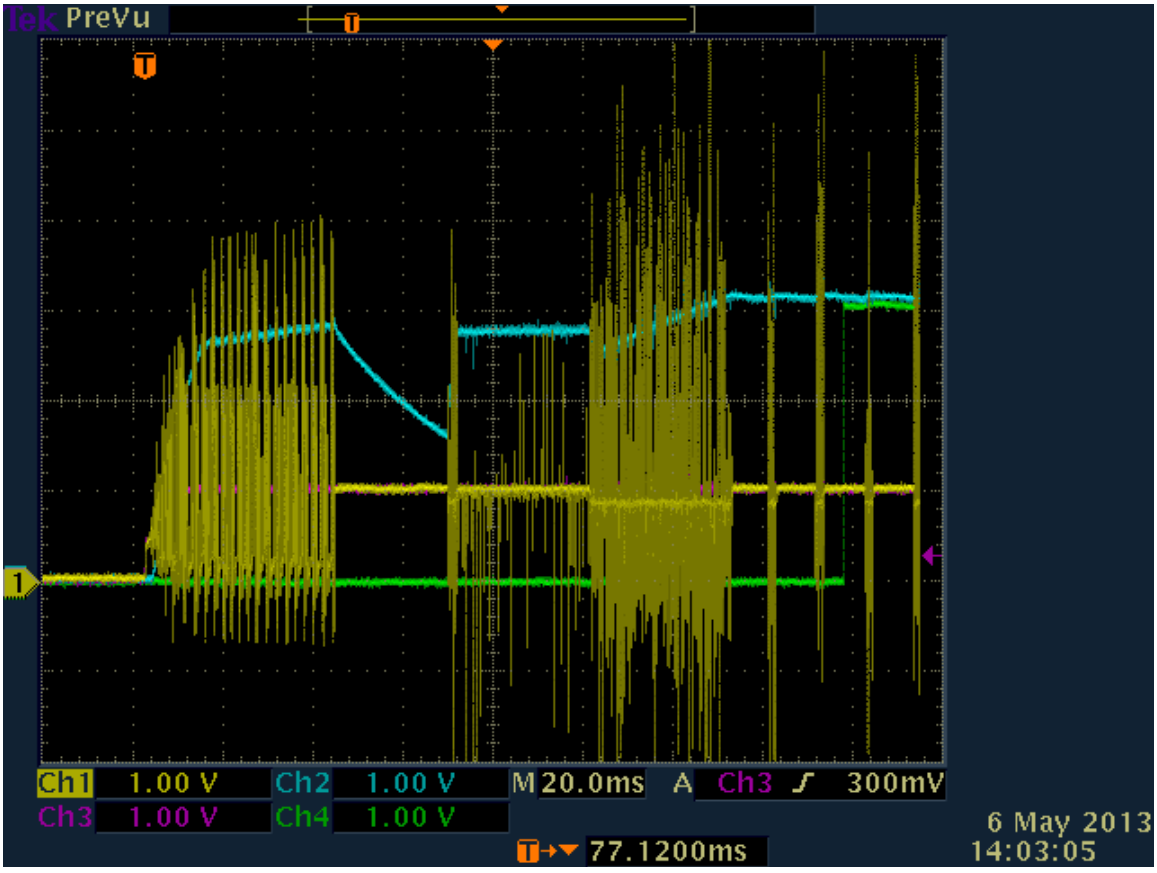

Figure 27. Measured startup with no battery and 10 kΩ load.

2. Startup with Battery Less Than UV

The next hardware experiment used the same setup as the first experiment except that a simulated battery is connected with a V_{BAT} = 1.9 V, which is below the UV setting of 2.2 V. With V_{BAT} < UV, V_{STOR}, which is connected to the load, is disconnected from V_{BAT} to prevent a deep discharge of the storage device. The expected waveforms of the UV experiment are shown in Figure 28. The converter switching pattern can be seen on channel one (V_{phase}), V_{STOR} is shown on channel two, $V_{p/s\#1}$ is shown on channel three and V_{IN} is shown on channel four. In the manufacturer example, V_{STOR} charges to 2.9 V initially and, since it is above the UV set point, V_{STOR} and V_{BAT} are shorted together, causing V_{STOR} to drop to V_{BAT}. The UV set point is sampled again, and now that V_{STOR} is less than the UV set point, V_{STOR} and V_{BAT} are disconnected, causing V_{STOR} to rise.

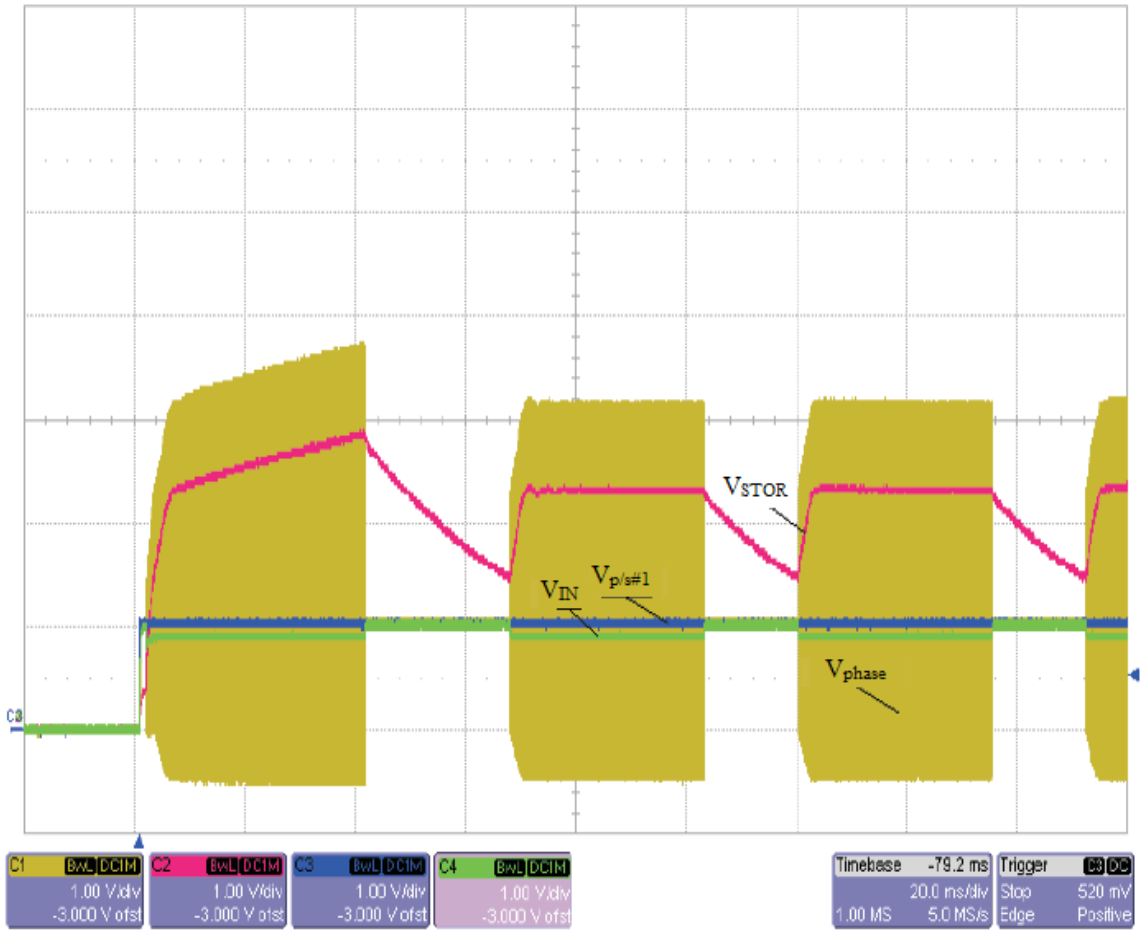

Figure 28. Expected startup with battery less than UV. (From [8])

The measured lab results were very similar to the expected waveforms and can be seen in Figure 29. The converter switching pattern can be seen on channel one, V_{STOR} is shown on channel two, $V_{p/s\#1}$ is shown on channel three, and V_{IN} is shown on channel four. The voltage V_{STOR} can be seen charging to 2.4 V, which is above the 2.2 V UV setting, allowing V_{STOR} to be connected to V_{BAT} to charge the storage element. The storage voltage V_{STOR} gets pulled down to about V_{BAT}, which is set to 1.9 V. The cycle continues in this way since the simulated battery never charges above the UV setting.

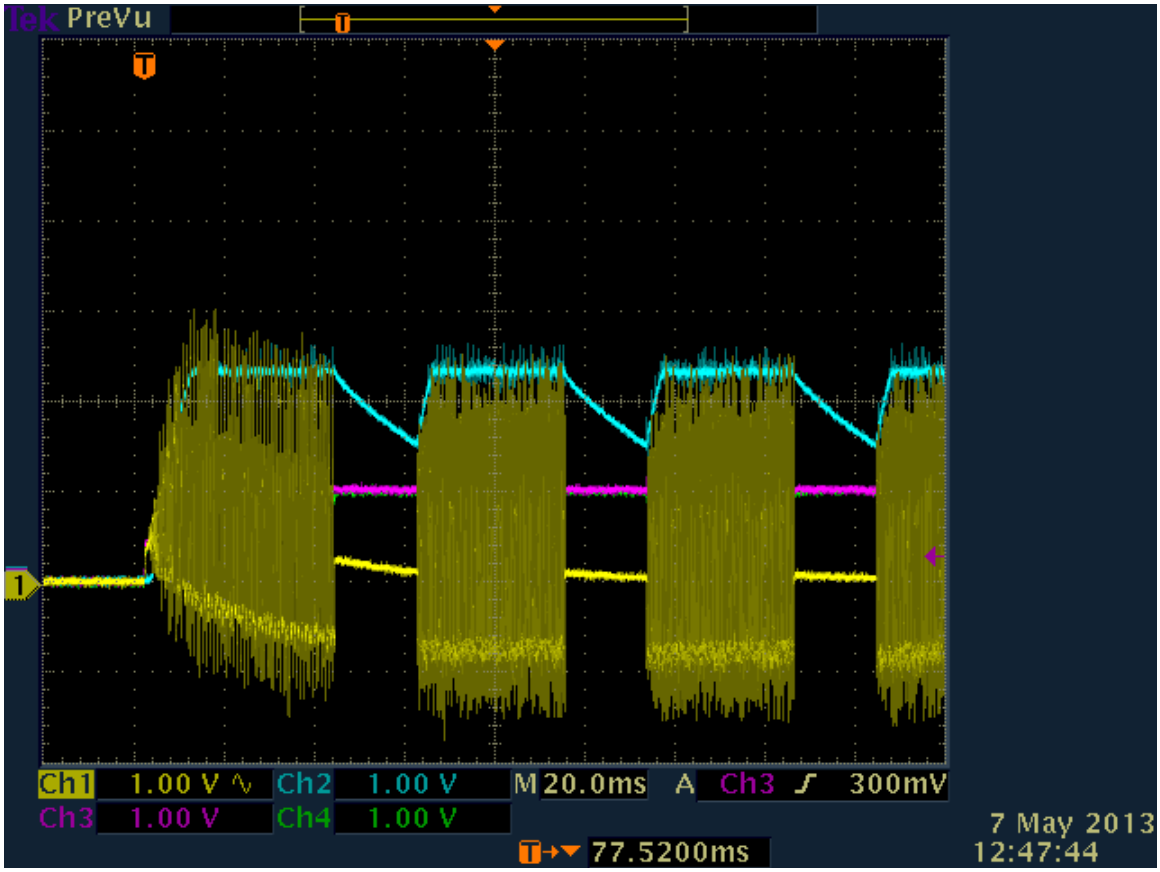

Figure 29. Measured startup with battery less than UV.

The MPPT setting was also demonstrated with the same setup as the UV experiment. For the initial MPPT verification, $V_{p/s\#1}$ was set to one V, and a MPPT setting was calculated from

$$MPPT = \frac{V_{IN}}{V_{p/s\#1}} \tag{15}$$

where a MPPT setting of 91.6 was observed. The MPPT regulation can be seen in Figure 30 where channel three is $V_{p/s\#1}$ and channel four is V_{IN}.

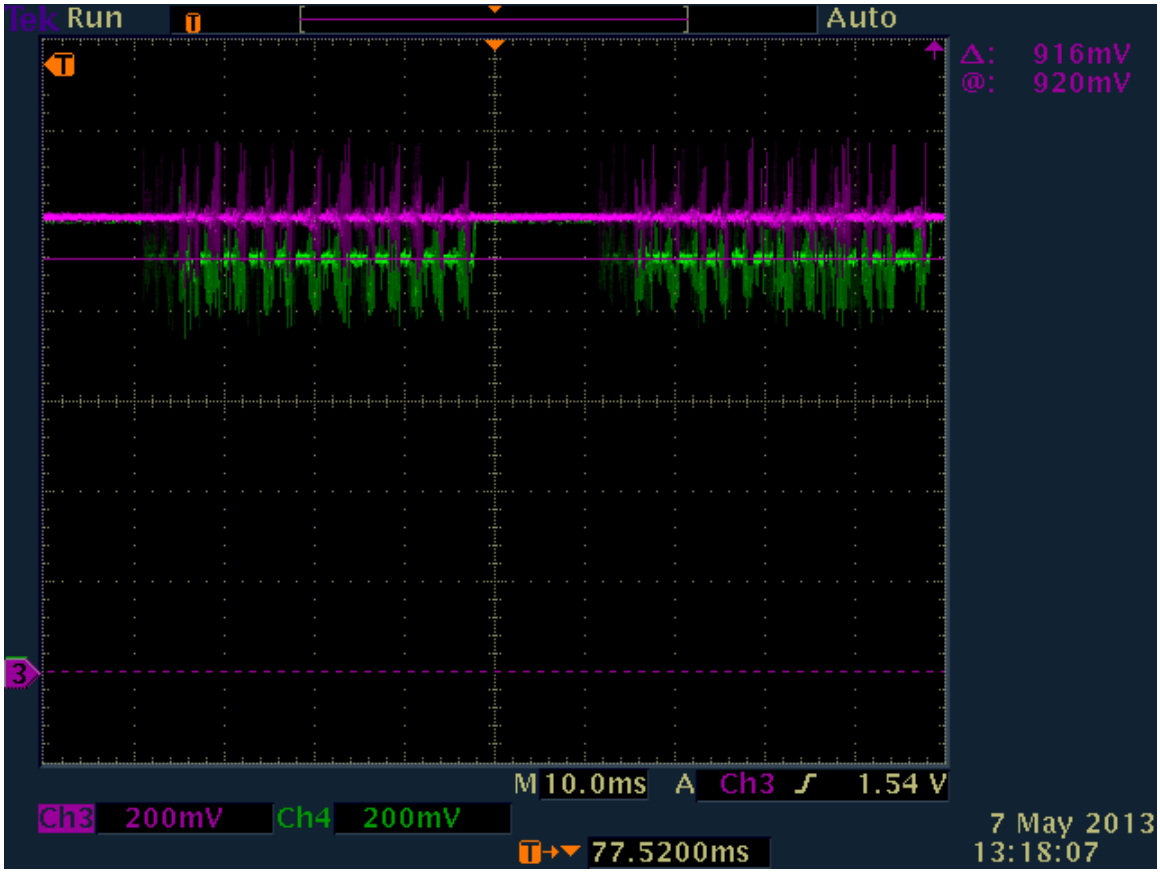

Figure 30. MPPT setting 90 percent with V_{IN} = 1.0 V.

The voltage $V_{p/s\#1}$ was then set to 1.5 V and, after the 16 s sampling of V_{REF} was accounted for, the MPPT setting was verified again. Using equation (15), we observed a MPPT setting of 90.6 percent. This demonstrates the ability of the boost converter to dynamically change the MPPT setting with changes in input voltage.

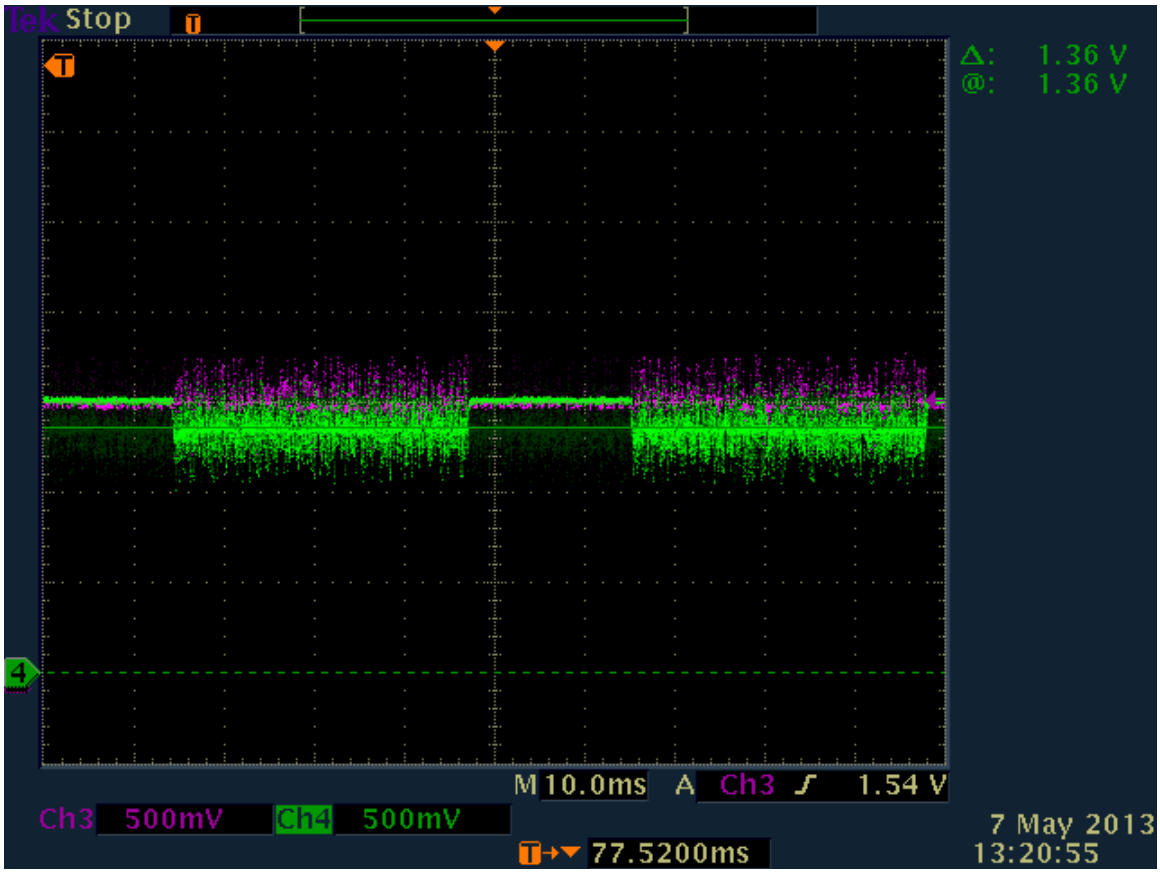

Figure 31. MPPT setting 90 percent with V_{IN} = 1.5 V.

3. Powering up with a Battery Above UV

For the next hardware experiment, the circuit was setup as in the UV experiment except that the simulated battery was adjusted to 2.4 V so that V_{BAT} would be above the UV setting of 2.2 V. The expected waveforms are shown in Figure 32, where the converter switching pattern can be seen on channel one (V_{phase}), V_{STOR} is shown on channel two, $V_{p/s\#1}$ is shown on channel three, and V_{IN} is shown on channel four. After the initial cycling of the converter, it starts up in normal mode since V_{STOR} is above the 1.8 V set point and the cold-start function does not occur. Since V_{BAT} is above the UV set point, V_{STOR} remains shorted to V_{BAT} and the converter operates normally.

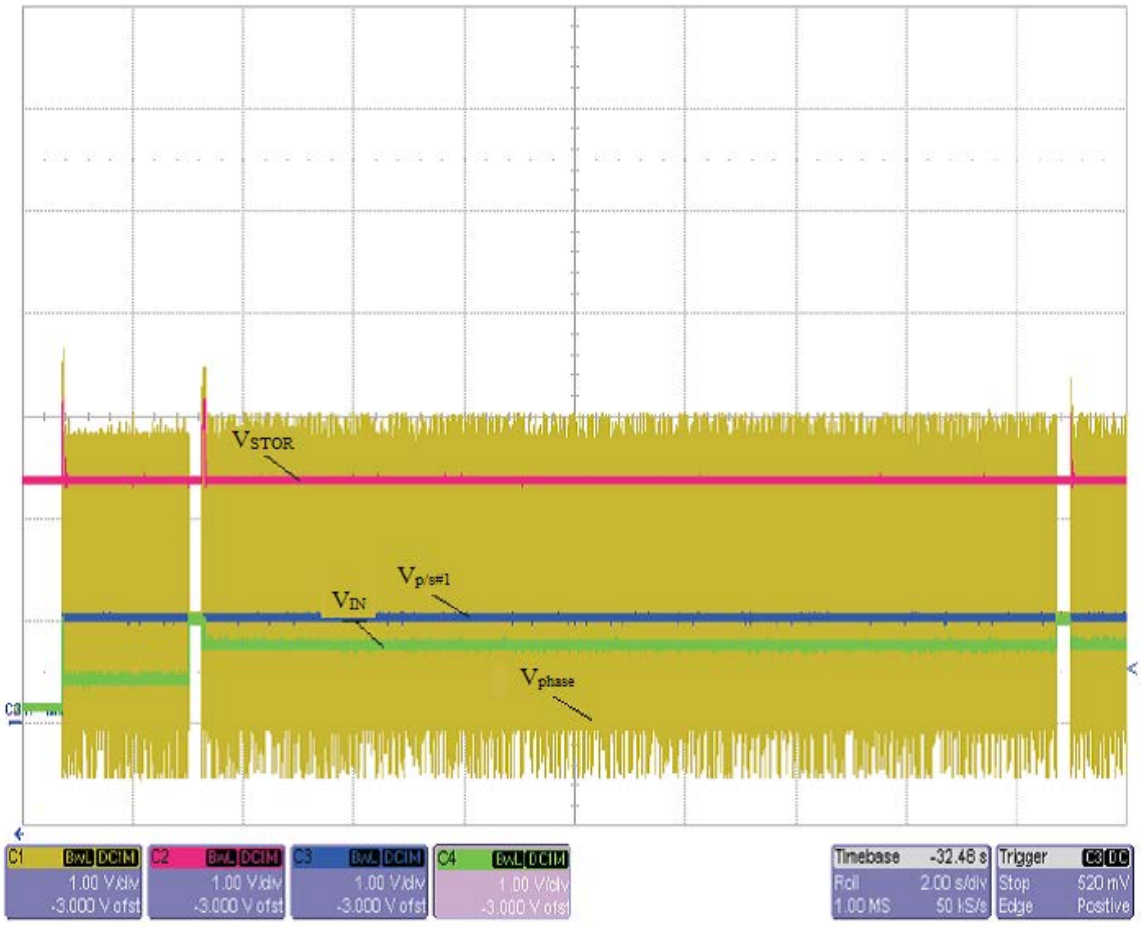

Figure 32. Expected power up with a battery above UV. (From [8])

The actual results from the hardware experiment are shown in Figure 33 where the converter switching pattern can be seen on channel one, V_{STOR} is shown on channel two, $V_{p/s\#1}$ is shown on channel three, and V_{IN} is shown on channel four. This verifies the expected waveforms, showing that V_{STOR} maintains a constant level and V_{IN} is constantly below $V_{p/s\#1}$ by the MPPT setting. This demonstrates the converter operating normally when V_{STOR} is above the UV setting.

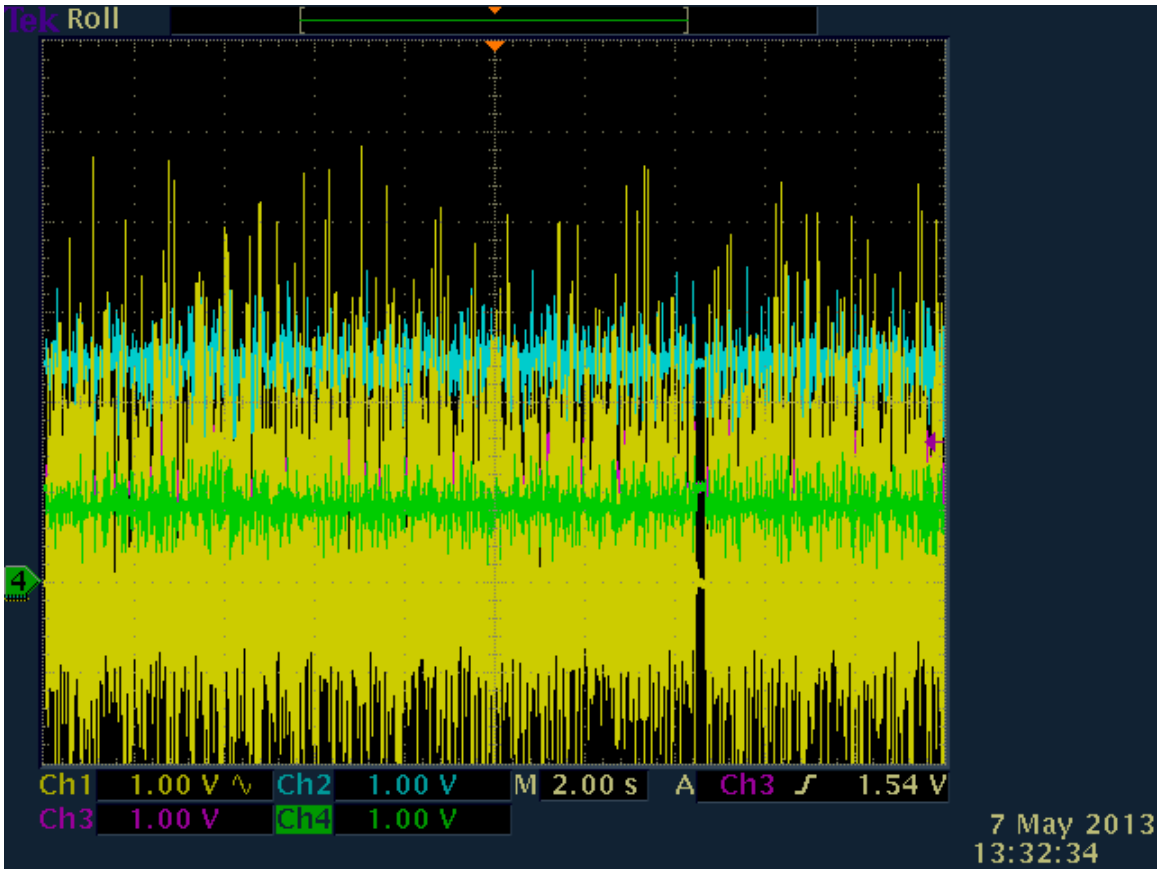

Figure 33. Measured power up with a battery above UV.

4. Basic Switching Converter

The following hardware experiment used the same setup as the UV experiment with the exception that the simulated battery was set to 2.5 V to ensure that V_{BAT} was above the UV setting. This experiment demonstrated the pulse frequency modulation (PFM) switching converter waveforms in detail. The expected switching converter waveform can be seen in Figure 34 where the converter switching pattern can be seen on channel one (V_{phase}), V_{STOR} is shown on channel two, V_{SOURCE} is shown on channel three, and V_{IN} is shown on channel four. As in the previous experiment, V_{STOR} is maintained constant due to being above the UV set point. Four pulses per cycle can be seen with the fourth cycle demonstrating an oscillating ring due to the inductor going into DCM.

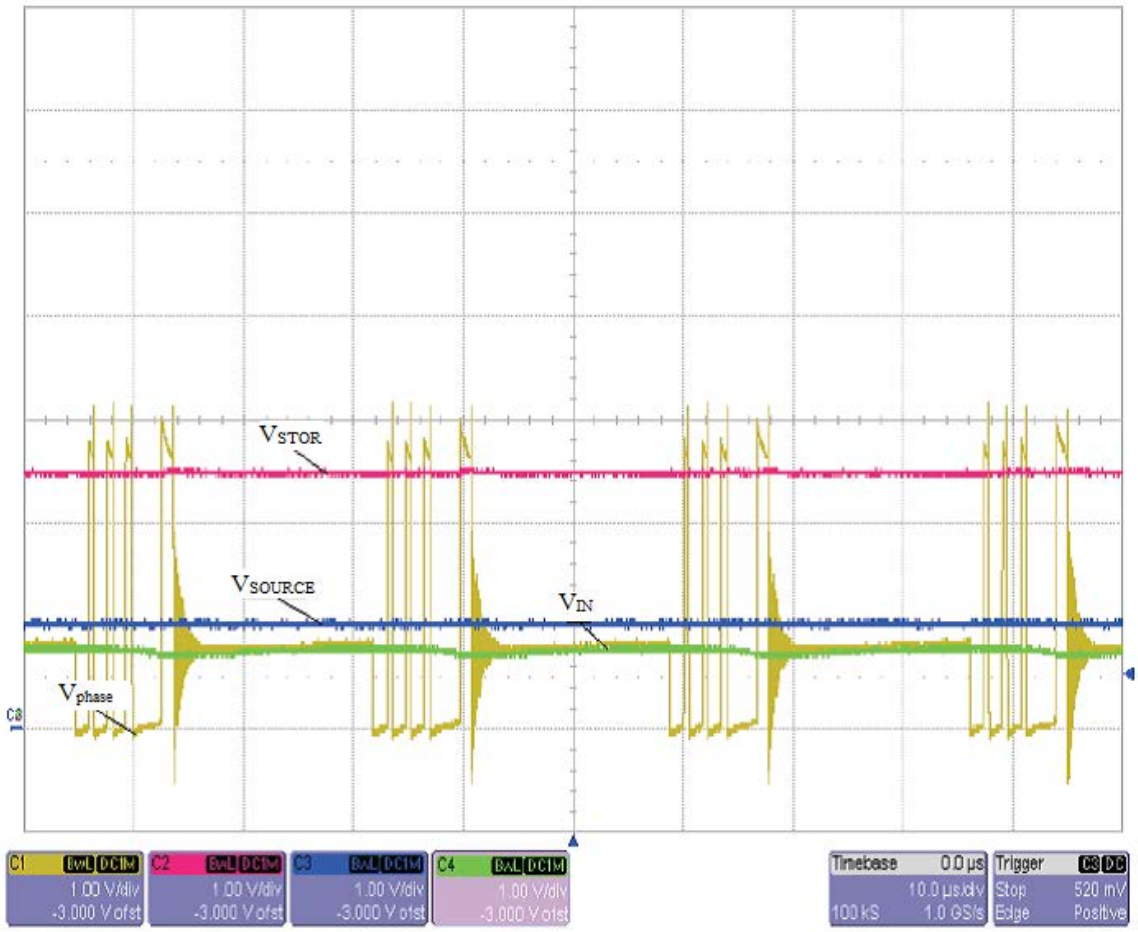

Figure 34. Expected basic PFM switching waveform. (From [8])

The actual hardware results are shown in Figure 35 and match very closely to the expected waveform. The converter switching pattern (V_{phase}) can be seen on channel one, V_{STOR} is shown on channel two, V_{SOURCE} is shown on channel three, and V_{IN} is shown on channel four. Four pulses are also seen, but the inductor DCM ringing is more pronounced. The excessive ringing could be due to equipment connections and component tolerances.

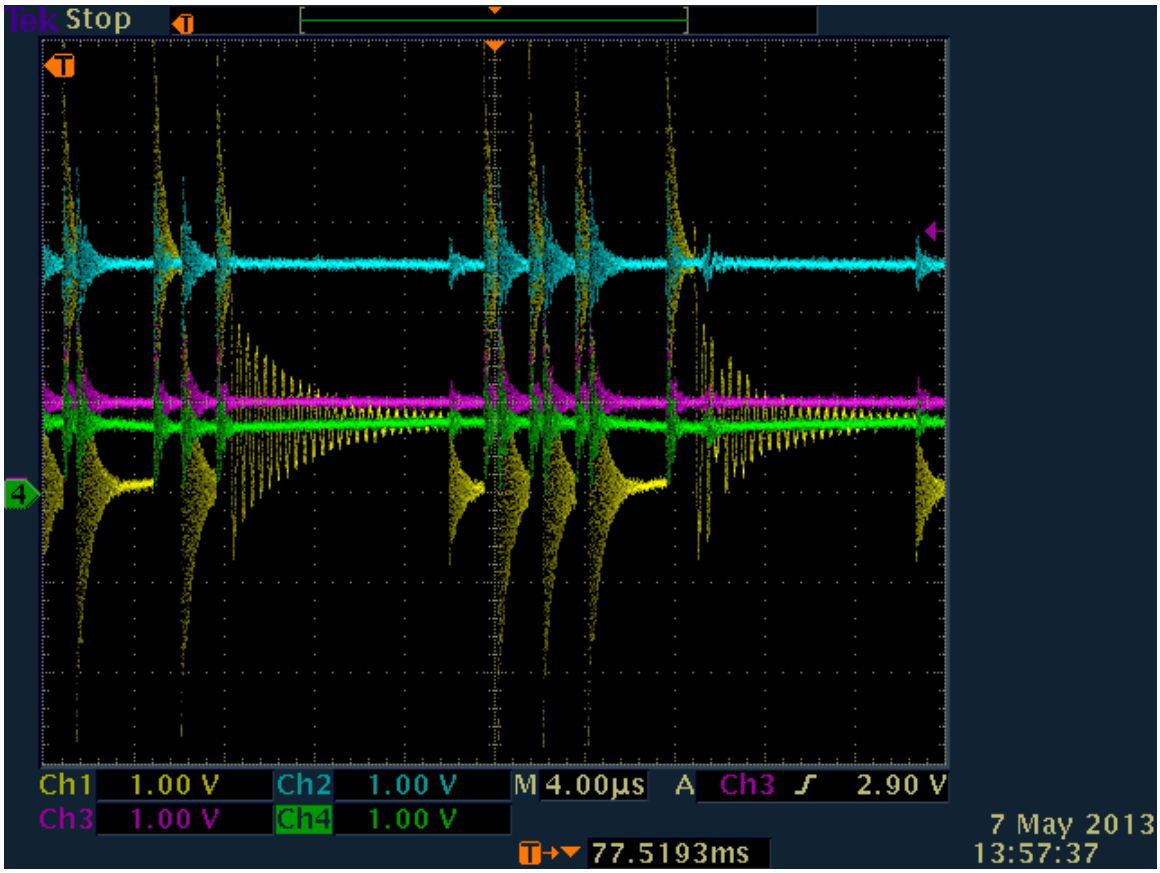

Figure 35. Measured PFM switching waveform.

C. EFFICIENCY

The efficiency of the circuit was measured in the hardware, and the results are shown in detail in Table 4. The input power P_{IN} was calculated as

$$P_{IN} = V_{IN} I_{IN} \tag{16}$$

where V_{IN} is the DC supply voltage and I_{IN} is the DC input current before the decoupling capacitors that service the converter. These quantities were measured using a multimeter. The output power was measured from

$$P_{OUT} = \frac{V^2}{R_{LOAD}}. \tag{17}$$

Efficiency was calculated from

$$\eta = \frac{P_{OUT}}{P_{IN}}. \tag{18}$$

Table 4. Hardware efficiency results.

Input Voltage (V)	Input Current (mA)	Output Voltage (V)	Input Power (mW)	Output Power (mW)	Efficiency (%)
3.00	0.365	3.07	1.095	0.943	86.1
2.80	0.384	3.07	1.075	0.943	87.7
2.60	0.410	3.07	1.066	0.943	88.4
2.40	0.456	3.07	1.094	0.943	86.1
2.20	0.504	3.07	1.109	0.943	85.0
2.00	0.608	3.07	1.216	0.943	77.5
1.80	0.684	3.07	1.231	0.943	76.6
1.60	0.782	3.07	1.251	0.943	75.3
1.40	0.965	3.07	1.351	0.943	69.8
1.20	1.130	3.07	1.356	0.943	69.5
1.00	1.300	3.07	1.300	0.943	72.5
0.80	1.675	3.07	1.340	0.943	70.3
0.60	2.330	3.07	1.398	0.943	67.4
0.50	2.920	3.07	1.460	0.943	64.6
0.40	3.510	3.02	1.404	0.912	65.0
0.39	1.833	0.76	0.715	0.058	8.1

The efficiency results in Table 4 are plotted in Figure 36 and match with the expected results that are shown in Figure 37. Unlike what is shown in the data sheet, the results from the experiments are not measured at a constant 10 mA. Although the input current was not constant, the general trend in efficiency is very similar. In the measured results, efficiency was above 60 percent and higher as long as V_{IN} was greater than 0.4 V. Once V_{IN} dropped below 0.4 V, the converter could not maintain the programmed output voltage of 3.07 V. As long as the converter was able to maintain the programmed output voltage, efficiency was relatively linear.

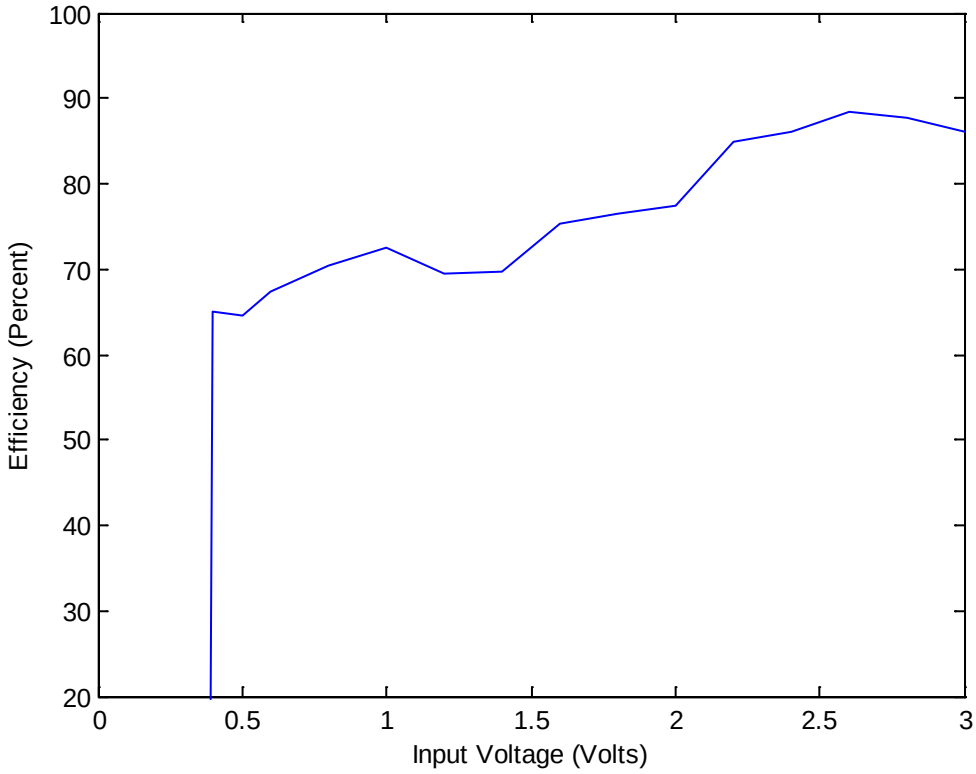

Figure 36. Hardware efficiency results (V_{STOR} = 3 V).

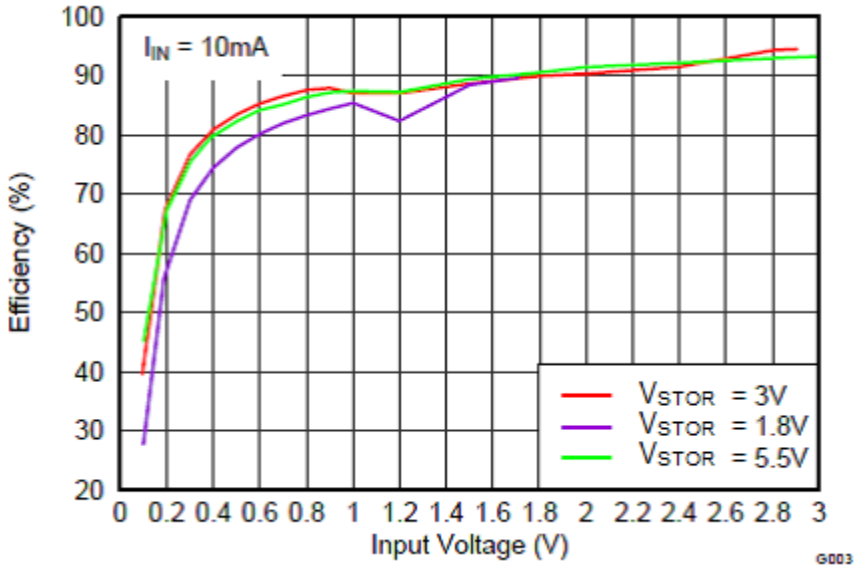

Figure 37. BQ25504 data sheet efficiency. (From [10])

D. CHARGING WITH A SOLAR CELL

The energy harvesting circuit was setup using a PV cell as an input and two 1.2 V AA size rechargeable batteries in series as the storage device. The circuit diagram is shown in Figure 38 and the equipment used can be seen in Figure 39. A 108.7 kΩ resistor was used for the system load.

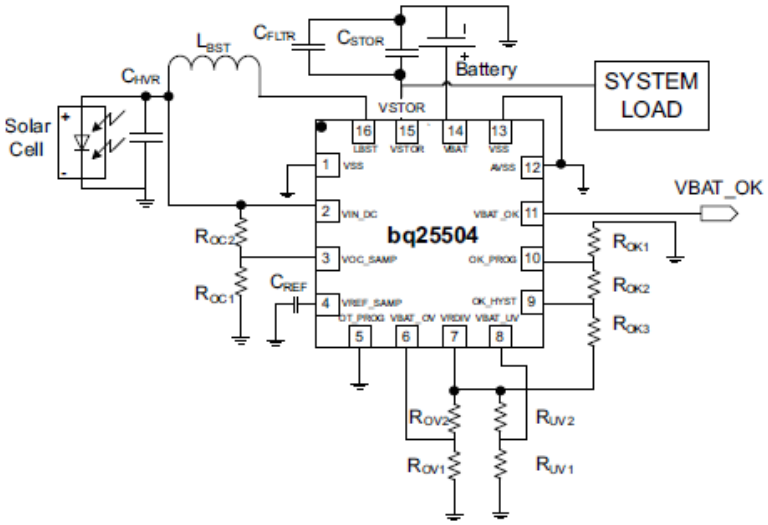

Figure 38. Solar cell charging setup. (From [10])

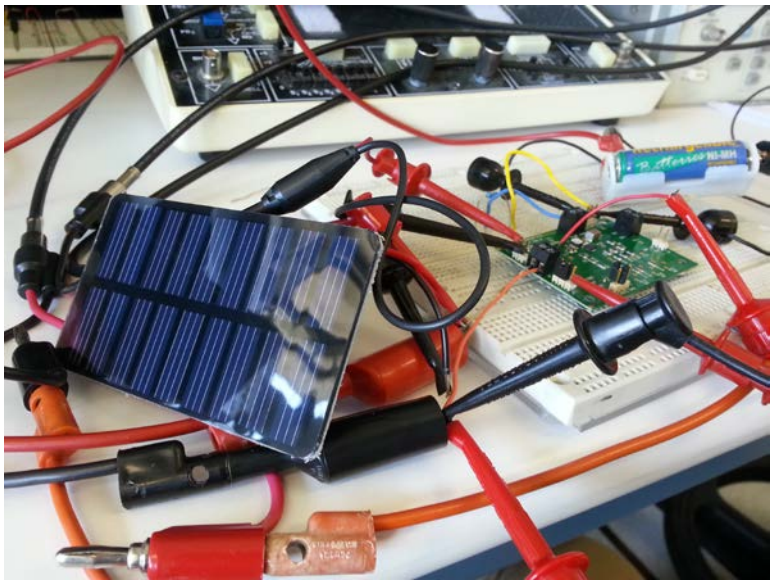

Figure 39. Solar cell charging equipment.

In Figures 40 through 43, the converter switching pattern, V_{phase}, can be seen on channel one, V_{STOR} is shown on channel two, and V_{IN} is shown on channel three. The initial battery voltage was above the UV set point at 2.46 V, which allowed V_{STOR} to be shorted to the battery. The load resistance R_{LOAD} was increased to 108.7 kΩ to lower the power draw on the relatively small solar cell. The V_{OC} was measured at 2.76 V for the initial setup. The boost converter output, illustrating the boost converter pulses and a V_{IN} of 2.15 V can be seen in Figure 40. The MPPT set point is calculated using equation (15) and was 77.9 percent.

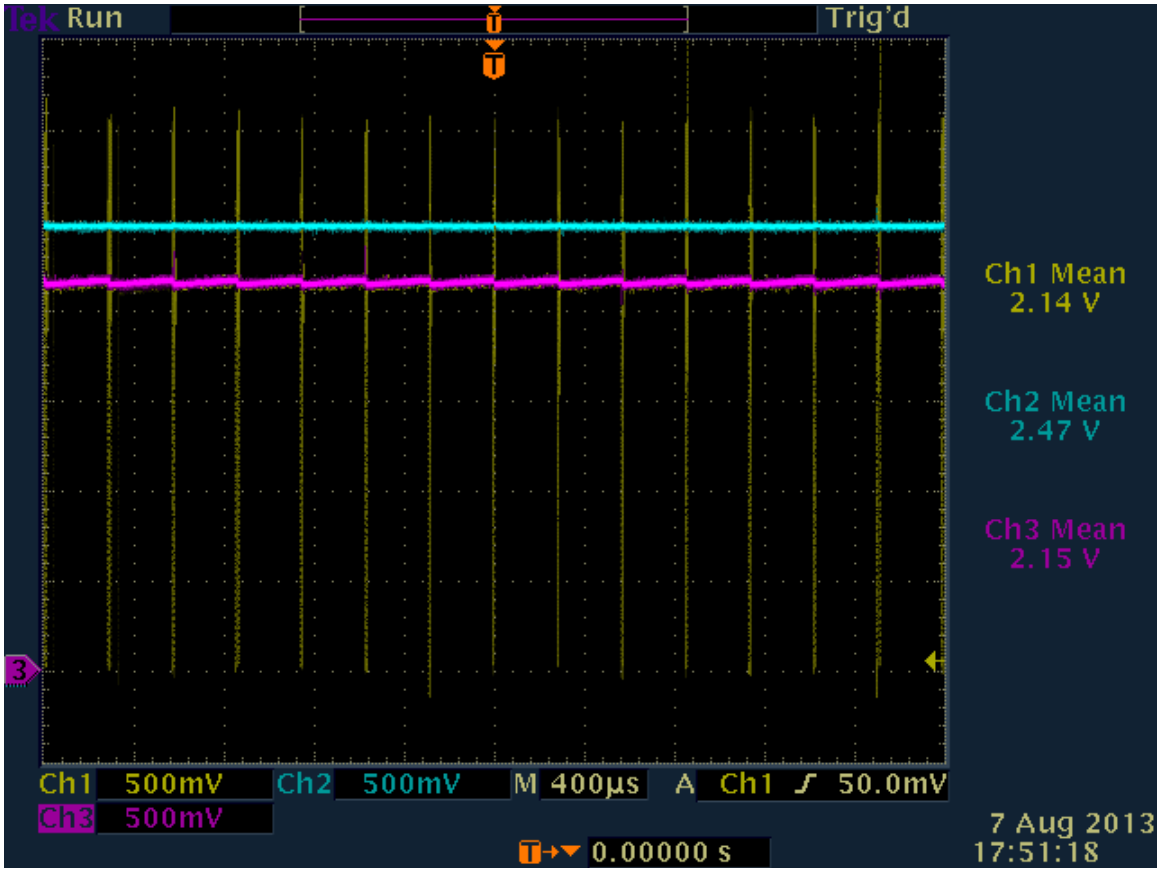

Figure 40. Measured boost converter output with V_{OC} = 2.76 V.

The solar cell output was lowered by decreasing the light intensity, and V_{OC} was measured at 2.01 V. The boost converter output, illustrating the boost converter pulses and a V_{IN} of 1.58 V, can be seen in Figure 41. The MPPT set point is calculated using

equation (15) and was 78.6 percent, demonstrating that the V_{IN} was maintained according to the MPPT setting within one percent.

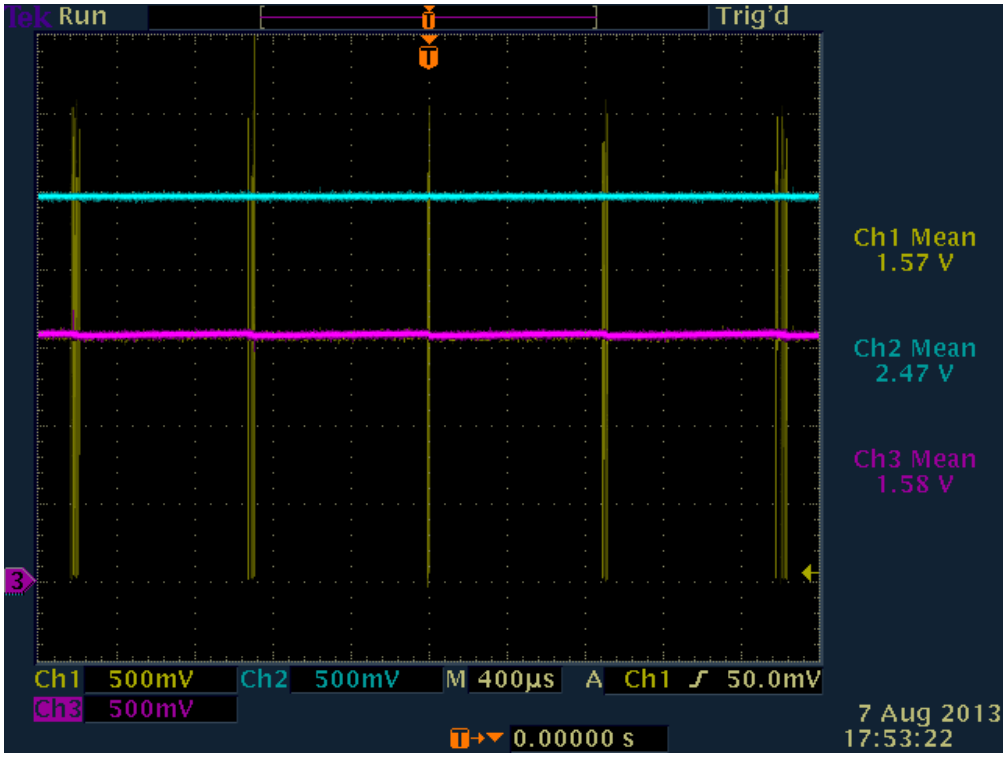

Figure 41. Measured boost converter output with V_{OC} = 2.01 V.

A more detailed view of the pulses generated by the converter is shown in Figure 42. A solar cell V_{OC} was measured at 2.7 V. Upon closer inspection, it can be seen that the converter only pulses twice. When V_{OC} was lowered to 1.7 V, it can be seen in Figure 43 that the converter now only pulses once due to the lower power produced by the solar cell.

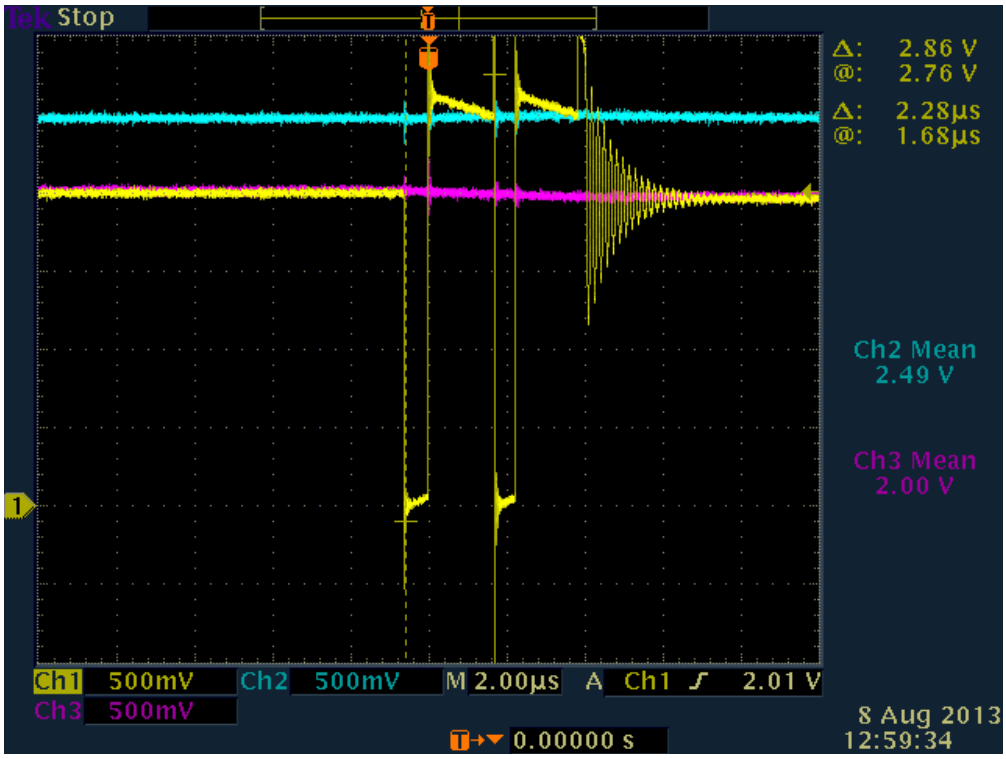

Figure 42. Converter pulses with a solar V_{OC} = 2.7 V.

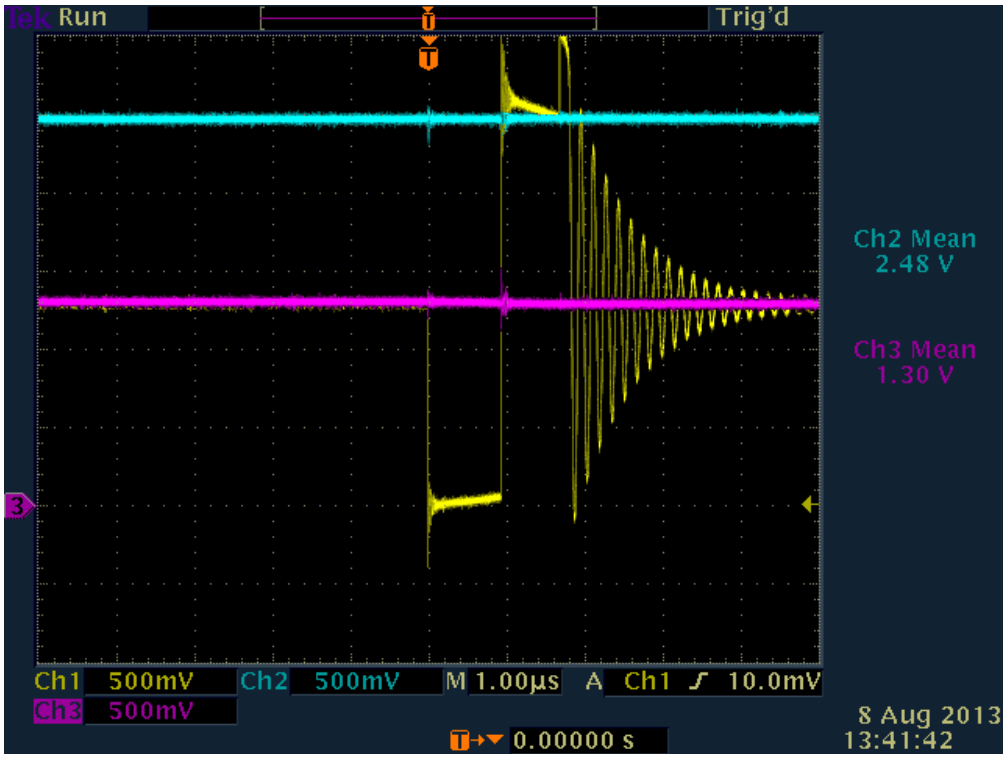

Figure 43. Converter pulses with solar V_{OC} = 1.7 V.

Finally, to show the increase in pulses provided by the converter due to the increase of the source power available, the converter was supplied by a lab power supply where V_{OC} = 1.0 V with a source resistance of 50 Ω. The increase in power results in more pulses generated by the converter as shown in Figure 44.

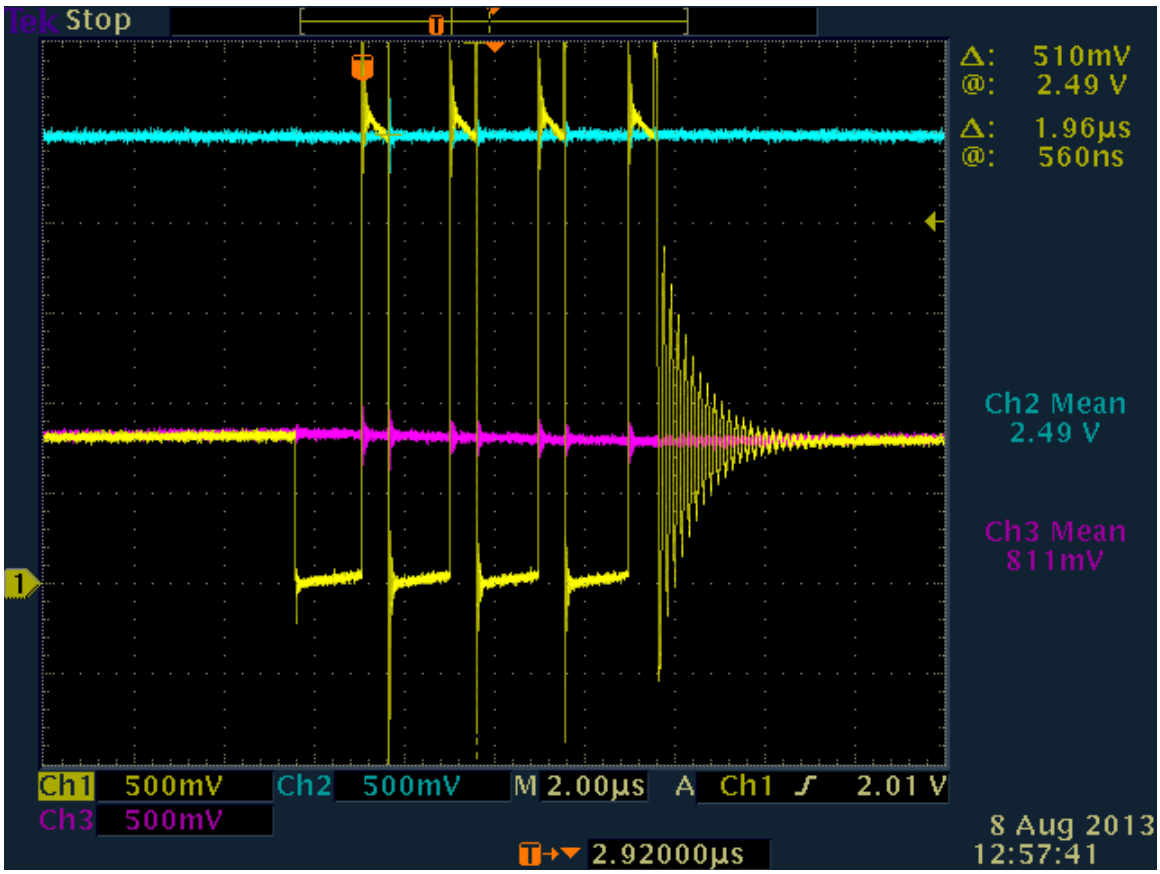

Figure 44. Converter pulses with 1.0 V power supply.

V. CONCLUSIONS AND RECOMMENDATIONS

A. ACCOMPLISHMENTS

The technologies that aid in harvesting micro-power sources were investigated in this thesis. Most importantly, an efficient means of boosting low-voltage sources was achieved by using a boost converter with synchronous rectification. Additional technologies such as MPPT and battery management were also demonstrated to provide additional means to improve harvesting efficiency. For low-voltage sources, an ultra-efficient converter such as the one studied in this thesis are beneficial to increasing efficiency. A conventional boost converter would not be able to utilize low sources of power as effectively.

B. FUTURE WORK

Further research could be done with the same converter used in this thesis. There are other smart features of this circuit that were not tested such as the temperature sensor and the battery status feature. This technology could show the ability of the circuit to protect the energy storage device. Another energy harvesting converter could also be tested and the efficiencies compared. Also, a similar experiment as completed by CAP-XX in the introduction could be studied to enhance the charging time of this particular converter.

THIS PAGE INTENTIONALLY LEFT BLANK

APPENDIX. BQ25504 DATA SHEET

This appendix contains the data sheet that is available on the Texas Instruments website [10]. It details the operating conditions and functions of the BQ25504 energy harvester converter that was studied in this thesis.

Ultra Low Power Boost Converter with Battery Management for Energy Harvester Applications

Check for Samples: bq25504

FEATURES

- Ultra Low Power With High Efficiency DC/DC Boost Converter/Charger
  - Continuous Energy Harvesting From Low Input Sources: V_{IN} ≥ 80 mV(Typical)
  - Ultra Low Quiescent Current: I_Q < 330 nA (Typical)
  - Cold-Start Voltage: V_{IN} ≥ 330 mV (Typical)
- Programmable Dynamic Maximum Power Point Tracking (MPPT)
  - Integrated Dynamic Maximum Power Point Tracking for Optimal Energy Extraction From a Variety of Energy Generation Sources
  - Input Voltage Regulation Prevents Collapsing Input Source
- Energy Storage
  - Energy can be Stored to Re-Chargeable Li-ion Batteries, Thin-film Batteries, Super-Capacitors, or Conventional Capacitors
- Battery Charging and Protection
  - User Programmable Undervoltage and Overvoltage Levels
  - On-Chip Temperature Sensor with Programmable Overtemperature Shutoff
- Battery Status Output
  - Battery Good Output Pin
  - Programmable Threshold and Hysteresis
  - Warn Attached Microcontrollers of Pending Loss of Power
  - Can be Used to Enable/Disable System Loads

APPLICATIONS

- Energy Harvesting
- Solar Charger
- Thermal Electric Generator (TEG) Harvesting
- Wireless Sensor Networks (WSN)
- Industrial Monitoring
- Environmental Monitoring
- Bridge and Structural Health Monitoring (SHM)
- Smart Building Controls
- Portable and Wearable Health Devices
- Entertainment System Remote Controls

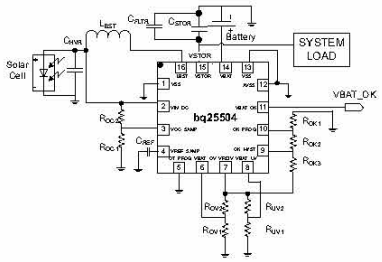

DESCRIPTION

The bq25504 is the first of a new family of intelligent integrated energy harvesting Nano-Power management solutions that are well suited for meeting the special needs of ultra low power applications. The product is specifically designed to efficiently acquire and manage the microwatts (μW) to miliwatts (mW) of power generated from a variety of DC sources like photovoltaic (solar) or thermal electric generators. The bq25504 is the first device of its kind to implement a highly efficient boost converter/charger targeted toward products and systems, such as wireless sensor networks (WSN) which have stringent power and operational demands. The design of the bq25504 starts with a DCDC boost converter/charger that requires only microwatts of power to begin operating.

These devices have limited built-in ESD protection. The leads should be shorted together or the device placed in conductive foam during storage or handling to prevent electrostatic damage to the MOS gates.

DESCRIPTION CONTINUED

Once started, the boost converter/charger can effectively extract power from low voltage output harvesters such as thermoelectric generators (TEGs) or single or dual cell solar panels. The boost converter can be started with VIN as low as 330 mV, and once started, can continue to harvest energy down to V_{IN} = 80 mV.

The bq25504 also implements a programmable maximum power point tracking sampling network to optimize the transfer of power into the device. Sampling the VIN_DC open circuit voltage is programmed using external resistors, and held with an external capacitor (CREF).

For example solar cells that operate at maximum power point (MPP) of 80% of their open circuit voltage, the resistor divider can be set to 80% of the VIN_DC voltage and the network will control the VIN_DC to operate near that sampled reference voltage. Alternatively, an external reference voltage can be provide by a MCU to produce a more complex MPPT algorithm.

The bq25504 was designed with the flexibility to support a variety of energy storage elements. The availability of the sources from which harvesters extract their energy can often be sporadic or time-varying. Systems will typically need some type of energy storage element, such as a re-chargeable battery, super capacitor, or conventional capacitor. The storage element will make certain constant power is available when needed for the systems. The storage element also allows the system to handle any peak currents that can not directly come from the input source.

To prevent damage to a customer's storage element, both maximum and minimum voltages are monitored against the user programmed undervoltage (UV) and overvoltage (OV) levels.

To further assist users in the strict management of their energy budgets, the bq25504 toggles the battery good flag to signal an attached microprocessor when the voltage on an energy storage battery or capacitor has dropped below a pre-set critical level. This should trigger the shedding of load currents to prevent the system from entering an undervoltage condition. The OV, UV and battery good thresholds are programmed independently.

All the capabilities of bq25504 are packed into a small foot-print 16-lead 3 mm x 3 mm QFN package.

ORDERING INFORMATION

PART NO.	PACKAGE	ORDERING NUMBER (TAPE AND REEL)(1)	PACKAGE MARKING	QUANTITY
bq25504	QFN 16 pin 3 mm x 3 mm	BQ25504RGTR	B5504	3000
		BQ25504RGTT	B5504	250

(1) The RGW package is available in tape on reel. Add R suffix to order quantities of 3000 parts per reel, T suffix for 250 parts per reel.

ABSOLUTE MAXIMUM RATINGS(1)

over operating free-air temperature range (unless otherwise noted)

		VALUE		UNIT
		MIN	MAX	
Input voltage	VIN_DC, VOC_SAMP, VREF_SAMP, VBAT_OV, VBAT_UV, VRDIV, OK_HYST, OK_PROG, VBAT_OK, VBAT, VSTOR, LBST (2)	–0.3	5.5	V
Peak Input Power, P_{IN_PK}			400	mW
Operating junction temperature range, T_J		–40	125	°C
Storage temperature range, T_{STG}		–65	150	°C

(1) Stresses beyond those listed under "absolute maximum ratings" may cause permanent damage to the device. These are stress ratings only and functional operation of the device at these or any other conditions beyond those indicated under "recommended operating conditions" is not implied. Exposure to absolute–maximum–rated conditions for extended periods may affect device reliability.
(2) All voltage values are with respect to V_{SS}/ground terminal.

THERMAL INFORMATION

THERMAL METRIC(1)(2)		bq25504 RGT (16 PINS)	UNITS
θ_{JA}	Junction-to-ambient thermal resistance	48.5	°C/W
θ_{JCtop}	Junction-to-case (top) thermal resistance	63.9	
θ_{JB}	Junction-to-board thermal resistance	22	
ψ_{JT}	Junction-to-top characterization parameter	1.8	
ψ_{JB}	Junction-to-board characterization parameter	22	
θ_{JCbot}	Junction-to-case (bottom) thermal resistance	6.5	

(1) For more information about traditional and new thermal metrics, see the *IC Package Thermal Metrics* application report, SPRA953.
(2) For thermal estimates of this device based on PCB copper area, see the TI PCB Thermal Calculator.

RECOMMENDED OPERATING CONDITIONS

		MIN	NOM	MAX	UNIT
$V_{IN\_(DC)}$	DC input voltage into VIN_DC(1)	0.13		3	V
VBAT	Battery voltage range(2)	2.5		5.25	V
C_{HVR}	Input capacitance	4.23	4.7	5.17	µF
C_{STOR}	Storage capacitance	4.23	4.7	5.17	µF
C_{BAT}	Battery pin capacitance or equivalent battery capacity	100			µF
C_{REF}	Sampled reference storage capacitance	9	10	11	nF
$R_{OC1} + R_{OC2}$	Total resistance for setting for MPPT reference.	18	20	22	MΩ
$R_{OK}1 + R_{OK}2 + R_{OK3}$	Total resistance for setting reference voltage.	9	10	11	MΩ
$R_{UV1} + R_{UV2}$	Total resistance for setting reference voltage.	9	10	11	MΩ
$R_{OV1} + R_{OV2}$	Total resistance for setting reference voltage.	9	10	11	MΩ
L_{BST}	Input inductance	19.8	22	24.2	µH
T_A	Operating free air ambient temperature	–40		85	°C
T_J	Operating junction temperature	–40		105	°C

(1) Maximum input power ≤ 300 mW. Cold start has been completed
(2) VBAT_OV setting must be higher than VIN_DC

ELECTRICAL CHARACTERISTICS

Over recommended temperature range, typical values are at T_A = 25°C. Unless otherwise noted, specifications apply for conditions of VIN_DC = 1.2V, VBAT = VSTOR = 3V. External components L_{BST} = 22 µH, C_{HVR} = 4.7 µF C_{STOR}= 4.7 µF.

PARAMETER		TEST CONDITIONS	MIN	TYP	MAX	UNIT
BOOST CONVERTER \ CHARGER STAGE						
$V_{IN(DC)}$	DC input voltage into VIN_DC	Cold-start completed	130		3000	mV
$I_{IN(DC)}$	Peak Current flowing from V_{IN} into VIN_DC input	0.5V < V_{IN} < 3 V; VSTOR = 4.2 V		200	300	mA
P_{IN}	Input power range for normal charging	VBAT > VIN_DC; VIN_DC = 0.5 V	0.01		300	mW
$V_{IN(CS)}$	Cold-start Voltage. Input voltage that will start charging of VSTOR	VBAT < VBAT_UV; VSTOR = 0 V; 0°C < T_A < 85°C		330	450	mV
$P_{IN(CS)}$	Minimum cold-start input power to start normal charging	VBAT < VBAT_UV; VSTOR = 0 V; Input source impedance 0 Ω		10	50	µW
V_{STOR_CHGEN}	Voltage on VSTOR when cold start operation ends and normal charger operation begins		1.6	1.77	1.95	V
$R_{BAT(on)}$	Resistance of switch between VBAT and VSTOR when turned on.	VBAT = 4.2 V; VSTOR load = 50 mA			2	Ω
$R_{DS(on)}$	Charger Low Side switch ON resistance	VBAT = 2.1 V			2	Ω
		VBAT = 4.2 V			2	
	Charger rectifier High Side switch ON resistance	VBAT = 2.1 V			5	Ω
		VBAT = 4.2 V			5	
f_{SW_BST}	Boost converter mode switching frequency				1	MHz

ELECTRICAL CHARACTERISTICS (continued)

Over recommended temperature range, typical values are at T_A = 25°C. Unless otherwise noted, specifications apply for conditions of VIN_DC = 1.2V, VBAT = VSTOR = 3V. External components L_{BST} = 22 µH, C_{HVR} = 4.7 µF C_{STOR}= 4.7 µF.

PARAMETER		TEST CONDITIONS	MIN	TYP	MAX	UNIT
BATTERY MANAGEMENT						
I_{VBAT}	Leakage on VBAT pin	VBAT = 2.1 V; VBAT_UV = 2.3 V, T_J = 25°C VSTOR = 0 V		1	5	nA
		VBAT = 2.1 V; VBAT_UV = 2.3 V, –40°C < T_J < 65°C, VSTOR = 0 V			80	nA
I_{VSTOR}	VSTOR Quiescent current Charger Shutdown in UV Condition	VIN_DC = 0V; VBAT < VBAT_UV = 2.4V; VSTOR = 2.2V, No load on VBAT		330	750	nA
	VSTOR Quiescent current Charger Shutdown in OV Condition	VIN_DC = 0V, VBAT > VBAT_OV, VSTOR = 4.25, No load on VBAT		570	1400	nA
V_{BAT_OV}	Programmable voltage range for overvoltage threshold (Battery voltage is rising)	VBAT increasing	2.5		5.25	V
$V_{BAT\_OV\_HYST}$	Battery voltage overvoltage hysteresis threshold (Battery voltage is falling), internal threshold	VBAT decreasing	18	35	89	mV
V_{BAT_UV}	Programmable voltage range for under voltage threshold (Battery voltage is falling)	VBAT decreasing; VBAT_UV > V_{BBM}	2.2		VBAT_OV	V
$V_{BAT\_UV\_HYST}$	Battery under voltage threshold hysteresis, internal thershold	VBAT increasing	40	80	125	mV
V_{BAT_OK}	Programmable voltage range for threshold voltage for high to low transition of digital signal indicating battery is OK,	VBAT decreasing	VBAT_UV		VBAT_OV	V
$V_{BAT\_OK\_HYST}$	Programmable voltage range for threshold voltage for low to high transition of digital signal indicating battery is OK,	VBAT increasing	50		VBAT_OV-VBAT_UV	mV
$V_{BAT\_ACCURACY}$	Overall Accuracy for threshold values, UV, OV, VBAT_OK	Selected resistors are 0.1% tolerance	–5%		5%	
V_{BAT_OKH}	VBAT OK (High) threshold voltage	Load = 10 µA			VSTOR-200mV	V
V_{BAT_OKL}	VBAT OK (Low) threshold voltage	Load = 10 µA			100	mV
TSD_PROTL	The temperature at which the boost converter is disabled and the switch between VBAT and VSTOR is disconnected to protect the battery	OT_Prog = LO		65		°C
TSD_PROTH		OT_Prog = HI		120		
OT_Prog	Voltage for OT_PROG High setting		2			V
	Voltage for OT_PROG Low setting				0.3	V
BIAS and MPPT CONTROL STAGE						
VOC_sample	Sampling period of VIN_DC open circuit voltage			16		s
VOC_Settling	Sampling period of VIN_DC open circuit voltage			256		ms
VIN_Reg	Regulation of VIN_DC during charging	0.5 V <V_{IN} < 3 V; I_{IN} (DC) = 10 mA	–10%		10%	
VIN_shutoff	DC input voltage into VIN_DC when charger is turned off		40	80	130	mV
MPPT_Disable	Threshold on VOC_SAMP to disable MPPT functionality		VSTOR-15 mV			V
VBIAS	Voltage node which is used as reference for the programmable voltage thresholds	VIN_DC ≥ 0.5V; VSTOR ≥ 1.8 V	1.21	1.25	1.27	V

DEVICE INFORMATION

RGT PACKAGE
(TOP VIEW)

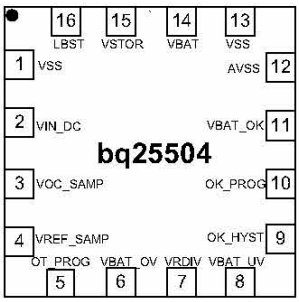

Figure 1. bq25504 3mm x 3mm QFN-16 Package

PIN FUNCTIONS

PIN		I/O TYPE	DESCRIPTION
NO.	NAME		
1	VSS	Input	General ground connection for the device
2	VIN_DC	Input	DC voltage input from energy harvesters
3	VOC_SAMP	Input	Sampling pin for MPPT network. To disable MPPT, connect to VSTOR
4	VREF_SAMP	Input	Switched node for holding the reference set by resistors on VOC_SAMP for MPPT. When MPPT is disabled, VREF_SAMP should not be left floating but either either be tied to an external reference voltage or tied to GND.
5	OT_PROG	Input	Digital Programming input for overtemperature threshold
6	VBAT_OV	Input	Resistor divider input for over voltage threshold
7	VRDIV	Output	Resistor divider biasing voltage.
8	VBAT_UV	Input	Resistor divider input for under voltage threshold
9	OK_HYST	Input	Resistor divider input for VBAT_OK hysteresis threshold
10	OK_PROG	Input	Resistor divider input for VBAT_OK threshold
11	VBAT_OK	Output	Digital battery good indicator referenced to VSTOR pin
12	AVSS	Supply	Signal ground connection for the device
13	VSS	Supply	General ground connection for the device
14	VBAT	I/O	Connection for storage elements
15	VSTOR	Output	Connection for the system load, output of the boost converter
16	LBST	Input	Inductor connection for the boost converter switching node

TYPICAL APPLICATION CIRCUITS

VIN_DC = 1.2 V, C_{STOR}= 4.7 µF, L_{BST}= 22 µH, C_{HVR}= 4.7 µF, C_{REF}= 10 nF, TSD_PROTL (65°C),
MPPT (V_{OC}) = 80% VBAT_OV = 3.1 V, VBAT_UV = 2.2 V, VBAT_OK = 2.4 V, VBAT_OK_HYST = 2.8 V,
R_{OK1} = 4.42 MΩ, R_{OK2} = 4.22 MΩ, R_{OK3} = 1.43 MΩ, R_{OV1} = 5.9 MΩ, R_{OV2} = 4.02 MΩ,
R_{UV1}= 5.6 MΩ, R_{UV2} = 4.42 MΩ, R_{OC1}= 15.62 MΩ, R_{OC2} = 4.42 MΩ

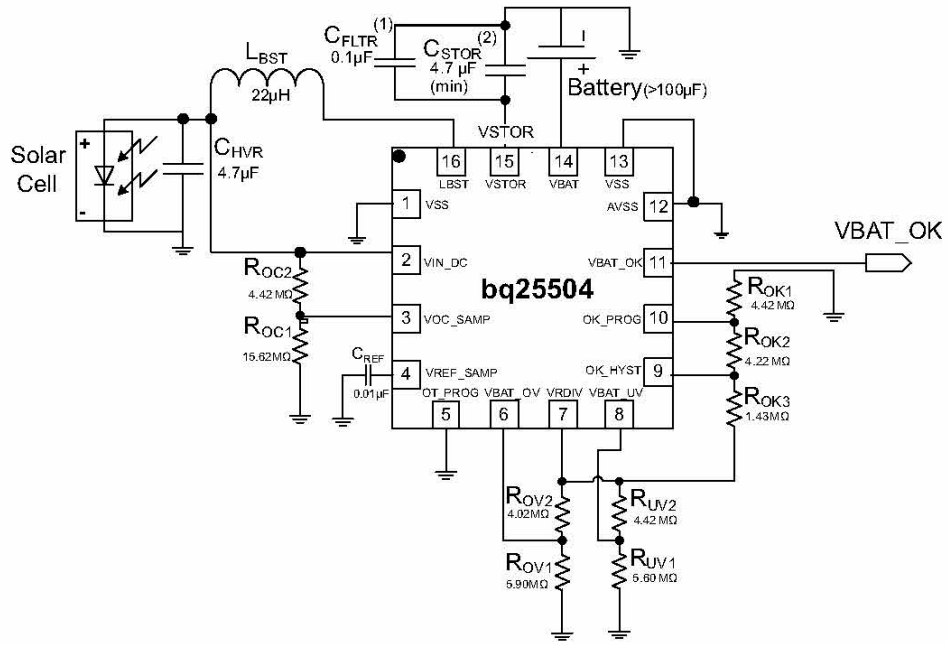

(1) Place close as possible to IC pin 15 (VSTOR) and pin 13 (VSS)
(2) See the Capacitor Selection section for guidance on sizing C_{STOR}

Figure 2. Typical Solar Application Circuit

VIN_DC = 0.5 V, C_{STOR} = 4.7 µF, L_{BST} = 22 µH, C_{HVR} = 4.7 µF, C_{REF} = 10 nF, TSD_PROTH (120°C), MPPT (V_{OC}) = 50% VBAT_OV = 4.2 V, VBAT_UV = 3.2 V, VBAT_OK = 3.5 V, VBAT_OK_HYST = 3.7 V, R_{OK1} = 3.32 MΩ, R_{OK2} = 6.12 MΩ, R_{OK3} = 0.542 MΩ, R_{OV1} = 4.42 MΩ, R_{OV2} = 5.62 MΩ, R_{UV1} = 3.83 MΩ, R_{UV2} = 6.12 MΩ, R_{OC1} = 10 MΩ, R_{OC2} = 10 MΩ

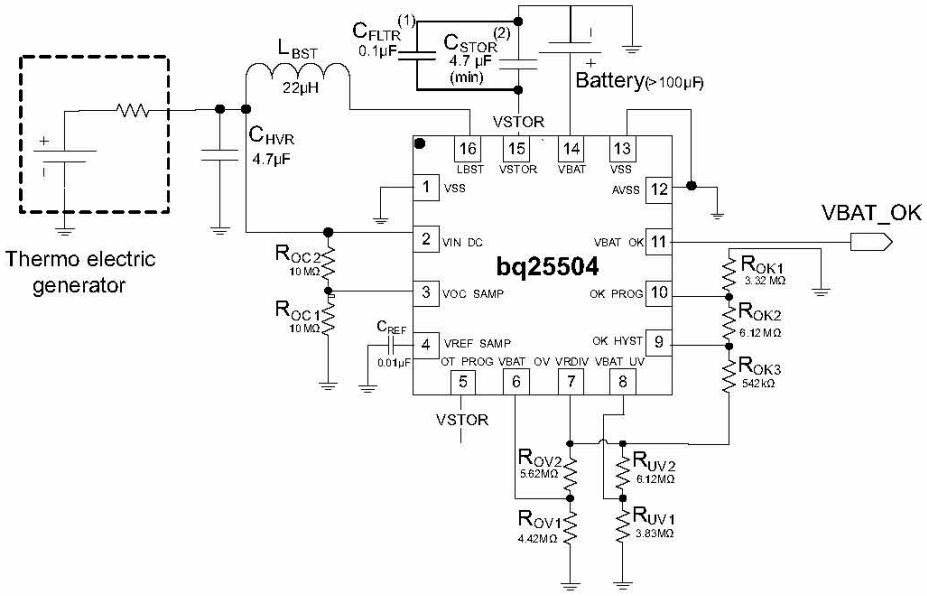

(1) Place close as possible to IC pin 15 (VSTOR) and pin 13 (VSS)
(2) See the Capacitor Selection section for guidance on sizing C_{STOR}

Figure 3. Typical TEG Application Circuit

VIN_DC = 1.2 V, C_{STOR} = 4.7 µF, L_{BST} = 22 µH, C_{HVR} = 4.7 µF, TSD_PROTL (65°C),
MPPT (V_{OC}) = Disabled VBAT_OV = 3.3 V, VBAT_UV = 2.2 V, VBAT_OK = 2.8 V, VBAT_OK_HYST = 3.1 V,
R_{OK1} = 3.97 MΩ, R_{OK2} = 5.05 MΩ, R_{OK3} = 0.976 MΩ, R_{OV1} = 5.56 MΩ,
R_{OV2} = 4.48 MΩ, R_{UV1} = 5.56 MΩ, R_{UV2} = 4.42 MΩ

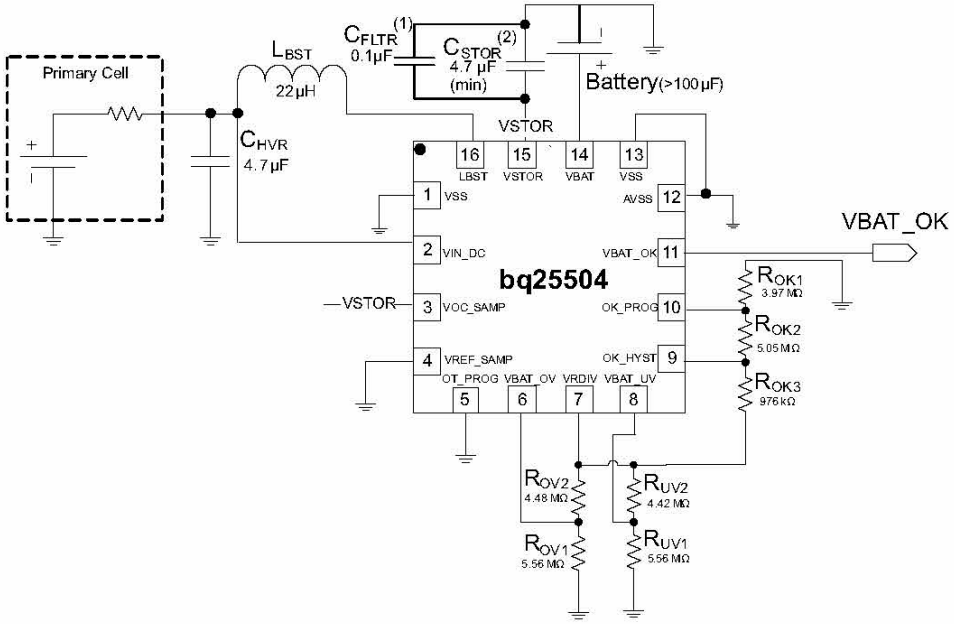

(1) Place close as possible to IC pin 15 (VSTOR) and pin 13 (VSS)
(2) See the Capacitor Selection section for guidance on sizing C_{STOR}

Figure 4. Typical MPPT Disabled Application Circuit

HIGH-LEVEL FUNCTIONAL BLOCK DIAGRAM

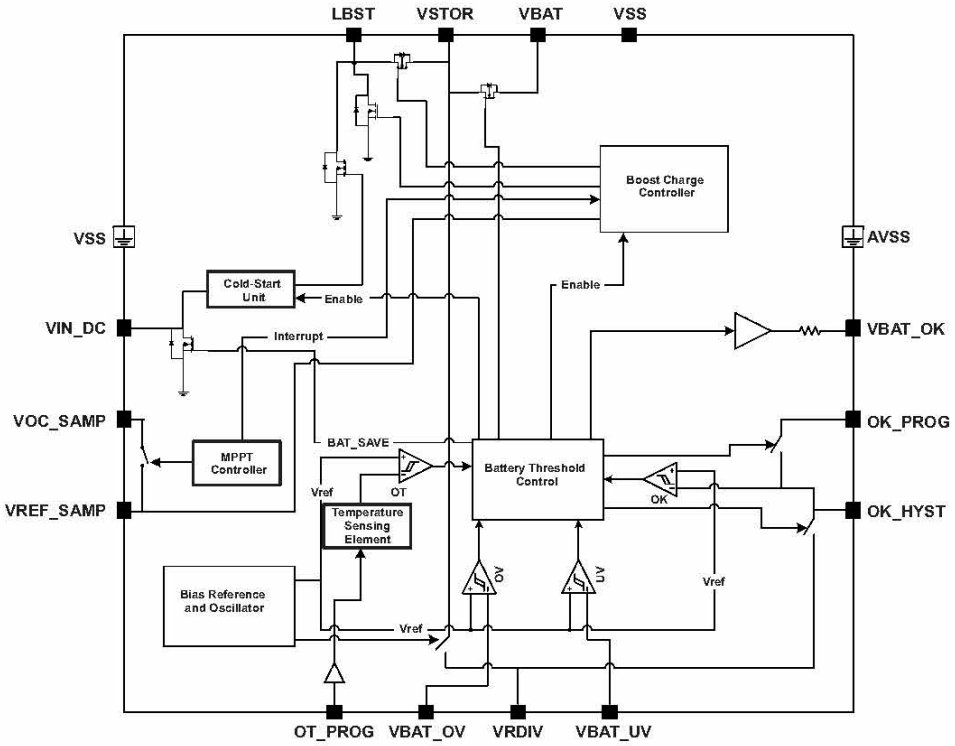

Figure 5. High-level Functional Diagram

TYPICAL CHARACTERISTICS

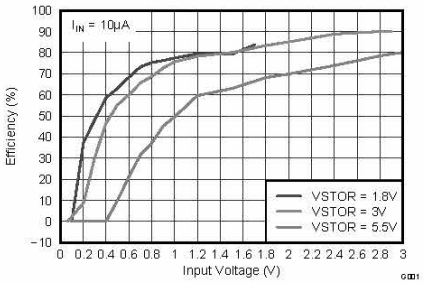

Figure 6. Efficiency vs Input Voltage

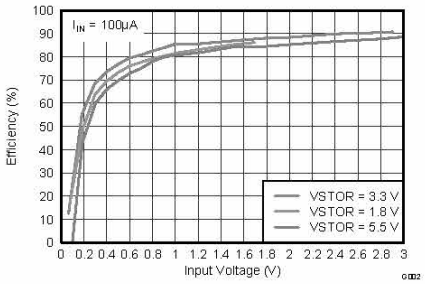

Figure 7. Efficiency vs Input Voltage

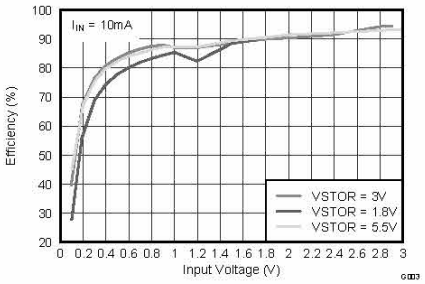

Figure 8. Efficiency vs Input Voltage

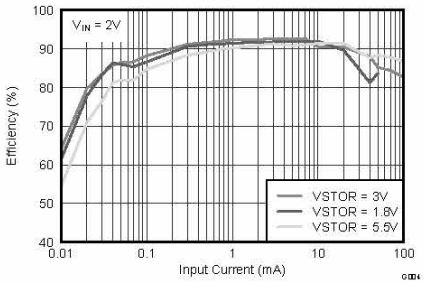

Figure 9. Efficiency vs Input Current

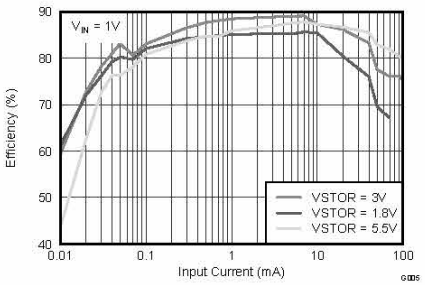

Figure 10. Efficiency vs Input Current

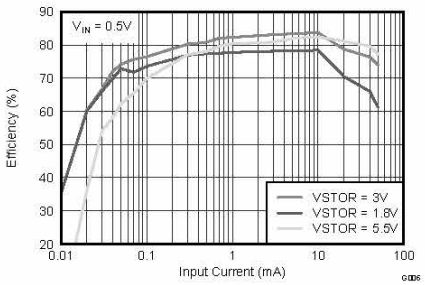

Figure 11. Efficiency vs Input Current

TYPICAL CHARACTERISTICS (continued)

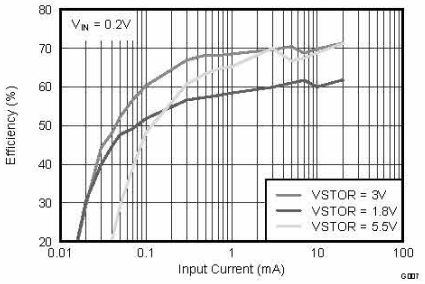

Figure 12. Efficiency vs Input Current

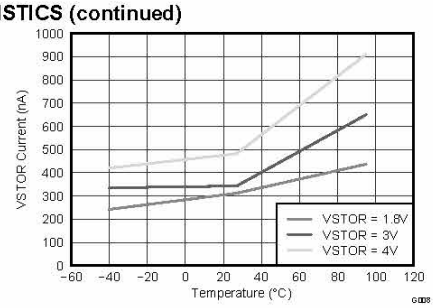

Figure 13. VSTOR Quiescent Current vs Temperature

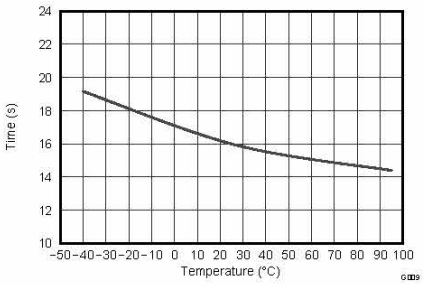

Figure 14. Sample Period vs Temperature

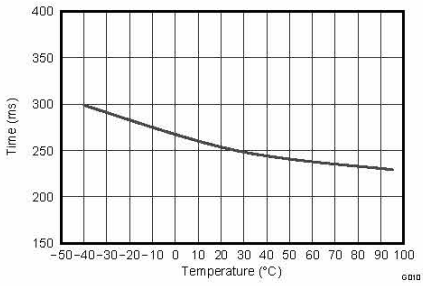

Figure 15. Settling Period vs Temperature

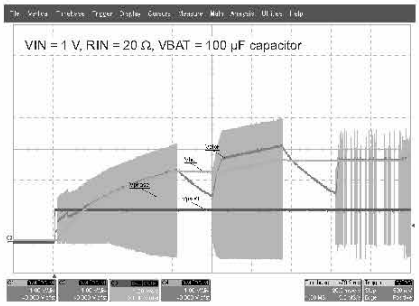

Figure 16. Example of Startup with no Battery and 10 KΩ Load

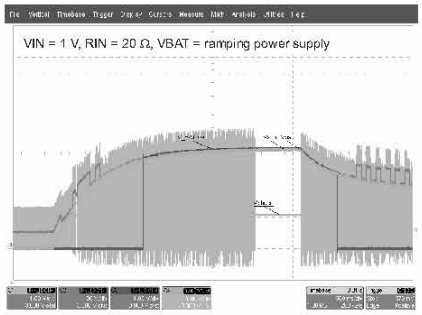

Figure 17. Example of VBAT_OK Operation, Ramping Battery From 0 V to 3.1 V

TYPICAL CHARACTERISTICS (continued)

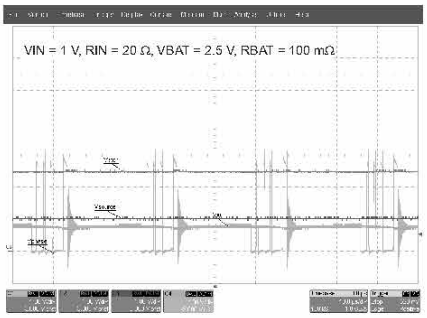

Figure 18. Example of PFM Switching Converter Waveform

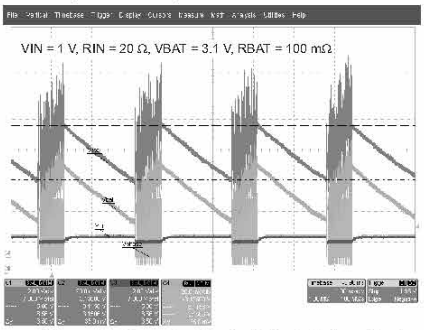

Figure 19. Example of Output Ripple Voltage During Operation at O V Setting

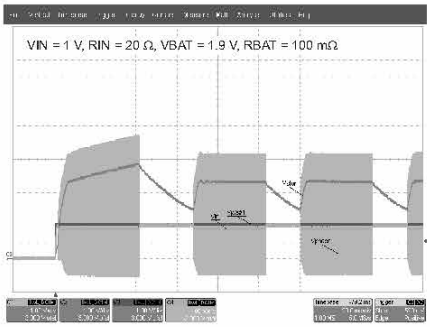

Figure 20. Example of Startup When VBAT is Held Below UV Setting

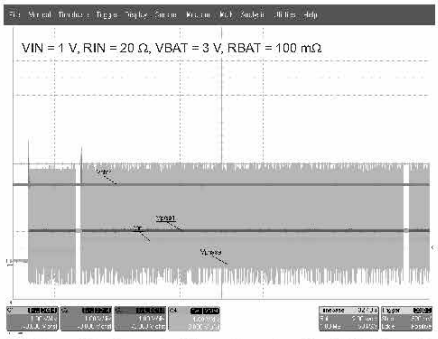

Figure 21. Example of Sampling Time for MPPT Operation

DETAILED PRINCIPLE OF OPERATION

OVERVIEW

The bq25504 is an ultra low quiescent current, efficient synchronous boost converter/charger. The boost converter is based on a switching regulator architecture which maximizes efficiency while minimizing start-up and operation power. The bq25504 uses pulse frequency modulation (PFM) to maintain efficiency, even under light load conditions. In addition, bq25504 also implements battery protection features so that either rechargeable batteries or capacitors can be used as energy storage elements. Figure 5 is a high-level functional block diagram which highlights most of the major functional blocks inside the bq25504.

Intended Operation

The bq25504's priority is to charge up the VSTOR capacitor, CSTOR, then power additional internal circuitry from VSTOR. When a storage element is attached (i.e. hot-plugged), the bq25504 will first attempt to charge up CSTOR from the storage element by turning on the internal PFET between the VSTOR and VBAT pins for approximately 45ms. See Storage Element section for guidance on selecting the storage element. If a system load tied to VSTOR prevent the storage element from charging VSTOR within 45 ms typical, it is recommended to add an external PFET between the system load and VSTOR. An inverted VBAT_OK signal can be used to drive the gate of the PFET. Once the VSTOR pin voltage reaches the user set under voltage threshold (VBAT_UV), the internal PFET stays on and the boost converter / charger begins to charge the storage element if there is sufficient power available at the VIN_DC pin, as explained below.If VSTOR does not reach VBAT_UV within 45 ms typical, then the PFET turns off and the Cold-Start subsystem turns on, also as explained below.

When no input source is attached, the VSTOR node should be discharged to ground before attaching a storage element. Hot-plugging a storage element that is charged (e.g., the battery protector is closed) and with VSTOR above ground results in the PFET between VSTOR and VBAT remaining off until a input source is attached and charging resumes. In addition, if a system load attached to VSTOR has fast transients that could pull VSTOR below VBAT_UV, the internal PFET switch will turn off in order to recharge the CSTOR capacitor. See the application section for guidance on sizing the VSTOR and/or VBAT capacitance to account for transients. If the voltage applied at VIN_DC is greater than VSTOR or VBAT then current may flow until the voltage at the input is reduced or the voltage at VSTOR and VBAT rise. This is considered an abnormal condition and the boost converter/charger does not operate.

Cold -Start Operation (VSTOR < V_{STOR_CHGN} and VIN_DC > $V_{IN(CS)}$)

When the voltage at pin VIN_DC exceeds the minimum input voltage with sufficient power, the cold-start subsystem turns on. The cold-start subsystem is essentially an unregulated boost converter. When the storage capacitor, CSTOR, voltage reaches V_{STOR_CHGEN} (1.8V typical), the main boost regulator starts up. The VSTOR voltage from the main boost regulator is now compared against battery undervoltage threshold (VBAT_UV). When the VBAT_UV threshold is reached, the PMOS switch between VSTOR and VBAT is turned on, which allows the energy storage element attached to VBAT to charge up. Cold start is not as efficient as the main boost regulator. If there is not sufficient power available it is possible that the cold start continuously runs and the VSTOR output does not increase to 1.8 V and start the main boost regulator.

Figure 22 shows the key threshold voltages. The battery management thresholds are explained later is this section.

Boost Converter, Charger Operation (VSTOR > V_{STOR_CHGN} and VIN_DC > $V_{IN(DC)-MIN}$)

The boost converter in bq25504 is used to charge the storage element attached at VBAT with the energy available from the DC input source. For the first 32 ms (typical) after the main converter is turned ON, the charger is disabled to let the input go up to its open-circuit voltage. This is needed to get the reference voltage which will be used for the remainder of the charger operation till the next MPPT sampling cycle turns ON. The boost converter employs pulse frequency modulation (PFM) mode of control to regulate the input voltage (VIN_DC) close to the desired reference voltage. The reference voltage is set by the MPPT control scheme as described in the next section. Input voltage regulation is obtained by transferring charge from the input to VSTOR only when the input voltage is higher than the voltage on pin VREF_SAMP. The current through the inductor is controlled through internal current sense circuitry. The peak current in the inductor is dithered internally to set levels to maintain high efficiency of the converter across a wide input current range. The converter nominally transfers up to a average of 100 mA of input current. The boost converter is disabled when the voltage on VSTOR reaches the OV condition to protect the battery connected at VBAT from overcharging.

Maximum Power Point Tracking

Maximum power point tracking (MPPT) is implemented in bq25504 in order to maximize the power extracted from an energy harvester source. MPPT is performed by periodically sampling a ratio of the open-circuit voltage of the energy harvester and using that as the reference voltage (VREF_SAMP) to the boost converter. The sampling ratio can be externally programmed using the resistors R_{OC1} and R_{OC2}. For solar harvesters, the resistive division ratio can be typically set between 0.7-0.8 and for thermoelectric harvesters; a resistive division ratio of 0.5 is typically used. The exact ratio for MPPT can be optimized to meet the needs of the input source being used.

Internally, the boost converter modulates the effective impedance of the energy transfer circuitry to regulate the input voltage (VIN_DC) to the sampled reference voltage (VREF_SAMP). A new reference voltage is obtained every 16s by periodically disabling the charger for 256ms and sampling a ratio of the open-circuit voltage. The reference voltage is set by the following expression:

$$VREF\_SAMP = VIN\_DC(OpenCircuit)\left(\frac{R_{OC1}}{R_{OC1} + R_{OC2}}\right) \quad (1)$$

The internal MPPT circuitry and the periodic sampling of VIN_DC can be disabled by tying the VOC_SAMP pin to VSTOR. When disabled an external reference voltage can be fed to the VREF_SAMP pin. The boost converter will then regulate VIN_DC to the externally provided reference. If input regulation is not desired, VREF_SAMP can be tied to GND.

Storage Element

When operating as a charger, the main storage elements must be connected to VBAT pin. Many types of elements can be used, such as capacitors, super capacitors or various battery chemistries. A storage element with 100uF equivalent capacitance is required to filter the pulse currents of the PFM switching converter. The equivalent capacitance of a battery can be computed as computed as C_{EQ} = 2 x $mAHr_{BAT(CHRGD)}$ x 3600 s/Hr / $V_{BAT(CHRGD)}$. In order for the storage element to be able to charge VSTOR capacitor (CSTOR) with in the 45ms window at hot-plug; therefore preventing the IC from entering cold start. The time constant created by he storage element's series resistance (plus the resistance of the internal PFET switch) and equivalent capacitance must be less than 45 ms (typical). For example, a battery's resistance can be computed as $R_{BAT} = V_{BAT} / I_{BAT(CONTIUOUS)}$ from the battery specifications. To take full advantage of the battery management, the load is normally tied to the VSTOR pin and not the VBAT pin. Also, if there are large load transients or the storage element has significant impedance then it may be necessary to increase the CSTOR capacitor from the 4.7uF minimum or add additional capacitance to VBAT in order to prevent a droop in the VSTOR voltage. See Capacitor Selection section in Application Information section for guidance on sizing the capacitor.

Battery Management

In this section the battery management functionality of the bq25504 integrated circuit (IC) is presented. The IC has internal circuitry to manage the voltage across the storage element and to optimize the charging of the storage element. For successfully extracting energy from the source, three different threshold voltages must be programmed using external resistors, namely the under voltage (UV) threshold, battery good threshold (VBAT_OK) and over voltage (OV) threshold. The three threshold voltages determine the region of operation of the IC. Figure 22 shows a plot of the voltage at the VSTOR pin and the various threshold voltages. For the best operation of the system, the VBAT_OK should be used to determine when a load can be applied or removed. A detailed description of the three voltage thresholds and the procedure for designing the external resistors for setting the three voltage thresholds are described next.

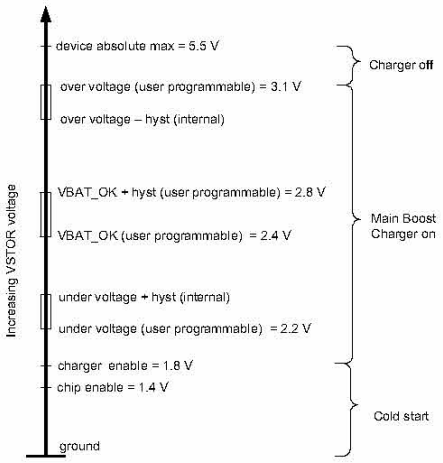

Figure 22. Figure Shows the Relative Position of Various Threshold Voltages (Threshold Voltages are From Typical Solar Application Circuit in Figure 2)

Battery Undervoltage Protection

To prevent rechargeable batteries from being deeply discharged and damaged, and to prevent completely depleting charge from a capacitive storage element, the undervoltage (VBAT_UV) threshold must be set using external resistors. The VBAT_UV threshold voltage when the battery voltage is decreasing is given by Equation 2:

$$VBAT\_UV = VBIAS\left(1 + \frac{R_{UV2}}{R_{UV1}}\right) \quad (2)$$

The sum of the resistors should be approximately, 10 MΩ that is, $R_{UV1} + R_{UV2}$ = 10 MΩ. The undervoltage threshold when battery voltage is increasing is given by UV_HYST. It is internal set to the under voltage threshold plus an internal hysteresis voltage denoted by VBAT_UV_HYST. For proper functioning of the IC and the overall system, the load must be connected to the VSTOR pin while the storage element must be connected to the VBAT pin. Once the VSTOR pin voltage goes above the UV_HYST threshold, the VSTOR pin and the VBAT pins are shorted. The switch remains closed until the VSTOR pin voltage falls below the under voltage threshold. The VBAT_UV threshold should be considered a fail safe to the system and the system load should be removed or reduced based on the VBAT_OK signal.

Battery Overvoltage Protection

To prevent rechargeable batteries from being exposed to excessive charging voltages and to prevent over charging a capacitive storage element, the over-voltage (VBAT_OV) threshold level must be set using external resistors. This is also the voltage value to which the charger will regulate the VSTOR/VBAT pin when the input has sufficient power. The VBAT_OV threshold when the battery voltage is rising is given by Equation 3:

$$VBAT\_OV = \frac{3}{2}VBIAS\left(1 + \frac{R_{OV2}}{R_{OV1}}\right) \quad (3)$$

The sum of the resistors should be approximately 10 MΩ that is, R_{OV1} + R_{OV2} = 10 MΩ. The overvoltage threshold when battery voltage is decreasing is given by OV_HYST. It is internal set to the over voltage threshold minus an internal hysteresis voltage denoted by VBAT_OV_HYST. Once the voltage at the battery exceeds VBAT_OV threshold, the boost converter is disabled. The charger will start again once the battery voltage falls below the VBAT_OV_HYST level. When there is excessive input energy, the VBAT pin voltage will ripple between the VBAT_OV and the VBAT_OV_HYST levels.

CAUTION

If VIN_DC is higher than VSTOR and VSTOR is higher than VBAT_OV, the input VIN_DC is pulled to ground through a small resistance to stop further charging of the attached battery or capacitor. It is critical that if this case is expected, the impedance of the source attached to VIN_DC be higher than 20 Ω and not a low impedance source.

Battery Voltage in Operating Range (VBAT_OK Output)

The IC allows the user to set a programmable voltage independent of the overvoltage and undervoltage settings to indicate whether the VSTOR voltage (and therefore the VBAT voltage when the PFET between the two pins is turned on) is at an acceptable level. When the battery voltage is decreasing the threshold is set by Equation 4

$$VBAT\_OK\_PROG = VBIAS\left(1 + \frac{R_{OK2}}{R_{OK1}}\right) \quad (4)$$

When the battery voltage is increasing, the threshold is set by Equation 5

$$VBAT\_OK\_HYST = VBIAS\left(1 + \frac{R_{OK2} + R_{OK3}}{R_{OK1}}\right) \quad (5)$$

The sum of the resistors should be approximately 10 MΩ i.e., R_{OK1} + R_{OK2} + R_{OK3}= 10 MΩ. The logic high level of this signal is equal to the VSTOR voltage and the logic low level is ground. The logic high level has ~20 KΩ internally in series to limit the available current to prevent MCU damage until it is fully powered. The VBAT_OK_PROG threshold must be greater than or equal to the UV threshold. For the best operation of the system, the VBAT_OK should be setup to drive an external PFET between VSTOR and the system load in order to determine when the load can be applied or removed to optimize the storage element capacity.

Thermal Shutdown

Rechargeable Li-ion batteries need protection from damage due to operation at elevated temperatures. The application should provide this battery protection and ensure that the ambient temperature is never elevated greater than the expected operational range of 85°C.

The bq25504 uses an integrated temperature sensor to monitor the junction temperature of the device. If the OT_PROG pin is tied low, then the temperature threshold for thermal protection is set to TSD_ProtL which is 65°C typically. If the OT_PROG is tied high, then the temperature is set to TSD_ProtH which is 120°C typically. Once the temperature threshold is exceeded, the boost converter/charger is disabled and charging ceases. Once the temperature of the device drops below this threshold, the boost converter and or charger can resume operation. To avoid unstable operation near the overtemp threshold, a built-in hysteresis of approximately 5°C has been implemented. Care should be taken to not over discharge the battery in this condition since the boost converter/charger is disabled. However, if the supply voltage drops to the VBAT_UV setting, then the switch between VBAT and VSTOR will open and protect the battery even if the device is in thermal shutdown.

APPLICATION INFORMATION

INDUCTOR SELECTION

For the bq25504 to operate properly, an inductor of appropriate value must be connected between Pin 16 (LBST) and Pin 2 (VIN_DC) for the boost converter.

For the boost converter and or charger, the inductor must have an inductance = 22 µH and have a peak current capability of ≥250 mA with the minimum series resistance to keep high efficiency.

CAPACITOR SELECTION

In general, all the capacitors need to be low leakage. Any leakage the capacitors have will reduce efficiency, increase the quiescent current and diminish the effectiveness of the IC for energy harvesting.

VREF_SAMP Capacitance:

The MPPT operation depends on the sampled value of the open circuit voltage and the input regulation follows the voltage stored on the CREF capacitor. This capacitor is sensitive to leakage since the holding period is around 16 seconds. As the capacitor voltage drops due to any leakage, the input regulation voltage also drops preventing proper operation from extraction the maximum power from the input source. Therefore, it is recommended that the leakage be less than 2 nA at 3 V bias.

VIN_DC Capacitance:

Energy from the energy harvester input source is initially stored on a capacitor CHVR tied to Pin 2 (VIN_DC) and ground (VSS, Pin 1). For energy harvesters which have a source impedance which is dominated by a capacitive behavior, the value of the harvester capacitor should scaled according to the value of the output capacitance of the energy source, but an initial value of 4.7 µF is recommended.

:VSTOR Capacitance

Operation of the BQ25504 requires a two capacitors to be connected between Pin 15 (VSTOR) and ground. A high frequency bypass capacitor of at 0.01 µF should be placed as close as possible between VSTOR and GND. In addition, a bulk capacitor of at least 4.7 µF should be connected between Pin 15 and ground to assure stability of the boost converter, especially when the battery is fully charged and the converter in output voltage limiting mode.

Additional Capacitance on VSTOR or VBAT:

If there are large, fast system load transients and, or the storage element has high resistance, then the CSTOR capacitors may momentarily discharge below the VBAT_UV threshold in response to the transient. This causes the bq25504 to turn off the PFET switch between VSTOR and VBAT and turn on the boost converter. Of, the CSTOR capacitors may further discharge below the VSTOR_CHGEN threshold and cause the bq25504 to enter Cold Start. For instance, some Li-ion batteries or thin-film batteries may not have the current capacity to meet the surge current requirements of an attached low power radio. To prevent VSTOR from drooping, either increase the CSTOR capacitance or add additional capacitance in parallel with the storage element is recommended. For example, if the bq25504 is configured to charge the storage element to 4.2 V and a 500 mA load transient of 50 µs duration infrequently occurs, then, solving I = C x dv/dt for CSTOR gives :

$$CSTOR \geq 500\ mA \times 50\ \mu s/(4.2\ V - 1.8\ V) = 10.5\ \mu F \quad (6)$$

Note that increasing CSTOR is the recommended solution but will cause the bq25504 to operate in the less efficient Cold Start mode for a longer period at startup compared to using CSTOR = 4.7 µF. If longer Cold Start run times are not desired, then place the additional capacitance in parallel with the storage element.

For a recommended list of standard components, see the EVM User's guide (SLUU654).

LAYOUT CONSIDERATIONS

As for all switching power supplies, the layout is an important step in the design, especially at high peak currents and high switching frequencies. If the layout is not carefully done, the boost converter/charger could show stability problems as well as EMI problems. Therefore, use wide and short traces for the main current path and for the power ground paths. The input and output capacitor, as well as the inductor should be placed as close as possible to the IC.

The resistors that program the thresholds should be placed as close as possible to the input pins of the IC to minimize parasitic capacitance to less than 2 pF.

To layout the ground, it is recommended to use short traces as well, separated from the power ground traces. This avoids ground shift problems, which can occur due to superimposition of power ground current and control ground current. Assure that the ground traces are connected close to the device GND pin.

THERMAL CONSIDERATIONS

Implementation of integrated circuits in low-profile and fine-pitch surface-mount packages typically requires special attention to power dissipation. Many system-dependent issues such as thermal coupling, airflow, added heat sinks and convection surfaces, and the presence of other heat-generating components affect the power-dissipation limits of a given component.

Three basic approaches for enhancing thermal performance are listed below.

- Improving the power-dissipation capability of the PCB design
- Improving the thermal coupling of the component to the PCB
- Introducing airflow in the system

For more details on how to use the thermal parameters in the Thermal Table, check the Thermal Characteristics Application Note (SZZA017) and the IC Package Thermal Metrics Application Note (SPRA953).

REVISION HISTORY

Changes from Original (October 2011) to Revision A **Page**

- Added C_{FLTR} and Notes 1 and 2 to Figure 2 6
- Added C_{FLTR} and Notes 1 and 2 to Figure 3 7
- Added C_{FLTR} and Notes 1 and 2 to Figure 4 8
- Added the INTENDED OPERATION section 13
- Changed the Cold -Start Operation section 13
- Changed the Boost Converter, Charger Operation section 13
- Changed the Storage Element section 14
- Changed the CAPACITOR SELECTION section 17

PACKAGING INFORMATION

Orderable Device	Status (1)	Package Type	Package Drawing	Pins	Package Qty	Eco Plan (2)	Lead/ Ball Finish	MSL Peak Temp (3)	Samples (Requires Login)
BQ25504RGTR	ACTIVE	QFN	RGT	16	3000	Green (RoHS & no Sb/Br)	CU NIPDAU	Level-2-260C-1 YEAR	
BQ25504RGTT	ACTIVE	QFN	RGT	16	250	Green (RoHS & no Sb/Br)	CU NIPDAU	Level-2-260C-1 YEAR	

(1) The marketing status values are defined as follows:
ACTIVE: Product device recommended for new designs.
LIFEBUY: TI has announced that the device will be discontinued, and a lifetime-buy period is in effect.
NRND: Not recommended for new designs. Device is in production to support existing customers, but TI does not recommend using this part in a new design.
PREVIEW: Device has been announced but is not in production. Samples may or may not be available.
OBSOLETE: TI has discontinued the production of the device.

(2) Eco Plan - The planned eco-friendly classification: Pb-Free (RoHS), Pb-Free (RoHS Exempt), or Green (RoHS & no Sb/Br) - please check http://www.ti.com/productcontent for the latest availability information and additional product content details.
TBD: The Pb-Free/Green conversion plan has not been defined.
Pb-Free (RoHS): TI's terms "Lead-Free" or "Pb-Free" mean semiconductor products that are compatible with the current RoHS requirements for all 6 substances, including the requirement that lead not exceed 0.1% by weight in homogeneous materials. Where designed to be soldered at high temperatures, TI Pb-Free products are suitable for use in specified lead-free processes.
Pb-Free (RoHS Exempt): This component has a RoHS exemption for either 1) lead-based flip-chip solder bumps used between the die and package, or 2) lead-based die adhesive used between the die and leadframe. The component is otherwise considered Pb-Free (RoHS compatible) as defined above.
Green (RoHS & no Sb/Br): TI defines "Green" to mean Pb-Free (RoHS compatible), and free of Bromine (Br) and Antimony (Sb) based flame retardants (Br or Sb do not exceed 0.1% by weight in homogeneous material)

(3) MSL, Peak Temp. -- The Moisture Sensitivity Level rating according to the JEDEC industry standard classifications, and peak solder temperature.

TAPE AND REEL INFORMATION

REEL DIMENSIONS

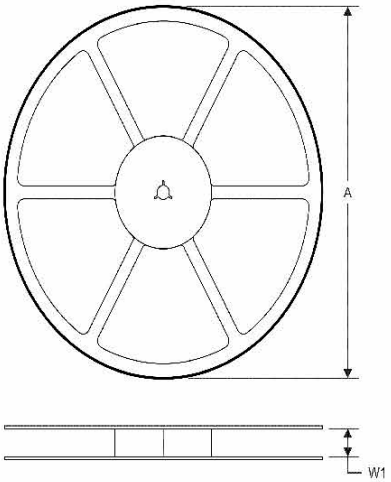

TAPE DIMENSIONS

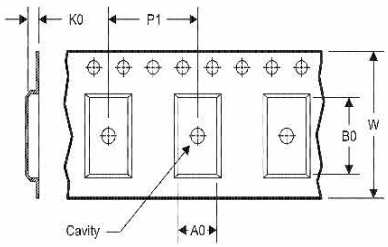

A0	Dimension designed to accommodate the component width
B0	Dimension designed to accommodate the component length
K0	Dimension designed to accommodate the component thickness
W	Overall width of the carrier tape
P1	Pitch between successive cavity centers

TAPE AND REEL INFORMATION

*All dimensions are nominal

Device	Package Type	Package Drawing	Pins	SPQ	Reel Diameter (mm)	Reel Width W1 (mm)	A0 (mm)	B0 (mm)	K0 (mm)	P1 (mm)	W (mm)	Pin1 Quadrant
BQ25504RGTR	QFN	RGT	16	3000	330.0	12.4	3.3	3.3	1.1	8.0	12.0	Q2
BQ25504RGTT	QFN	RGT	16	250	180.0	12.4	3.3	3.3	1.1	8.0	12.0	Q2

TAPE AND REEL BOX DIMENSIONS

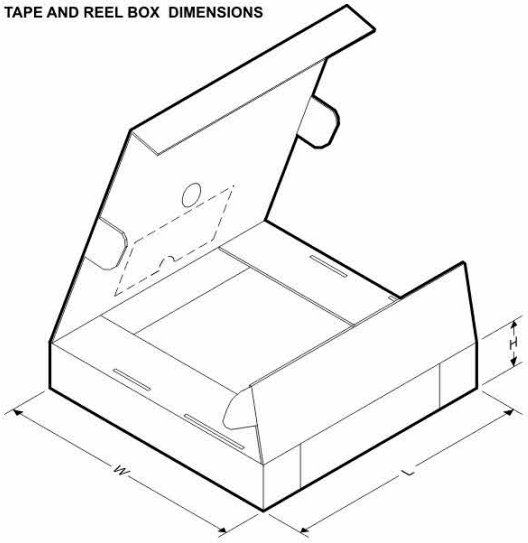

*All dimensions are nominal

Device	Package Type	Package Drawing	Pins	SPQ	Length (mm)	Width (mm)	Height (mm)
BQ25504RGTR	QFN	RGT	16	3000	367.0	367.0	35.0
BQ25504RGTT	QFN	RGT	16	250	210.0	185.0	35.0

RGT (S–PVQFN–N16) PLASTIC QUAD FLATPACK NO–LEAD

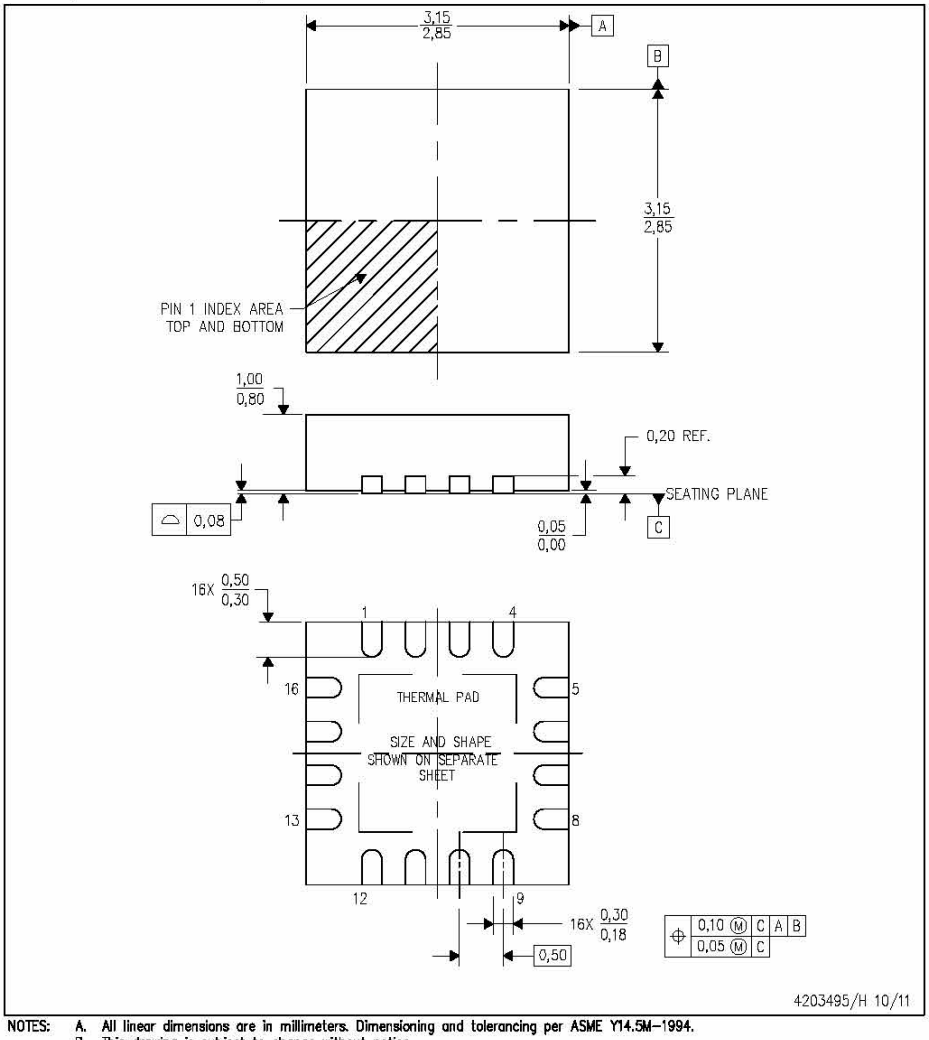

NOTES:
A. All linear dimensions are in millimeters. Dimensioning and tolerancing per ASME Y14.5M–1994.
B. This drawing is subject to change without notice.
C. Quad Flatpack, No–leads (QFN) package configuration.
D. The package thermal pad must be soldered to the board for thermal and mechanical performance.
E. See the additional figure in the Product Data Sheet for details regarding the exposed thermal pad features and dimensions.
F. Falls within JEDEC MO–220.

TEXAS INSTRUMENTS
www.ti.com

RGT (S–PVQFN–N16) PLASTIC QUAD FLATPACK NO–LEAD

THERMAL INFORMATION

This package incorporates an exposed thermal pad that is designed to be attached directly to an external heatsink. The thermal pad must be soldered directly to the printed circuit board (PCB). After soldering, the PCB can be used as a heatsink. In addition, through the use of thermal vias, the thermal pad can be attached directly to the appropriate copper plane shown in the electrical schematic for the device, or alternatively, can be attached to a special heatsink structure designed into the PCB. This design optimizes the heat transfer from the integrated circuit (IC).

For information on the Quad Flatpack No–Lead (QFN) package and its advantages, refer to Application Report, QFN/SON PCB Attachment, Texas Instruments Literature No. SLUA271. This document is available at www.ti.com.

The exposed thermal pad dimensions for this package are shown in the following illustration.

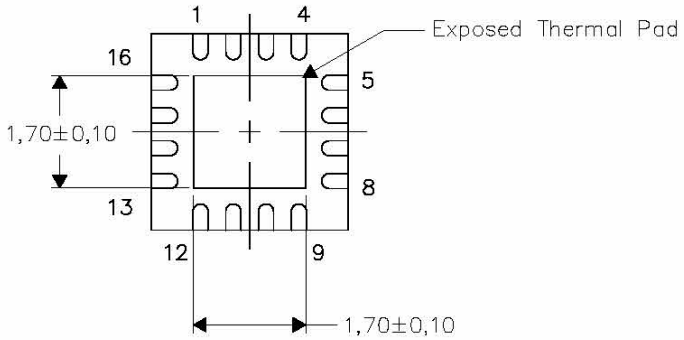

Bottom View

Exposed Thermal Pad Dimensions

4206349–4/Q 10/11

NOTE: All linear dimensions are in millimeters

RGT (S–PVQFN–N16) PLASTIC QUAD FLATPACK NO–LEAD

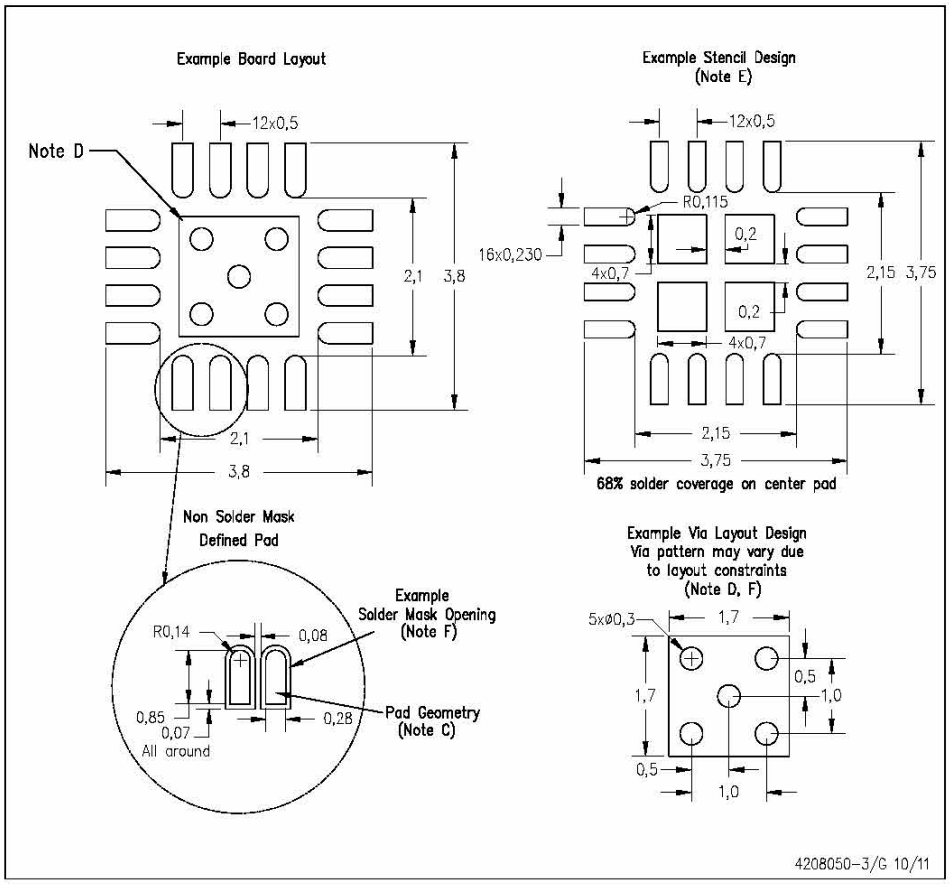

NOTES:
A. All linear dimensions are in millimeters.
B. This drawing is subject to change without notice.
C. Publication IPC–7351 is recommended for alternate designs.
D. This package is designed to be soldered to a thermal pad on the board. Refer to Application Note, QFN/SON PCB Attachment, Texas Instruments Literature No. SLUA271, and also the Product Data Sheets for specific thermal information, via requirements, and recommended board layout. These documents are available at www.ti.com <http://www.ti.com>.
E. Laser cutting apertures with trapezoidal walls and also rounding corners will offer better paste release. Customers should contact their board assembly site for stencil design recommendations. Refer to IPC 7525 for stencil design considerations.
F. Customers should contact their board fabrication site for minimum solder mask web tolerances between signal pads.

IMPORTANT NOTICE

Texas Instruments Incorporated and its subsidiaries (TI) reserve the right to make corrections, enhancements, improvements and other changes to its semiconductor products and services per JESD46, latest issue, and to discontinue any product or service per JESD48, latest issue. Buyers should obtain the latest relevant information before placing orders and should verify that such information is current and complete. All semiconductor products (also referred to herein as "components") are sold subject to TI's terms and conditions of sale supplied at the time of order acknowledgment.

TI warrants performance of its components to the specifications applicable at the time of sale, in accordance with the warranty in TI's terms and conditions of sale of semiconductor products. Testing and other quality control techniques are used to the extent TI deems necessary to support this warranty. Except where mandated by applicable law, testing of all parameters of each component is not necessarily performed.

TI assumes no liability for applications assistance or the design of Buyers' products. Buyers are responsible for their products and applications using TI components. To minimize the risks associated with Buyers' products and applications, Buyers should provide adequate design and operating safeguards.

TI does not warrant or represent that any license, either express or implied, is granted under any patent right, copyright, mask work right, or other intellectual property right relating to any combination, machine, or process in which TI components or services are used. Information published by TI regarding third-party products or services does not constitute a license to use such products or services or a warranty or endorsement thereof. Use of such information may require a license from a third party under the patents or other intellectual property of the third party, or a license from TI under the patents or other intellectual property of TI.

Reproduction of significant portions of TI information in TI data books or data sheets is permissible only if reproduction is without alteration and is accompanied by all associated warranties, conditions, limitations, and notices. TI is not responsible or liable for such altered documentation. Information of third parties may be subject to additional restrictions.

Resale of TI components or services with statements different from or beyond the parameters stated by TI for that component or service voids all express and any implied warranties for the associated TI component or service and is an unfair and deceptive business practice. TI is not responsible or liable for any such statements.

Buyer acknowledges and agrees that it is solely responsible for compliance with all legal, regulatory and safety-related requirements concerning its products, and any use of TI components in its applications, notwithstanding any applications-related information or support that may be provided by TI. Buyer represents and agrees that it has all the necessary expertise to create and implement safeguards which anticipate dangerous consequences of failures, monitor failures and their consequences, lessen the likelihood of failures that might cause harm and take appropriate remedial actions. Buyer will fully indemnify TI and its representatives against any damages arising out of the use of any TI components in safety-critical applications.

In some cases, TI components may be promoted specifically to facilitate safety-related applications. With such components, TI's goal is to help enable customers to design and create their own end-product solutions that meet applicable functional safety standards and requirements. Nonetheless, such components are subject to these terms.

No TI components are authorized for use in FDA Class III (or similar life-critical medical equipment) unless authorized officers of the parties have executed a special agreement specifically governing such use.

Only those TI components which TI has specifically designated as military grade or "enhanced plastic" are designed and intended for use in military/aerospace applications or environments. Buyer acknowledges and agrees that any military or aerospace use of TI components which have ***not*** been so designated is solely at the Buyer's risk, and that Buyer is solely responsible for compliance with all legal and regulatory requirements in connection with such use.

TI has specifically designated certain components which meet ISO/TS16949 requirements, mainly for automotive use. Components which have not been so designated are neither designed nor intended for automotive use; and TI will not be responsible for any failure of such components to meet such requirements.

Products		**Applications**	
Audio	www.ti.com/audio	Automotive and Transportation	www.ti.com/automotive
Amplifiers	amplifier.ti.com	Communications and Telecom	www.ti.com/communications
Data Converters	dataconverter.ti.com	Computers and Peripherals	www.ti.com/computers
DLP® Products	www.dlp.com	Consumer Electronics	www.ti.com/consumer-apps
DSP	dsp.ti.com	Energy and Lighting	www.ti.com/energy
Clocks and Timers	www.ti.com/clocks	Industrial	www.ti.com/industrial
Interface	interface.ti.com	Medical	www.ti.com/medical
Logic	logic.ti.com	Security	www.ti.com/security
Power Mgmt	power.ti.com	Space, Avionics and Defense	www.ti.com/space-avionics-defense
Microcontrollers	microcontroller.ti.com	Video and Imaging	www.ti.com/video
RFID	www.ti-rfid.com		
OMAP Applications Processors	www.ti.com/omap	**TI E2E Community**	e2e.ti.com
Wireless Connectivity	www.ti.com/wirelessconnectivity		

Mailing Address: Texas Instruments, Post Office Box 655303, Dallas, Texas 75265

LIST OF REFERENCES

[1] R. Mabus. "Message from the Secretary of the Navy," in *Naval Energy, A Strategic Approach*, October 2009. [Online]. Available: http://www.onr.navy.mil/naval-energy-forum/~/media/5EFD428CFEB0412391CC321DCAF67138.ashx (accessed June 2012).

[2] Texas Instruments. "Industry's most efficient boost charger for nano power energy harvesting applications." [Online]. Available: http://www.ti.com/ww/en/analog/bq25504_boost_converter_charger_ic/index.html?DCMP=hpa_pmp_bq25504_en&HQS=bq25504 (accessed June 2012).

[3] N. Hoffman, "A miniature electromechanical generator design utilizing human motion," M.S. thesis, Dept. Electrical and Computer Eng., Naval Postgraduate School, Monterey, CA, 2010.

[4] CAP-XX. "Charging a supercapacitor from a solar cell with a bq25504 PPT energy harvesting IC." [Online]. Available: http://www.cap-xx.com/news/news.php (accessed July 2012).

[5] S. Bandyopadhyay and A. Chandrakasan, "Platform architecture for solar, thermal, and vibration energy combining with MPPT and single inductor," *IEEE Journal of Solid-State Circuits*, vol. 47, no. 9, pp. 2199–2215, September 2012.

[6] M. Pinuela *et al*., "Current state of research at Imperial College London in RF harvesting and inductive power transfer," London, UK: Imperial College London, Dept. Elect. And Electronic Eng., [Online]. Available: https://workspace.imperial.ac.uk/opticalandsemidev/Public/Publications/2012_05_IWWETH.pdf (accessed July 2012)

[7] A. Emadi *et al*., *Integrated Power Electronic Converters and Digital Control*. Boca Raton, FL: CRC Press, 2009.

[8] R. Ashton. "Popular direct-coupled DC-DC converters," class notes for EC3150, Dept. of Electrical and Computer Engineering, Naval Postgraduate School, Monterey, CA, summer 2012.

[9] National Instruments. "Maximum power point tracking," July 2009. [Online]. Available: http://www.ni.com/white-paper/8106/en/ (accessed June 2012)

[10] Texas Instruments, "BQ25504 datasheet," in *BQ25504 EVM Ultra Low Power Boost Converter with Battery Management for Energy Harvester Applications*. Dallas, TX: Texas Instruments, October 2011 [Revised September 2012].

[11] Texas Instruments, *BQ25504 EVM Ultra Low Power Boost Converter with Battery Management for Energy Harvester Applications* [user's guide]. Dallas, TX: Texas Instruments, October 2011 [Revised October 2011].

INITIAL DISTRIBUTION LIST

1. Defense Technical Information Center
   Ft. Belvoir, Virginia

2. Dudley Knox Library
   Naval Postgraduate School
   Monterey, California